

Aus dem Friedrich-Baur-Institut der Medizinischen Fakultät  
an der Neurologischen Klinik und Poliklinik  
der Ludwig-Maximilians-Universität München  
(Direktorin: Univ.-Prof. Dr. med. Marianne Dieterich)



**Immortalization of primary myoblasts from the DMD pig -  
hTERT/CDK4 prevent cellular senescence in primary porcine myoblasts**

Dissertation zum Erwerb des Doktorgrades der Humanmedizin  
an der Medizinischen Fakultät  
der Ludwig-Maximilians-Universität München

vorgelegt von  
Nicolas Ulrich Schumacher  
aus  
Hilden  
2022

---

**Mit Genehmigung der Medizinischen Fakultät der Universität München**

Berichterstatlerin: Priv.-Doz. Dr. med. Dr. phil. Sabine Krause

Mitberichterstatler: Prof. Dr. Daphne Merkus  
Priv.-Doz. Dr. Joachim Scheßl

Dekan: Univ.-Prof. Dr. med. Thomas Gudermann

Tag der mündlichen Prüfung: 21.07.2022

---

**Teile dieser Arbeit wurden veröffentlicht in:**

**Publikationen:**

Papadimas GK, Paraskevas GP, Zambelis T, Karagiaouris C, Bourbouli M, Bougea A, Walter MC, **Schumacher NU**, Krause S, Kapaki E. The multifaceted clinical presentation of VCP-proteinopathy in a Greek family, Acta Myologica, 2017; XXXVI: p. 1-4

**Publizierte Abstracts:**

**Schumacher NU**, Kessler B, Blutke A, Wolf E, Stucka R, Walter MC, Krause S. Immortalisierung von primären Myoblasten aus dem DMDPig [abstract]. In: 23. Kongress des wissenschaftlichen Beirates der Deutschen Gesellschaft für Muskelkranke e.V.; 2017 Feb 16-17; München; Nervenheilkunde 2017; 36: abstract 100

**Vorträge:**

**Schumacher NU** (2017, February), Immortalisierung von primären Myoblasten aus dem DMDPig; präsentiert auf dem 23. Kongress des Wissenschaftlichen Beirates der Deutschen Gesellschaft für Muskelkranke e.V., München

---

# I. Inhaltsverzeichnis

I. INHALTSVERZEICHNIS .....	4
II. ZUSAMMENFASSUNG .....	6
III. ABSTRACT .....	7
IV. INTRODUCTION .....	8
IV.1. The muscular system and myopathies.....	8
IV.2. The Duchenne and Becker muscular dystrophy .....	9
IV.3. Animal models of Duchenne muscular dystrophy .....	19
IV.4. Hereditary inclusion body myopathies.....	28
IV.4.1. GNE myopathy.....	28
IV.4.2. VCP proteinopathy .....	29
IV.5. immortalization of cell lines.....	30
V. AIM OF THE PROJECT .....	35
VI. MATERIALS AND METHODS .....	36
VI.1. Cell lines.....	36
VI.1.1. Pigs ( <i>Sus scrofa</i> ).....	36
VI.1.2. Patients.....	36
VI.1.3. Additional cell lines.....	37
VI.2. Basics of cell cultivation .....	37
VI.3. Plasmids.....	39
VI.4. Use of genetically modified organisms (GMOs) .....	40
VI.5. Test of antibiotic resistance .....	40
VI.6. Transfection of producer cell line .....	42
VI.7. Porcine myoblasts.....	45
VI.7.1. Transduction of myoblasts .....	45
VI.7.2. Cell doublings and cell counting .....	48
VI.7.3. Limited dilution.....	48
VI.7.4. Fusion of myoblasts.....	48
VI.7.5. Immunofluorescence staining.....	49
VI.8. Further molecular genetic analyses.....	50
VI.8.1. Sequence analysis in myoblasts .....	50
VI.8.2. Sequencing of CDK4 and hTERT genes in producer cell line.....	50
VI.9. Molecular genetic analyses of hereditary degenerative neuromuscular diseases .....	51
VI.9.1. Primers .....	51
VI.9.2. Polymerase chain reaction protocol .....	51
VI.9.3. Gel electrophoresis .....	52
VI.9.4. DNA-sequencing and analysis of data .....	52

<b>VII. RESULTS</b> .....	<b>53</b>
VII.1. Concentration of prepared plasmids .....	53
VII.2. Testing of antibiotic resistance .....	54
VII.3. Transfection of producer cell line .....	56
VII.4. Viral titers .....	57
VII.5. Porcine myoblasts .....	59
VII.5.1. Transduction of primary myoblasts .....	59
VII.5.1. Cell doublings and cell counting .....	73
VII.5.2. Limited dilution .....	75
VII.5.4. Fusion of myoblasts .....	76
VII.5.5. Immunofluorescence staining .....	80
VII.6. Further molecular genetic analyses .....	81
VII.6.1. Sequence analysis in myoblasts .....	81
VII.6.2. Sequencing of <i>CDK4</i> and <i>hTERT</i> genes in producer cell lines .....	82
VII.7. Molecular genetic analyses of hereditary degenerative neuromuscular diseases .....	82
VII.7.1. Patient #1 .....	83
VII.7.2. Patient #2 .....	84
VII.7.3. Patient #3 .....	86
<b>VIII. DISCUSSION</b> .....	<b>88</b>
VIII.1. The path to immortalized cells .....	88
VIII.2. immortalization of porcine myoblasts .....	89
VIII.3. Limitations .....	93
VIII.4. Molecular genetic analyses of patients .....	95
VIII.5. Outlook .....	96
<b>IX. REFERENCE LIST</b> .....	<b>98</b>
<b>X. ANNEX</b> .....	<b>108</b>
X.1. List of abbreviations .....	108
X.2.1. pBABE-puro-hTERT .....	110
X.2.2. pBABE-hygro-CDK4-R24C .....	111
X.2.3. pBABE-neo-IRES-eGFP .....	112
X.2.3. Plasmid sequence maps .....	114
X.3. Primer sequences .....	116
IX.3.1. pBABE .....	116
X.3.2. GNE .....	116
X.3.3. VCP .....	117
X.4. GenBank accession numbers .....	117
X.5. List of figures and tables .....	118
X.6. Danksagung .....	120
X.7. Eidesstattliche Versicherung .....	121
X.8. Curriculum vitae .....	122

## II. Zusammenfassung

Die X-chromosomal rezessive Muskeldystrophie Duchenne ist die häufigste erbliche Myopathie und betrifft einen von 3'500 bis 5'000 Jungen. Symptomatische Therapiekonzepte haben das Überleben und die Lebensqualität der betroffenen Patienten verbessert. Die Forschung zu ursächlichen Therapien wird durch das Fehlen ausreichender *in vitro*- und *in vivo*-Testmaterialien und zahlenmäßig kleine Patientenkohorten behindert. Das DMD-Schwein stellt ein exzellentes *in vivo*-Modell der Erkrankung dar. Es besitzt die häufigste genetische Mutation des Menschen, eine Deletion des Exon 52 des *DMD*-Gens, und ähnelt dem menschlichen Phänotyp sehr. Aufgrund der starken Abnahme des verfügbaren primären humanen Zellmaterials bei deutlichem Rückgang der durchgeführten Muskelbiopsien bei gleichzeitig zunehmender Notwendigkeit von *in vitro*-Hochdurchsatzverfahren für neue Therapien, sind immortalisierte Zellsysteme für die Kultivierung großer Zellmengen und stabile *in vitro*-Testbedingungen unabdingbar.

Der Einsatz zweier zellzyklusaktiver Gene, humane Telomerase Reverse Transkriptase (*hTERT*) sowie Cyclin-abhängige Kinase 4 (*CDK4*), und deren stabile Integration in primäre Zellen mittels retroviralem, auf dem Moloney murinen Leukämievirus basierendem Vektorsystem führte bei primären humanen Myoblasten zur Umgehung der replikativen Seneszenz und vermehrter proliferativer Kapazität.

In diesem neuen Versuch wiesen porcine DMD-Myoblasten- und Wildtyp (WT)-Kontrollzelllinien nach Transduktion mit *hTERT* und *CDK4* eine signifikante Verlängerung der Lebensspanne und Vermehrungsfähigkeit auf. So persistierte nach 250 Tagen ein konstantes Wachstum. Konsekutives Auszählen der Zellen bewies die erhaltene Proliferationskapazität der transduzierten gegenüber den nicht-transduzierten Zellen. Die DMD-Zellen behielten ihre initiale Morphologie und Eigenschaften mit erfolgreicher Myoblastenfusion und Differenzierung zu mehrkernigen Myotuben nach 250 Tagen bei. Desmin als Myogenitätsmarker war in Zellkulturen höherer Passagen reduziert. Mit Stand November 2021 ist dies die erste berichtete Immortalisierung porciner Muskelzellen. Diese Zelllinien haben das Potential als leistungsfähige Werkzeuge für die zukünftige präklinische und translationale Forschung der Muskeldystrophie Duchenne zu dienen.

Erbliche Myopathien umfassen eine Vielzahl von Erkrankungen. Die Identifizierung einer heterozygoten Punktmutation im *VCP*-Gen (c.476G>A, p.R159H) bestätigte in zwei Patienten die Diagnose einer VCP-Proteinopathie und beleuchtete die ausgeprägte Genotyp-Phänotyp-Variabilität dieser Erkrankung. Zusätzlich wurde in einer weiteren bulgarischen Roma-Patientin eine neue, heterozygote Compound-Mutation im *GNE*-Gen (c.178A>G, p.M60V und c.1853T>C, p.I618T) entdeckt, die die Diagnose einer GNE-Myopathie bestätigte.

### III. Abstract

X-linked Duchenne muscular dystrophy (DMD) is the most common hereditary myopathy, affecting one in 3'500 -5'000 boys. Symptomatic therapy has improved survival and quality of life of affected patients. But research into more causative treatment is constrained by the lack of a sufficient amount of *in vitro* and *in vivo* testing materials and small patient cohorts. The DMD pig large animal model represents an excellent *in vivo* model for DMD, as it features the most common genetic mutation in humans, a deletion of exon 52 of the *DMD* gene and resembles the human phenotype closely. To counteract the growing disparity in the recent decline in available human primary cell material due to a sharp reduction in muscle biopsies and the increased need for *in vitro* high throughput testing of new therapies, an immortalized cell system is required to enable the cultivation of large amounts of cell material and ensure stable *in vitro* testing conditions.

The use of two cell cycle active genes, human telomerase reverse transcriptase (*hTERT*) and cyclin-dependent kinase 4 (*CDK4*) and their stable integration in primary cells using a retroviral delivery system based on the Moloney murine leukemia virus has been shown to successfully overcome replicative senescence and induce extended proliferative capabilities in primary human myoblasts.

In this new experiment, porcine DMD myoblasts and a wild type (WT) control line transduced with *hTERT* and *CDK4* featured a significant extension of life span and proliferation abilities, showing persistent constant growth to a hallmark of 250 days. Consecutive cell counting proved the preservation of proliferation capacity of transduced DMD and WT cells compared to non-transduced controls. The DMD cells retained their initial morphologic and functional properties, including successful myoblast fusion into terminally differentiated multinucleated myotubes after proliferation span of 250 days. However, immunofluorescence staining of desmin as a marker of myogenicity was reduced in cell cultures of higher population doublings. As of November 2021, this is the first reported immortalization of porcine myogenic cells. These cell lines have the potential to serve as a powerful tool for future preclinical and translational research in Duchenne muscular dystrophy.

Hereditary myopathies encompass a variety of different diseases. The identification of a heterozygous point mutation in the *VCP* gene (c.476G>A, p.R159H) in two patients suspected of VCP proteinopathy using Sanger sequencing, added to the broad variation in genotype-phenotype-correlation in this disease. Additionally, a new compound heterozygous mutation (c.178A>G, p.M60V and c.1853T>C, p.I618T) in the *GNE* gene was identified in one Bulgarian Roma patient, confirming the diagnosis of GNE myopathy.

## IV. Introduction

### IV.1. The muscular system and myopathies

In humans, the muscular system represents 45 % of the total human lean body mass [1]. Although the ratio is dependent on sex and physical fitness, it highlights that muscles are an important structure of our body.

The muscular system serves many purposes in human physiology. It can be divided into smooth muscle, primarily located in internal organs and blood vessels, and the striated muscle, which can be further sectioned into cardiac and skeletal muscle, located in the heart and muscles of the body [2]. The striated muscle is a complex tissue with the main purpose of contraction and relaxation. It is the motor of the body, transferring chemical energy into mechanical force and warmth and thus being responsible for movement [3]. Skeletal muscle is derived from the mesoderm and the linear arrayed multinucleated cells are clustered on several levels from muscular fasciculi to myofibrils. The latter contain the sarcomere as complex functional unit for the interaction of actin and myosin in muscle contraction and the costamere and intermediate filaments as stabilizers and connectors to neighboring cells. The term “striated muscle” is derived from the visible lines in the structure of the sarcomere [2].

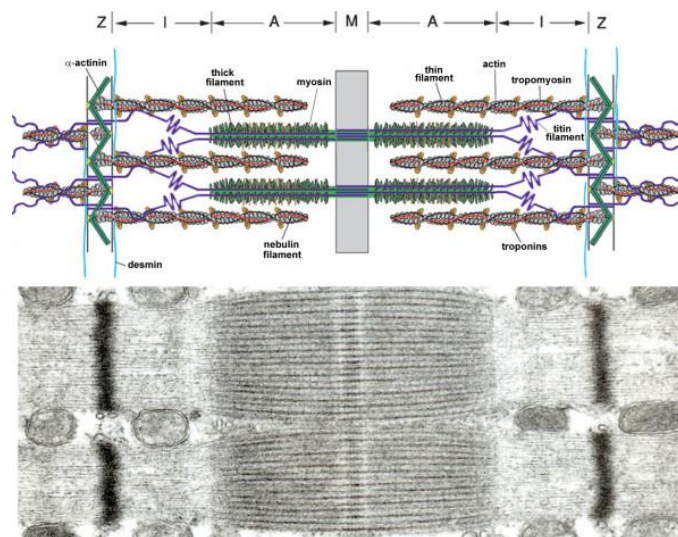


**Figure 1: top: Overview of two adjacent sarcomeres; bottom: electron microscopic image of ultrastructural organization of sarcomeres in parallel [4]. (Published under Creative Commons Attribution License - CC BY 2.0.)**

Primary myogenesis during embryogenesis originates from the respective somite in the paraxial mesoderm. During migration of the myogenic progenitor cells into the limb bud, a phasic complex and tightly regulated cascade of myogenic determination factor expression takes place, i.e. among others, Pax3, Pax7, Myf5, MRF, Myogenin and MyoD, which results into

formation of multinucleated myotubes and myofibres. As these cells are postmitotic, adult muscle regeneration relies on satellite cells, a group of quiescent stem cells with retained proliferation capabilities located between basal lamina and sarcolemma or near the capillaries. These cells can be activated and induce postnatal muscle growth or muscular regeneration by fusing with the damaged muscle fibre, expressing similar myogenesis factors, e. g. Pax3 or Pax7 [5-7]. Minor damage can be corrected by mechanisms initiated by the fibre itself [8, 9].

Naturally, a structure this large and important can harbor defects and hence, there is a wide array of myopathies, i. e. diseases of the muscle. They can be hereditary, e. g. the complex group of progressive muscular dystrophies, including congenital muscular dystrophies, Duchenne and Becker muscular dystrophy, Emery-Dreifuss muscular dystrophy, distal muscular dystrophies, limb-girdle diseases and facioscapulohumeral or oculopharyngeal muscular dystrophies. These afflictions are caused by genetic mutations in genes coding for relevant proteins of the muscle [10, 11]. Congenital and metabolic myopathies and myopathies of ion channels constitute other hereditary diseases. Acquired myopathies include myositis due to autoimmune reactions or pathogens. Toxic or endocrine myopathies and critical-illness-myopathies are other variants which develop due to toxic agents or unphysiological conditions of the body [12]. In this work we will focus on two different myopathies: first, the most common form in children, the Duchenne muscular dystrophy and second, the hereditary inclusion body myopathy, amongst others, caused by mutations in the *VCP* and *GNE* genes.

## **IV.2. The Duchenne and Becker muscular dystrophy**

The Duchenne (DMD) and Becker (BMD) muscular dystrophy are X-linked progressive muscular diseases. DMD is the most common muscular dystrophy. A generally accepted estimate is that DMD affects one in 3'500-5'000 and BMD one in 12'000 boys [13, 14]. In epidemiological studies an incidence of 15.9 to 19.5 per 100'000 live male births was found [15-17].

The affected mostly male patients show signs of progressive muscular weakness with an onset at the age of two to three years. Elevated levels of serum creatine kinase (CK) up to 10 - 20-fold can be frequently detected before occurrence of manifest clinical symptoms [16]. Usually, the peak of CK elevation is reached at 2 years of age. A normalization of levels over time is possible [12, 18].

Typical first signs suggestive for DMD, starting in early childhood, include weakness, clumsiness, difficulties in stair climbing or toe walking, and the presentation of Gowers's sign, a typical way of standing up by using the hands (Figure 2) [19].

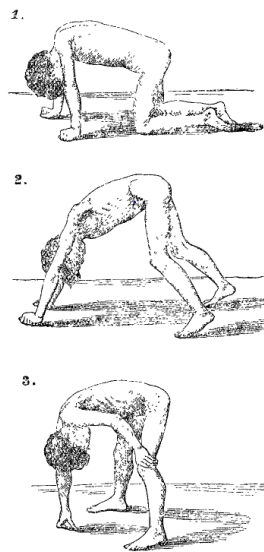


**Figure 2: Typical sequence of Gowers's sign [20]. (Reprint permission granted from copyright holder.)**

The muscular weakness typically initiates at the proximal muscle of the lower limb and later the upper limbs before affecting the distal muscles. This leads to a progressive impairment of movement in the children. They exhibit a progressively slow and waddling gait with subsequent scoliosis, lumbar lordosis and pseudohypertrophy of calf muscles and more infrequently of the quadriceps muscle. Additionally, pain, mainly in hips and lower back, decreased endurance or head control, and most strikingly an inability to keep up with peers may occur. Other clinical features may include shortening of the Achilles tendon, hypotonia or hypo- to areflexia [21, 22].

DMD patients also suffer from dilated cardiomyopathy (DCM). Incidence of DCM and subsequent arrhythmias increase over the course of the disease [23-27]. DMD patients feature a growth delay compared to peers [28]. Furthermore, many DMD patients suffer from fractures, mostly due to falling. Ambulatory independent patients have the highest incidence of fractures, even sometimes leading to permanent immobility, and DMD patients treated with glucocorticoids have an elevated risk of vertebral compression fractures [29-31].

Additionally, a small proportion of DMD patients exhibit considerable cognitive impairment and reading deficits or increased rates in attention-deficit / hyperactivity disorder, anxiety disorders, autism spectrum disorders, epilepsy and obsessive-compulsive disorders [32].

BMD patients manifest a later onset and slower progression of symptoms. Even cases with an onset of symptoms after 60 years of age have been reported. BMD patients often present a mild or even subclinical skeletal muscle involvement but feature a severe phenotype of dilated cardiomyopathy [33-36]. BMD patients can also display signs of mental impairment [10].

Some patients exhibit an intermediate phenotype, which lies in between those of DMD and BMD and cannot be certainly assigned to one of the groups [37]. X-linked dilated cardiomyopathy is

another rare form of dystrophinopathy which affects expression or function of dystrophin mostly or exclusively in the cardiac muscle and therefore spares the skeletal muscle [38-42].

Most female carriers of a dystrophin mutation are asymptomatic but can also present typical symptoms of DMD to a varying degree and age of onset. A study conducted by Hoogerwaard et al. showed that at least a fifth of carriers do exhibit signs of muscular weakness or dilated cardiomyopathy [43-45]. Newer findings through MRI screening indicate higher incidence of cardiomyopathy among carriers [46]. There are also reports of cardiac transplantation for DMD carriers [47]. Carriers do feature elevated CK levels in 70 % for DMD and 50 % for BMD. CK levels exhibit the same kinetics with highest values in younger carriers [18].

The loss of ambulation occurs at about thirteen years of age. The most common causes of death for DMD patients are respiratory insufficiency, induced by progressive weakness, pneumonia or scoliosis or dilated cardiomyopathy with conduction abnormalities in their twenties or late teens [24]. Survival beyond 30 years of age used to be rare, but supportive therapy now enables many patients to reach the fourth decade of life [48]. Loss of ambulation in BMD patients varies from adolescence onwards but they exhibit a significantly longer life expectancy [10].

Apart from the obvious clinical features, DMD has a significant impact on quality of life of the patients, their families and caregivers and often represents a substantial financial burden [49].

The disease was first described in 1852 by Edward Meryon and in 1867 by Guillaume-Benjamin Duchenne in “the pathology of paralysis with muscular degeneration (paralysie myosclerotique), or paralysis with apparent hypertrophy” [50, 51]. Initially the cause and mechanism of the illness was unknown, amongst others leading to the description as “eine im hohen Maße befremdliche Erscheinung” - a highly strange appearance, by my great-grandfather in his dissertation about case histories of the dystrophia muscularis progressiva in 1892 [52]. BMD was first described by Peter Emil Becker in 1955 [53]. Only in 1986 the dystrophin gene and one year later the dystrophin protein were identified in humans [11, 54].

DMD and BMD are caused by genetic mutations in the dystrophin gene (*DMD*; OMIM #310200) located at locus Xp21.2-p21.1 on the short arm of the X chromosome. It is the largest human gene with a size of 2.4 million base pairs (bp) and contains 79 exons. Its mRNA consists of 14 kilobases and encodes for a 427 kD protein comprised of 3.685 amino acids [55]. The existence of at least seven independent, tissue-different promoters and two polyA-addition sites leads to the expression of various dystrophin isoforms [32].

In striated muscle, dystrophin serves as main component of the dystrophin-glycoprotein complex (DGC), situated at the sarcolemma, connecting the inner cytoskeleton and extracellular matrix (ECM). It is part of the costamere, which is responsible for protection against mechanical stress and important for intercellular signaling and ion homeostasis. Dystrophin is a cytoplasmic rod-shaped member of the spectrin superfamily made up by an N-terminal actin binding domain (N-ABD or ABD1), a central rod like domain composed of 24 spectrin-like repeats with four hinge regions and a second actin binding domain (ABD2). These tandem calponin-homology domains are used for binding F-Actin. A cysteine-rich domain and a C-terminal domain are linking the protein to other members of the DGC. Dystrophin exhibits several more structures that facilitate protein-protein-interaction, e. g. a WW domain, two EF-hand motifs, a zinc finger (ZZ) domain, coiled coils at the C-terminal domain or binding sites for ankyrin B and the intermediate filament synemin. Actin is bound by the ABD1 and ABD2 and therefore, dystrophin links the actin-based cytoskeleton with the extracellular matrix and protects actin filaments against depolymerization. The lack of dystrophin leads to a loss of mechanical mounting of the cytoskeleton and muscle cell membrane damage. Additionally, loss of ion homeostasis, especially calcium, and deranged intracellular signaling result in cellular stress and increased protein degradation [56-72].

The dystrophin-glycoprotein complex also includes the  $\alpha$ -,  $\beta$ -,  $\gamma$ -, and  $\delta$ -sarcoglycan subcomplex. These single-pass transmembrane proteins promote interactions between cytoskeleton and ECM and stabilize sarcospan with its four transmembrane domains, which lies in proximity of the sarcoglycan complex. The dystrophin-associated glycoprotein, called dystroglycan, expressing an  $\alpha$ - and  $\beta$ -subunit, provides linkage to laminin of the extracellular matrix and therefore improves stability of the cell. Other proteins, including dystrobrevin and syntrophin, both expressed in several isoforms, also take part in the DGC's functions, e. g. binding to a neuronal nitric oxidase synthase (nNOS), which is crucial for regulation of vasodilatation of blood vessels and therefore prevention of exercise-induced fatigue through its product nitric oxide. Mutations in several DGC components can lead to various myopathies, e. g. sarcoglycanopathies or limb-girdle muscular dystrophies [57, 58, 70, 73-77].

Utrophin, also called dystrophin-related protein, is a dystrophin functional and structural homologue located on human chromosome six, sharing an 80 % homology with the actin-binding domain and the following cysteine-rich domain of dystrophin. In adult muscle tissue, it is present primarily at myotendinous and neuromuscular junctions. It is upregulated in dystrophin-deficient humans and mice and then can also be detected at the sarcolemma. In mdx mice, upregulation of utrophin leads to a more benign DMD phenotype. Dystrophin and utrophin can be co-expressed at the sarcolemma [78]. Utrophin expression in DMD is thought to support muscle integrity and function [77, 79-81].

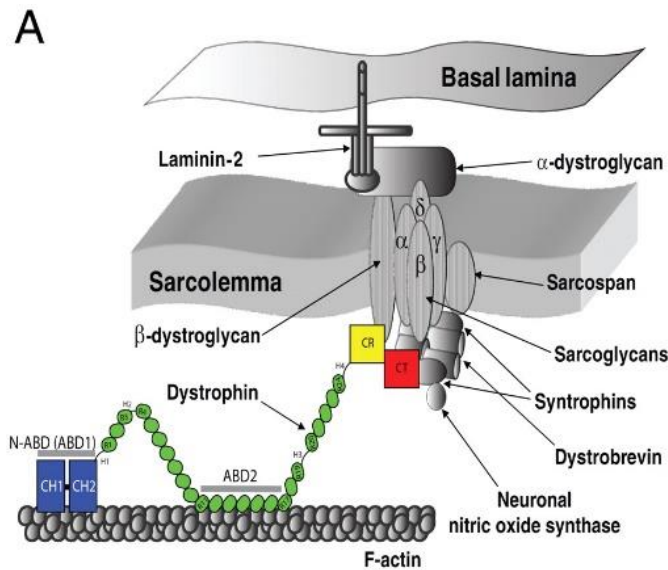


**Figure 3: Overview of the structure of the dystrophin-glycoprotein complex [56]. (Reprint permission granted from copyright holder.)**

Different 427 kD dystrophin isoforms are Dp427m in muscle, Dp427c in brain, Dp427p in Purkinje cells and historically Dp427l in lymphoblastoids, whose significance is heavily disputed [54, 60, 82-85]. Shorter variants of dystrophin can be found in the retina (Dp260), central nervous system and kidney (Dp140) and in the Schwann cells of the peripheral nervous system (Dp116) [86, 87]. Short isoforms (Dp71, Dp40) are expressed ubiquitously [88-90]. Some isoforms also exhibit different splicing patterns (Figure 4).

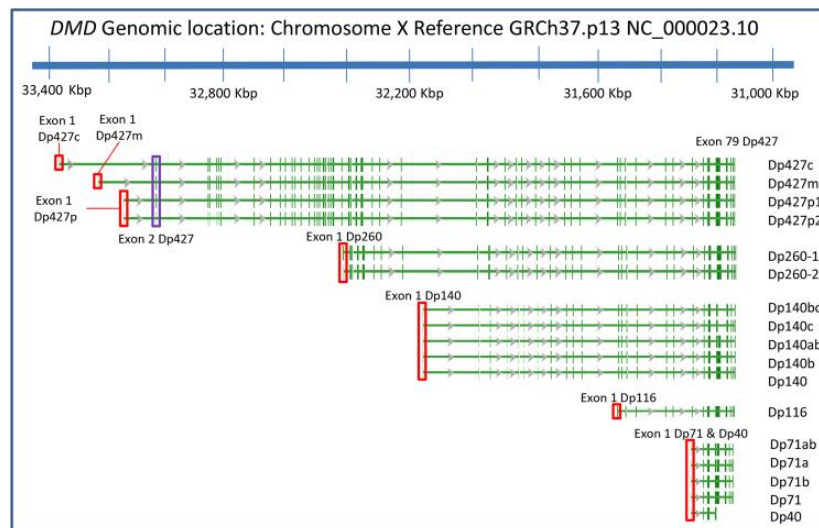


**Figure 4: Overview of human dystrophin isoforms [32]. (Published under Creative Commons Attribution 4.0 International License – CC BY 4.0.)**

Diagnosis of DMD and BMD is carried out using clinical features, laboratory parameters as elevated levels serum creatine kinase, and a molecular genetic testing of the patient. Conducting a muscle biopsy with immunohistological staining or western blotting as an invasive

diagnostic measure to prove absence of dystrophin is not recommended anymore as first-step diagnostics by national guidelines, e. g. by the German Society of Neurology (DGN). It is only required when no genetic mutation could be found through multiplex ligation-dependent probe amplification (MLPA) or next generation sequencing (NGS). A genetic testing should also be offered to female relatives in order to assess their carrier status [12, 19].

In 2015 Bladen et al. conducted a large analysis of the TREAT-NMD DMD Global Database with more than 7'000 DMD patients that showed 80 % of DMD patients featured a large mutation in the *DMD* gene. These are deletions of one or more exons in 86 % and gene duplications in 14 % of cases. Smaller mutations, such as single nucleotide variants, small deletions or insertions or splice-site variants represent 20 % of cases. Most of them (52 %) were point mutations, comprised of nonsense (96 %) or missense mutations (4 %). Other small mutations include small deletions (25 %), small insertions (9 %), splice-site mutations (14 %) and mid-intronic mutations (0.3 %). BMD features a different distribution of mutations than DMD, e. g. less nonsense mutations (3 % vs 19 %), more splice-site mutations (9 % vs 5 %) and large deletions (67 % vs 60 %), as found by Takeshima et al. in Japanese patients. There are two hot spots for mutations in humans in the regions of exon 2 to 20 and exon 45 to 55. One third of mutations in the *DMD* gene are *de novo*. [14, 91-94].

According to the reading frame hypothesis, genotype-phenotype correlations are dependent on the integrity of mRNA reading frame. DMD is caused by out-of-frame mutations that lead to production of an unstable, dysfunctional dystrophin protein which is more susceptible to degradation, or none at all. On the other hand, in-frame mutations causative for BMD result in a shortened but largely functional dystrophin protein. In BMD, the phenotype is linked to the structure of translated dystrophin protein. This rule has been found to be accurate in more than 90 % of cases, although exceptions in BMD seem to be higher. Generally, exceptions of the rule are possible, e. g. DMD patients with in-frame mutations or BMD patients with out-of-frame mutations. It is believed that disruption of critical sites or splicing patterns are causative [92, 95-98].

DMD is a lethal disease with currently no cure available. For proper care and family planning an exact diagnosis with molecular genetic testing is crucial [99]. Supportive care carried out by a multiprofessional team with regular fixed visits, targeting the symptoms of DMD, leads to an increased life span, prolongation of ambulation, decreasing contractures and scoliosis and increasing the ability to participate in life and life quality [19].

Recent DMD care considerations state that physical therapy or orthotic interventions are to be conducted to counteract the risks of progressive contractures and deformities and represent one of the mainstays of supportive care. Patients with DMD should participate in regular

submaximal activity, e. g. swimming or cycling, but avoid high-energy exercise. All necessary procedures or equipment, e. g. electric wheelchairs, aim at the patient retaining participation in all areas of life [19].

Glucocorticoid treatment with prednisone or deflazacort results in an improvement of strength, timed motor function, pulmonary function and delays the onset of cardiomyopathy. Additionally, it was shown that it reduces the need of scoliosis surgery and improves survival [100, 101]. Glucocorticoids defer loss of ambulation and delay disease progression [102]. Patients show side effects like growth alterations leading to short stature, increase in body mass index (BMI), hirsutism, cushingoid appearance and delayed puberty [103-105]. In addition, rapid cessation of glucocorticoid therapy bears the risk of adrenal insufficiency. New anti-inflammatory drugs called vamorolone and edasalonexent are currently subject to further investigation [106, 107]. Another supplement with potential for increased muscle strength is creatine monohydrate, which showed moderate benefits in clinical studies [108-110].

Detection of growth impairment or of delayed puberty, especially in cases of glucocorticoid treatment, should result in additional medical care by an endocrine specialist. In addition, frequent evaluation by a dietician is recommended to minimize the risk of malnutrition, obesity or underweight, depending on age and glucocorticoid therapy. In case of further symptoms, e. g. dysphagia, gastro-esophageal reflux disease or gastrointestinal dysmotility, a speech-language pathologist or gastroenterologist should be consulted. Additionally, due to high incidence of osteoporosis and resulting higher rates of fractures among DMD patients, adequate osteoporosis management has to be initiated and sufficient intake of calcium and vitamin D must be ensured [19].

Respiratory care includes regular assessment of parameters for lung function. In case of weight-gain or symptoms of sleep-disorders, a polysomnography with capnography should be carried out. Depending on the stage of disease, assisted coughing, nocturnally assisted ventilation, either non-invasively or via tracheostomy, and, with proceeding disease, daytime ventilation improve survival. Additionally, progressive scoliosis impairing respiratory function can require surgical correction to prevent further worsening. Surgery in DMD patients bears higher risks due to higher incidence of rhabdomyolysis and hypercalcemia as reactions to the muscle relaxant succinylcholine or inhalative anesthetics. Furthermore, immunizations against pneumococcus and influenza should be carried out to prevent life threatening acute respiratory illnesses [111-113].

A leading cause for death of DMD is cardiomyopathy [27]. Regular assessment of cardiac function by electrocardiogram and non-invasive imaging should begin at the time of diagnosis

of DMD and is to be intensified after onset of cardiac symptoms, including cardiac MRI. Cardiac therapy targets the possible effects of heart failure, arrhythmias and thromboembolism. Initiation of treatment with inhibitors of ACE is recommended by the age of ten for all DMD patients. Left ventricular assist devices, implantable cardioverter defibrillators and heart transplantations can be considered, depending on the individual's case [111].

As DMD patients have a higher incidence of mental impairment and psychiatric conditions, adequate psychological and educational support are necessary [114].

### DMD therapies

In recent years, novel therapies have been introduced, which targeted patients with specific mutations. Most of them aim at restoration of dystrophin expression. In mouse studies and human patients higher expression ratios of dystrophin tend to result in a more favorable phenotype [115, 116].

One approach is the re-establishment of mRNA read-through. Ataluren (PTC124) selectively induces ribosomal read-through of premature but not terminal stop codons. These occur in 10-15 % of patients. Application of the drug in human and mdx mice myoblasts resulted in production of full-length functional dystrophin [117, 118]. Studies proved the safety and non-toxicity of the drug, with the main side effect of vomiting, but they showed only marginal benefits for clinical improvement. In 2014 Ataluren, called Translarna, received conditional approval in the European Union for treatment of DMD patients aged two years or older who are able to walk and carry a nonsense mutation. Effectiveness of the drug has yet to be proven in clinical studies [119-121].

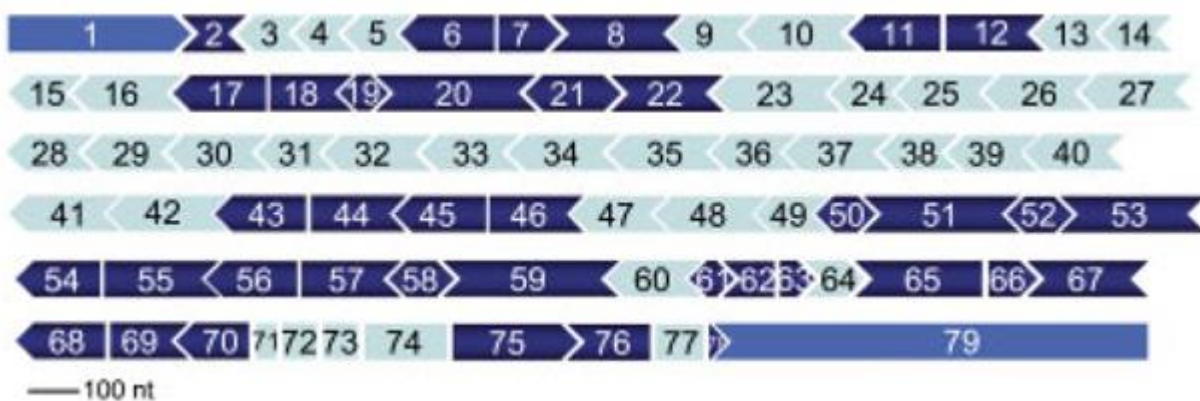


**Figure 5: Overview of exons coding for Dp427m. The reading frame is restored, when exons flanking the deletion have congruent ends, e. g. skipping of exon 51 and a deletion of exon 52 leads to a restored reading frame between exons 50 and 53 [122]. (Reprint permission granted from copyright holder).**

Another therapeutic approach is based on exon-skipping on pre-messenger RNA or DNA level and therefore restoring the dystrophin transcript. The fundamental principle of exon-skipping is

restoration of the reading frame and subsequent production of a shorter, but functional protein by excluding certain parts of the transcript. In pre-mRNA antisense oligonucleotides (AON), chemically modified DNA or RNA analogues used as steric blockers, bind to exon-internal sequences and manipulate the splicing site to receive an in-frame transcript to produce a Becker-like dystrophin [123, 124]. In theory, antisense-mediated exon skipping, although being mutation-specific, could be applicable in 83 % of all DMD patients and exon 51 skipping in particular represents a therapeutic option for up to 13 % of all patients. Even multi-exon skipping would be possible, although the challenges of low efficacy and possible high toxicity due to use of several drugs need to be tackled [122, 124].

In animal models and clinical trials exon-skipping has been used to restore local dystrophin expression, although its effects last only temporarily and hence regular injections must be carried out [125-128]. Intravenous or subcutaneous injections are necessary for systemic application, leading to limited efficacy of injections due to liver uptake and clearance by the kidneys [122, 128]. Different classes of AONs and chemical modifications have been tested *in vitro* and *in vivo* in animal models to overcome the high-first pass effect, toxicity issues and to lead to a more efficient delivery to skeletal and cardiac muscle, with some drugs moving on to clinical trials [129, 130]. Classes include 2'-O-methyl-RNA with phosphorothioate backbone (2OMePS), phosphorodiamidate morpholino oligomers (PMO) and cell-penetrating peptide-conjugated PMO (PPMO), which exhibit a better delivery to the cardiac muscle, but also a more severe panel of adverse effects in animal models, e. g. tubular degeneration of kidneys in monkeys [124, 131].

Approval of exon-skipping drugs for use in human medicine has been full of challenges. In 2016 approval of drisapersen, a drug designed for exon 51 skipping, was rejected by the U.S. Food and Drug Administration (FDA) after failing to show effectiveness in clinical trials and raising concerns about safety as adverse effects like renal toxicity, injection site reaction and thrombocytopenia occurred [132, 133]. By now, two drugs using the exon-skipping approach are in clinical use. One of them is called Eteplirsen, a PMO, able to induce exon 51 skipping and restore the reading frame in pre-mRNA. In 2016 an accelerated approval was issued by the FDA for this drug [134]. The approval has been criticized because of design and results of the conducted studies which showed increased levels of dystrophin expression, but did not prove a clear clinical improvement by drug application [135-137]. The European Medicines Agency (EMA) refused approval in 2018 [138]. Two other drugs, Golodirsen and Casimersen, have already received accelerated approval by the FDA to be used in DMD patients with mutations amenable to exon 53 or exon 45 skipping respectively, although the clinical benefits are still being investigated [139, 140].

Engineered endonucleases pose a new tool for repair of the *DMD* gene on DNA-level, using their ability to induce DNA double-strand breaks and stimulating homologous recombination or non-homologous end-joining which lead to micro-deletions and -insertions. With the right design a repair of the reading frame of the *DMD* gene is possible and an increase in dystrophin expression is visible. Techniques used include the application of zinc finger nucleases, meganucleases, transcription activator-like effector nucleases (TALEN) or more recently using the CRISPR/CAS9-system (clustered regularly interspaced short palindromic repeats with CRISPR-associated protein 9) delivered by adeno-associated virus vectors (AAV). These studies were carried out using *in vitro* and *in vivo* animal models and human cells, e. g. myogenic and stem cells. Especially the latter technique has been widely used and has shown recovery of dystrophin expression or even improvement in DMD phenotype in different animals, including dystrophin-deficient mice, dogs and pigs [141-151].

Another therapeutic approach is gene replacement. The large size of the *DMD* gene complicates induction of the full *DMD* sequence. Non-viral direct plasmid injection of full-length *DMD* gene in animal models and a phase I clinical trial have shown only limited and transient success [152-155]. Viruses with large packaging capacities, like an enhanced adenovirus or herpes simplex virus, were able to deliver full-length *DMD* cDNA *in vivo* and *in vitro* in mice, but safety concerns regarding toxicity and immune response have been limiting their application [156-158]. Before application of adenoviral vectors in a patient, immunization against viral capsid proteins and transgene products would have to be excluded and repetitive procedure would therefore not be possible, as its injection might lead to an immune response in larger animals [159]. Retroviral transduction of cells is restricted to mitotic cells and therefore not practical for use in postmitotic myotubes [160]. Currently AAV is the most common type of vector, although it features a limited packaging capacity of 5 kb, which is not sufficient for the *DMD* coding sequence with a size of 14 kb. Tri-AAV vectors were successfully used to transduce and express full length *DMD* cDNA in mdx and mdx<sup>4cv</sup> mice by being packaged in three parts and recombined in the host [161, 162]. Additionally, AAV have been used to improve exon-skipping by delivering U7 small nuclear RNA (snRNA) with antisense sequence to target exon splicing enhancers *in vitro* and *in vivo* in mice and dogs, which resulted in increased dystrophin expression [163-165]. A new approach includes the use of mini- or microdystrophins, shortened but functional forms of the protein, whose genetic sequence is transduced using AAV. Human patients have been reported to feature large multiexon deletions and to exhibit a benign phenotype, implying a possible therapeutic use of drastically shortened versions of DMD [166]. Minidystrophins were shown to increase dystrophin expression in mice [167, 168]. Extensive research and studies have enabled AAV-mediated gene therapy to be further assayed for use in humans. A phase I trial ended in 2012, showed the potential of designed AAV vectors to

reduce immune responses [169]. Current clinical trials with limited numbers of participants include a phase I/IIa clinical trial for rAAVrh74.MHCK7-micro-dystrophin, a phase Ib trial for PF-06939926, being rAAV9 with microdystrophin, and a phase I/IIa trial for AAV9 U7snRNA for treatment of exon 2 duplications [170-172]. Nevertheless, the challenge of high prevalence of preexisting antibodies against different serotypes of AAV remains a limiting factor for therapeutic application [173].

Idebenone is a synthetic short-chain benzoquinone, acting as an antioxidant and improving mitochondrial function and restoring ATP-production. Clinical trials proved a significant reduction in decline of respiratory function and a smaller number of bronchopulmonary complications and hospitalization due to respiratory events [174, 175].

Other therapeutic approaches currently under investigation, include upregulation of utrophin as compensatory mechanism. Recent AAV-mediated gene therapy of mdx mice targeting the GALGT2 gene led to an increased glycosylation of  $\alpha$ -dystroglycan and utrophin expression which resulted in retained heart function [78, 176]. Inhibition of myostatin, a transforming growth factor-beta superfamily member functioning as a negative regulator of muscle growth, results in increased muscle growth and regeneration in mice. Several clinical trials testing antibodies against myostatin have taken place but no clinical benefits have been proven [177-180]. Furthermore, isolation and transplanting skeletal muscle progenitor cells have shown to partially restore dystrophin expression in mdx mice and humans *in vivo*, but required immunosuppression [181-184]. Additionally, there are other approaches for DMD therapy and constantly new ones are presented, e. g. histone deacetylase inhibitors, antibodies against connective tissue growth factor and use of allogenic cardiosphere-derived cells (reviewed in [185]).

As of November 2021, clinicaltrials.gov of the U.S. National Library of Medicine reports more than 83 active or planned clinical trials for Duchenne muscular dystrophy, obviously not including preclinical trials or studies conducted with animal models [186].

### **IV.3. Animal models of Duchenne muscular dystrophy**

Since the first description of Duchenne muscular dystrophy in 1867 several spontaneous occurring or engineered dystrophin-deficient animal models have been developed in order to study the disease and pose the key to understanding the potential efficacy of different DMD therapies. [187]. Nearly 60 different animal models based on mammalian and non-mammalian species have been established by now [188].

## Small animal models

Murine models are the most widely used form of animal models. Many different variants of mice have been bred to mirror the human condition as exactly as possible. The first murine animal model (*Mus musculus*) with X-chromosome-linked muscular dystrophy was discovered in 1984 after detection of elevated plasma levels of muscle creatine kinase [189]. It features a lack of dystrophin [11] and reduced dystrophin RNA levels [190]. Further analysis showed that a single base substitution (c.3185C>T) in exon 23 of the *DMD* gene is responsible for changing a glutamine codon (CAA) into a stop codon (TAA) and leading to a truncated dystrophin protein by inducing premature translation termination at 27 % length of the polypeptide [191]. Being the most widely used animal model due to its genetic and biochemical features, the benign phenotype of the mdx mouse limits its translational potential for clinical trials in DMD patients [192]. Mdx mice do show a reduced lifespan [193]. The mdx mouse model does not show the typical histological hallmarks of DMD, especially the lack of detectable weakness nor progressive degeneration of limb muscles of younger mdx mice. But typical changes of a progressive DMD are shown to be present in the diaphragm [194, 195]. Older mice are found to show a more progressive muscular weakness, loss of myofibers, and replacement with connective tissue and therefore some similarity to the human phenotype [196].

Mdx mice have been crossbred onto different backgrounds in order to modify disease severity, for example DBA/2J mouse with a more severe phenotype [197] and a series of mice (mdx2cv, mdx3cv, mdx4cv, mdx5cv) with chemically induced mutations and therefore expression of different dystrophin isoforms [198]. Other noteworthy dystrophin-deficient mice include the mdx52 mouse with a targeted disruption of exon 52 [199], the *Dmd*-null mice with a deletion of the entire dystrophin gene [200], a model with knock-in of the complete human *DMD* gene in chromosome 5 of the mouse genome [201] or other transgenic mice. But still those mice express a phenotype with limited comparability to the human one [187, 202]. Alternative approaches include the creation of immune-deficient dystrophin-deficient mouse lines in order to eliminate the effects of the host's immune system on the progression of the disease [188].

Other mouse models were developed to mimic the human DMD phenotype by conducting a double knock-out of dystrophin and other proteins associated with the dystrophin complex or muscle cell repair, most prominently utrophin [79] or alpha 7 integrin [203, 204], which have been found to be upregulated in dystrophin-deficient mice and are believed to improve the disease's appearance. These mouse lines were established in order to worsen and therefore assimilate the murine phenotype to the human one by eliminating the potentially confounding effects of genes, which are upregulated in case of dystrophin-deficiency. Although most of the double knock-out models feature a more severe phenotype and show an accelerated disease

progression, transfer of findings is limited as DMD patients don't actually lack a second gene [188].

In general the translation of findings in mice suffers from the problem of scale, as humans are up to 3'000 times larger than mice, and feature different growth and regeneration patterns apart from further physiological differences [205].

An extensive list of established mouse models for studying the Duchenne muscular dystrophy is stated below (Figure 6).

<b>Dystrophin-deficient mice</b>	
Mdx	Exon 23 point mutation, on C57BL/10 background, also on other backgrounds as Albino Mdx, Mdx/BALB/c, Mdx/BL6, Mdx/C3H, Mdx/DBA2 [197], Mdx/FVB
Mdx2cv, mdx3cv, mdx4cv, mdx5cv	Chemically induced intron 42 point mutation, intron 65 point mutation, exon 53 mutation or exon 10 point mutation
CRKHR1	Unsequenced, dystrophin deficiency confirmed by immunofluorescence staining
Mdx52	Exon 52 deletion
Mdx $\beta$ geo	Insertion of the $\beta$ -geo gene trap cassette in intron 63
DMD-null	Entire DMD gene deletion
Dp71-null	Selective elimination of Dp71 by insertion of a $\beta$ -geo cassette in intron 62, disruption of Dp71 unique exon 1
Dup2	Exon 2 duplication
<b>Immune deficient mdx mice</b>	
NSG-mdx4cv	Prkdc and IL2rg double deficient on the mdx4cv background, B cell, T cell and NK cell, innate immunity and multiple cytokine signaling pathway deficient
Rag2 <sup>-</sup> Il2rb <sup>-</sup> Dmd <sup>-</sup>	Rag2 and IL2rb double deficient on the mdx $\beta$ geo background, B cell, T cell, NK cell and multiple cytokine signaling pathway deficient with no revertant fiber
Scid mdx	DNA-dependent protein kinase catalytic subunit deficient (prkdc) on the mdx background, B cell and T cell deficient
W41 mdx	C-kit receptor and haematopoietic deficient
<b>Phenotypic dko mice</b>	
$\alpha$ 7/dystrophin dko or mdx/ $\alpha$ 7 <sup>-/-</sup>	$\alpha$ 7-Integrin/ dystrophin double deficient
Adbn <sup>-/-</sup> mdx	$\alpha$ -Dystrobrevin/ dystrophin double deficient
Cmah-mdx	Cmah/dystrophin double deficient
d-Dko	$\delta$ -Sarcoglycan/ dystrophin double deficient
Desmin <sup>-/-</sup> mdx4cv	Desmin/dystrophin double deficient
Dmd <sup>mdx</sup> /Large <sup>myd</sup>	like-glycosyltransferase (LARGE)/dystrophin double deficient
DMD-null; Adam8 <sup>-/-</sup>	ADAM8 deficient and entire DMD gene deletion
Dysferlin/dystrophin dko	Dysferin/dystrophin double deficient
IL-10 <sup>-/-</sup> /mdx	Interleukin-10/dystrophin double deficient
mdx/mTR	Telomerase RNA/dystrophin double deficient
mdx:MyoD <sup>-/-</sup>	MyoD/dystrophin double deficient
mdx:utrophin <sup>-/-</sup> or mdx/utrophin <sup>-/-</sup>	Utrophin/dystrophin double deficient
PAI-1 <sup>-/-</sup> mdx	Plasminogen activator inhibitor-1 (PAI-1)/dystrophin double deficient
<b>Dko mice with phenotype similar to mdx</b>	
msDKO	Cytosolic $\gamma$ -actin/dystrophin double deficient
iNOS-null mdx or iNOS/Dys DKO	iNOS/dystrophin double deficient
PVKO-mdx	Parvalbumin/dystrophin double deficient
<b>Dko mice with reduced disease</b>	
clAP1 <sup>-/-</sup> ;mdx	Cellular inhibitor of apoptosis 1 (clAP1)/ dystrophin double deficient
Fib <sup>-/-</sup> mdx	Fibrinogen/dystrophin double deficient
Finp1 <sup>-/-</sup> mdx4CV	Folliculin interacting protein-1 (Fnip1) deficient mice on the mdx4cv background.
Mdx-casp	Caspase-12/dystrophin double deficient

mdx/Mkp5 <sup>-/-</sup>	Mitogen-activated protein kinases phosphatase-5 (Mkp5)/dystrophin double deficient
mdx/myd88 <sup>-/-</sup>	Myeloid differentiation primary response protein 88 (myd88)/dystrophin double deficient
mdx/q <sup>-/-</sup>	Protein kinase C q (PKCq)/dystrophin double deficient
mdx/sgk1 <sup>-/-</sup>	Serum-and glucocorticoid-induced kinase 1 (sgk1) and dystrophin double deficient
mdx-Xist <sup>Δhs</sup>	Xist/dystrophin double knockout
Mstn <sup>-/-</sup> /mdx	Myostatin/dystrophin double deficient
OPN DMM	Osteopontin (OPN)/dystrophin double deficient
<b>Transgenic mdx mice</b>	
Full-length dystrophin transgenic mdx	Transgenic over-expression of full-length dystrophin in the mdx background
Dp71 transgenic mdx	Transgenic over-expression of Dp71 in the mdx background
Dp116 transgenic mdx4cv	Transgenic over-expression of Dp116 in the mdx4cv background
Dp116:mdx:utrophin <sup>-/-</sup>	Transgenic over-expression of Dp116 in the utrophin/dystrophin dko background
Dp260 transgenic mdx	Transgenic over-expression of Dp260 in the mdx background
Dp260 in mdx/utrn <sup>-/-</sup>	Transgenic over-expression of Dp260 in the utrophin/dystrophin dko background
Δ17-48 transgenic mdx	Transgenic over-expression of the naturally occurring Δ17-48 mini-dystrophin gene in the mdx background
ΔH2-R19 transgenic mdx	Transgenic over-expression of the synthetic ΔH2-R19 mini-dystrophin gene in the mdx background
Cardiac-specific ΔH2-R19 transgenic mdx	Transgenic over-expression of the synthetic ΔH2-R19 mini-dystrophin gene in the heart of mdx mice
ΔH2-R15 transgenic mdx	Transgenic over-expression of the synthetic ΔH2-R15 mini-dystrophin gene in the mdx background
Micro-dystrophin transgenic	Transgenic over-expression of various synthetic micro-dystrophin genes in the mdx background
Fiona	Transgenic over-expression of full-length utrophin in the mdx background
Laminin α1 transgenic mdx	Transgenic over-expression of the laminin α1 chain in the mdx background

**Figure 6: Overview of important DMD mouse models, modified after [188]**

Two other DMD rodent animal models using rats have been designed using the CRISPR/Cas9-system targeting *DMD* exons 3 and 16 or TALE nucleases targeting *DMD* exon 23. This creates a premature stop codon and results in a loss of dystrophin expression and an exhibition of muscle degeneration, although with varying phenotypes between the two rat models [206, 207].

Recently rabbits have been used to develop a new animal model for DMD by co-injecting Cas9 mRNA and sgRNA targeting exon 51 into rabbit zygotes. DMD KO rabbits exhibit a strong phenotype including muscular dystrophy and cardiomyopathy, but a high incidence of premature death [208].

Non-mammalian animal models include the nematode worm *Caenorhabditis elegans* [209, 210] and the *Drosophila* fly [211]. In addition, several dystrophin-deficient zebrafish animal models have been developed to make use of the optical clarity of zebrafish embryos and larvae to visualize dynamic molecular processes and screen small-molecule drugs *in vivo*. The models are based on different types of genetic mutations [212]. Non-mammalian animals have limitations in their comparability to humans [202].

## Large animal models

As DMD mutations in dogs occur spontaneously, dystrophin-deficient muscular dystrophies have been reported in several breeds. Some of them have served as basis for DMD animal models. The most prominent one is the Golden Retriever muscular dystrophy dog model (GRMD) that contains the mutation of a single base change in the 3' consensus splice site of intron 6, leading to skipping of exon 7 and to a premature stop codon in exon 8 [213, 214]. Through crossbreeding a beagle-based canine X-linked muscular dystrophy model (CXMDj) has been established [215]. Other dystrophin-deficient dog breeds currently held in colonies are the Cavalier King Charles Spaniel (CKCS) with an intron 50 hot spot mutation [216], the Welsh Corgi with a long interspersed repetitive element-1 (LINE-1) insertion of intron 13, which led to introduction of new exon containing a stop codon [217] and the Labrador retriever dystrophic dog. These large animal models share a phenotype far more similar to human DMD than mouse models. However, variable inter-individually different dystrophic phenotypes with the same genetic mutation and even in the same litter make it difficult to ascertain functional endpoints in studies [187, 202, 218, 219]. As possible reasons epigenetic effects and modifier genes are discussed [220, 221]. At the same time, the GRMD suffers from the contradiction of premature death and, if the animal survives the first year, a relatively long period of ambulation ([219] reviewed in [205]). Reports of dystrophin-deficient dogs by breeds are listed in the table below (Figure 7).

Alaskan malamute dystrophic dog	Confirmed dystrophin deficiency, but unknown mutation
Cavalier King Charles Spaniel (CKCS-MD)	Spontaneous intron 50 point mutation resulting in exon 50 exclusion from the mRNA
Cocker spaniel dystrophic dog	Deletion of four nucleotides in exon 65
CXMDj	GRMD crossed to beagle background
GLRMD	Hybrid of GRMD and Labrador Retriever
Grand Basset Griffon Vendéen dystrophic dog	Confirmed dystrophin deficiency, but unknown mutation
Golden Retriever (GRMD)	Intron 6 point mutation resulting in the exclusion of exon 7 from the mRNA
German short haired pointer (GSHP MD)	Spontaneous whole gene deletion
Hybrid cDMD dogs with mixed genetic background and multiple mutations	Generated by crossing different cDMD breeds
Japanese spitz dystrophic dog	Case report of inversion between intron 19 of dystrophin gene and retinitis pigmentosa GTPase regulator gene (RPGN)
Labrador Retriever BMD dog	Unknown mutation, case report with low-level uniform expression of a ~135 kDa dystrophin protein and mild phenotype.
Labrador Retriever dystrophic dog	Confirmed dystrophin deficiency, but unknown mutation
Labrador Retriever dystrophic dog	Spontaneous repetitive element insertion in intron 19
Lurcher dystrophic dog	Confirmed dystrophin deficiency, but unknown mutation
Miniature schnauzer dystrophic dog	
Norfolk Terrier dystrophy	
Old English sheepdog dystrophic dog	
Rat terrier dystrophic dog	
Rottweiler dystrophic dog	Nonsense point mutation in exon 58
Tibetan terrier dystrophic dog	Exons 8-29 deletion
Weimaraner dystrophic dog	Confirmed dystrophin deficiency, but unknown mutation

Welsh Corgi MD	Spontaneous LINE-1 insertion in intron 13
----------------	---

**Figure 7: Reports of dystrophin-deficient dogs, modified after [188]**

Spontaneous mutations have led to the generation of feline muscular dystrophy models. A hypertrophic feline muscular dystrophy model (HFMD) has been developed in order to study the disease in cats. The afflicted animals suffer, apart from cardiac symptoms, from pronounced appendicular and axial muscular hypertrophy with involvement of diaphragm and tongue, which complicates handling of these animals. In 1994 the causative mutation was identified as a deletion of Dp427 promoter and exon 1 in dystrophin muscle and Purkinje cell isoforms. Additionally, HFMD cats exhibit a lethal peracute rhabdomyolysis with severe hypercalcemia during inhalative anesthesia with isoflurane. [187, 222-225]. Cats with a non-hypertrophic dystrophy have been reported, too [226].

Recently a rhesus monkeys DMD model (*Macaca mulatta*) was created using the CRISPR/Cas9-system targeting *DMD* exons 4 and 46. It resulted in mosaic mutation and a variable genotype and phenotype. In some monkeys a partial depletion of dystrophin and early muscle degeneration were reported [227].

### **Porcine animal models**

In 2012 an exon 41 missense mutation, causative for BMD, was found in slaughter-weight pigs leading to a loss of dystrophin of up to 50 % compared to healthy littermates. The pigs showed only minimal dystrophic phenotype but were susceptible to stress-induced sudden death [228]. Chances of detecting genetic disorders in pigs are especially high in the meat industry, where a case of fatty muscular dystrophy occurred. The pig showed no abnormalities during lifetime, but a post-mortem dissection identified unusually pale, discolored skeletal muscle with prominent fat infiltrations. Dystrophin staining was considerably reduced and showed a similar pattern like human BMD. Genetic testing was not carried out [229].

Finally, in 2013 a new large animal model for the Duchenne muscular dystrophy was developed based on the domestic pig (*Sus scrofa*). Pigs have several advantages over other animals as models for human diseases. Pigs have been domesticated animals for over 10.500 years and lived closely alongside men ever since [230]. They share a common ancestor with humans and therefore, the physiological and genetic structure of the porcine and human body are similar. Both being mammals, physiological and pathophysiological mechanisms, like the human cardiovascular, immune, respiratory, skeletal muscle or metabolic system, can be mirrored excellently in pigs [231-233]. Pigs are highly reproductive with an early onset of sexual maturity of five to eight months, maintain all season breeding, a short generation interval of 12-18 months and multiple offspring per litter, making them easy to breed, especially as breeding conditions have been optimized over generations [234, 235]. In 2012 a full sequence analysis of a female

Duroc pig was completed [209]. Concerning DMD, the high sequence homology of the dystrophin gene of 94 % promised further benefits [236]. Genetic engineering of large animal models has proven to be difficult in the past, but new genetic techniques simplify the creation of new large animal models, including the pig [233, 234].

The DMD pig based on the German landrace pig was at first developed in 2013 by the working groups of Maggie Walter and Eckhard Wolf at LMU, Munich, Germany, using gene targeting of exon 52 in male pig cells and generating offspring by nuclear transfer. Klymiuk et al. used a bacterial artificial chromosome (BAC) carrying the relevant part of the porcine DMD and replaced the region corresponding to human *DMD* exon 52, one of the most common mutations on humans, by recombineering with a neomycin resistance cassette, which led to a frame shift [146, 237].

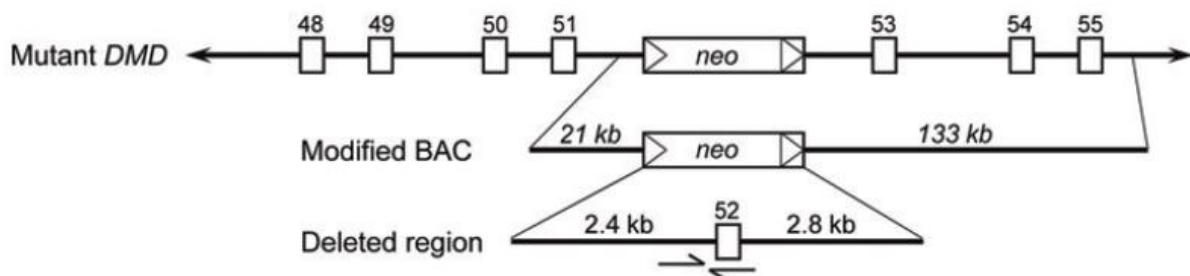


**Figure 8: Schematic picture of replacement of exon 52 by a neomycin cassette [237]. (Reprint permission granted from copyright holder.)**

Klymiuk et al. continued to transfect these modified BACs into primary kidney cells from a 3-month-old piglet. After positive selection using G418 as selective agent, the clones were screened using quantitative polymerase chain reaction. Successfully targeted cell clones were used for nuclear transfer (SCNT). Cloned embryos were transferred into recipient gilts in order to establish pregnancy. Genotyping by polymerase chain reaction proved the absence of *DMD* exon 52 in the piglets. RNA-sequencing of the *DMD* transcript profile proved missing exon 52 sequences and showed the introduction of two stop codons in exon 53 and four stop codons in exon 54 by the +1-frame shift mutation [237].

All porcine cells used in our experiments for this doctoral thesis were derived from dystrophin-deficient individuals or their wild-type siblings held in colony at Oberschleißheim, Germany. The DMD pigs exhibited absence of dystrophin in skeletal muscles with reduced levels of the dystrophin-associated proteins  $\alpha$ -sarcoglycan and  $\beta$ -dystroglycan, mirroring the human condition.

The piglets showed increased serum creatine kinase levels up to ten-fold of wild type values and progressive dystrophic changes in skeletal muscles. As described in Klymiuk et al. they suffered from a strikingly impaired mobility, muscle weakness and a maximum life span of three months due to respiratory impairment. Some pigs died shortly after birth, which is uncommon in human DMD babies. The pigs exhibited an accelerated development of muscular dystrophy compared to human patients. Muscular weakness was depicted by the failure of DMD piglets in locomotion studies, i. e. to climb a platform of 25 cm height or disturbances in the pig's gait patterns. There is a negative correlation between birth weight and life expectancy and a large variation in birth weights in positive correlation with phenotype severity, which may be caused by the cloning method, most likely due to epigenetic dysregulation [237-239].

Histopathological analyses showed typical hallmarks of DMD including excessive fibre size variations, rounded hypertrophic and branching fibres, central nuclei and intestinal fibrosis and mononuclear inflammatory cell infiltration which intensified and progressed with the age of the pigs. Scattered clusters of segmentally necrotic fibres, as well as regenerating fibres were visible. Cardiac muscle analysis in the first litter showed no strong signs of involvement. Furthermore, with increased age distribution of muscle fibre diameters shifted from a normal pattern, visible in two-day-old DMD piglets and their age-matched wild type controls, to a biphasic, broadened distribution, which is a typical sign for progressive DMD. The detected changes were progressive and more severe in three-month-old pigs than two-day-old ones. An upregulation of utrophin was detected in two-day-old-DMD-piglets compared with age-matched wild type controls, although in immunohistochemistry there was no sarcolemmal utrophin expression and only a strong staining associated with blood vessels, presumably responsible for the increase in protein. The utrophin upregulation shows heavy progress in three-month-old-DMD-pigs with positive sarcolemmal utrophin staining [233, 237].

Transcriptome analyses of biceps femoris muscle were performed. The changes detected in three-month-old pigs were comparable to the alterations in human DMD showing degeneration, regeneration, inflammation, fibrosis and impaired metabolic activity. In contrast the changes in two-day-old piglets were comparable to a mechanical stress signature after acute exercise muscle injury [237].

Klymiuk et al. also conducted an extensive muscle proteome analysis which showed an increased progression of pathological changes in DMD muscles over time. Already at two days of age signs of early derangement of the DMD muscle were detectable. At the age of three months an increase in proteins connected to muscle repair and a decrease in several respiratory chain proteins, indicating disturbances in aerobic energy production, and functional muscle tissue was observed in comparison to age matched wild type controls [233].

This DMD pig reflects pathological hallmarks and clinical severity of human DMD better than the widely used mdx mouse. Due to carrying the most frequent human mutation of the DMD gene, it is advantageous over the GRMD as a large animal model for DMD. However, the DMD pig exhibits a markedly accelerated progression of DMD compared to humans. Possible reasons to be further investigated are accelerated post-natal growth, lack of sarcolemmal utrophin upregulation or genetic downregulation leading to both reduced inflammation and regeneration [233].

Due to reduced life expectancy, the DMD pig hardly reaches reproductive maturity and successful mating. It is a typical symptom in animal models for X-linked genetic disorders like DMD that male animals show impaired growth, higher neonatal lethality and a reproductive disability, hindering a normal reproduction of these models [240]. As described above, nuclear transfer technology leads to a great variability in size and phenotype severity. An approach using natural mating, *in vitro* fertilization or artificial insemination is preferred. In recent studies DMD boars, chimeric in somatic and germ cells, have been created and were able to reach sexual maturity but only displayed a significantly weaker phenotype. The generated sperm was successfully used to create offspring through *in vitro* fertilization [240]. Klymiuk et al. also generated female DMD carrier pigs using SCNT. Mating of female carrier with wild type boar resulted in male DMD piglets according to the Mendelian ratio [233].

In 2014 an application for a U.S. patent for a transgenic, large non-human animal model of DMD, BMD and DMD-associated dilated cardiomyopathy was filed by Rogers and Swart. Excision of exon 52 of a Yucatan mini pig using Cre-Lox recombination and replacement with a Neo<sup>R</sup> cassette was described, as well as using gene targeting and somatic cell nuclear transfer (SCNT) with subsequent breeding in order to establish a colony of live animals with mutation [241]. The application was granted in 2019. As of November 2021, no further reports about a DMD or BMD pig were published by the applicants, although porcine models for other diseases have been developed, i.e. a cystic fibrosis pig [242], a neurofibromatosis type 1 pig [243] or the ExeGen™ low density lipoprotein receptor mini swine for studying diet-related atherosclerosis [244]. These are further proof of the versatility and usefulness of the pig as a translational animal model.

In 2016 another DMD pig with a deletion of exon 27 in a Chinese Diannan miniature pig was created by Yu et al. through co-injecting zygotes using the CRISPR/Cas9 system. They reported a lower dystrophin expression in skeletal muscle, heart and intestine, despite higher relative expression levels of DMD mRNA. A lower birth weight and muscle weakness was observed in comparison to a wild-type control. The ratio of central nuclei in fibres was elevated, also supporting the induction of a DMD phenotype in the minipigs [245].

The dystrophin-deficient pig model (DMD $\Delta$ 52) of Klymiuk et al. has already proven to be a useful tool to conduct *in vivo* experiments for therapeutic approaches to treat DMD by conducting somatic gene editing. Moretti et al. injected 10 - 14 days old DMD pigs i. v. and i. m. with AAV9-Cas9-gE51, adeno-associated virus 9 carrying Cas9 and guide RNAs targeting exon 51, in order to eliminate exon 51 from the *DMD* gene. The snipping of exon 51 results in production of a shortened, partially functional dystrophin  $\Delta$ 51-52. After six weeks, an increased expression of the truncated dystrophin and colocalization with members of the DGC, i. e.  $\gamma$ -sarcoglycan and  $\beta$ -dystroglycan, was shown in skeletal muscle. The structure of the skeletal muscle was improved compared to the untreated DMD pigs and exhibited less interstitial fibrosis and decreased mononuclear cell infiltration. This led to an improvement of muscle function and mobility of the animals. The incident of severe malignant arrhythmias, a common danger in DMD, was reduced and life span prolonged [146]. This is an excellent example of the translational possibilities and therapeutic achievements by utilizing pigs as an animal model for DMD. Pigs and other animal models for DMD are necessary for evaluation of efficacy and safety of new drugs or therapeutic concepts [234].

### **IV.4. Hereditary inclusion body myopathies**

Another group of rare neuromuscular diseases is called hereditary inclusion body myopathies (hIBM), characterized by the presence of characteristic rimmed vacuoles in muscle biopsies with typical absence of inflammation and hereditary transmission of disease. They should not be confused with sporadic inclusion body myositis (sIBM), which is the most common form of acquired muscular disease in older patients [246, 247].

#### **IV.4.1. GNE myopathy**

One form of hIBM is caused by mutations in the *GNE* gene (*GNE*; OMIM 603824), located on chromosome nine [248-250]. This gene codes for a bifunctional UDP-*N*-acetylglucosamine 2-epimerase/ *N*-acetylmannosamine kinase. Its key enzymatic activities catalyze the first steps of the sialic acid biosynthesis pathway and regulate cell surface sialylation [251, 252]. Sialic acids are widely expressed as terminal carbohydrates on glycoconjugates and are important for cellular functions like cell adhesion or signal recognition [253]. The disease pathomechanism is not fully understood yet. *GNE* has been found to be expressed at normal levels and usual localizations in affected patients, suggesting impaired *GNE* function and not expression as cause of *GNE* [254]. In addition, *GNE* has been shown to be essential in embryonic development, as inactivation of *GNE* leads to early embryonic death in mice [253]. Hyposialylation of muscle glycans was a suspected pathogenetic mechanism. However, overall level of sialylation was shown to be normal, although reduced levels were found in some tissues

of GNE-deficient mice [255, 256]. NE was shown to be located in the Golgi complex and the nucleus, which indicates a possible role as a nucleocytoplasmic shuttling protein [257]. GNE is also a factor in survival-apoptosis pathways, oxidative stress, cell proliferation and gene expression [258-260]

Autosomal-recessive GNE myopathy was first described in 1981 and 1985 in Japanese and Iranian Jewish families by Nonaka et al. and Argov and Yarom. The onset of symptoms lies usually in early adulthood with distal weakness of the legs, especially with difficulties in dorsal extension of feet. Mm. tibiales anteriores are primarily affected, while the Mm. quadriceps femoris are noticeably spared. Levels of CK were normal or moderately elevated. Muscle biopsies showed rimmed vacuoles and very little evidence of inflammatory, necrotic or regenerative processes. In the course of disease upper limb and proximal legs are also affected, leading to progressive impairment. In a study conducted by Nishino et al., 18 % of included patients developed cardiac symptoms up to sudden cardiac death. Cases of combined skeletal and cardiac muscle affection have been reported. Respiratory symptoms are no typical sign of the illness. GNE myopathy does not affect facial or bulbar muscles or lead to cognitive impairment [261-267]. Homozygous patients exhibit a more severe phenotype than those with compound heterozygous mutations [268]. Disease progression varies significantly, even between siblings with the same mutation, indicating a possible role of genetic modifying factors. Studies found the average time between disease onset and loss of ambulation to be ten to twelve years [264, 269].

Initially described in Japanese and Iranian Jewish patients, several founder mutations in clusters of patients have been discovered, e. g. in p.I618T in people of Bulgarian Roma ethnicity or p.M743T in Middle Eastern populations. In certain ethnic communities, e. g. Japan or Iranian Jews, the disease is more common. Based on allele-frequencies a carrier rate of 1/203 was estimated, leading to an approximated prevalence of GNE myopathy of 6/1'000'000 or 40'000 in total, making the disease highly underdiagnosed with only 950 patients known in 2018 [265, 269-271].

Currently there is no curative therapy for GNE myopathy. Several therapeutic approaches are under investigation, targeting hyposialylation through upregulation of production or substitution of sialic acid or conducting gene editing to restore GNE function (reviewed in [265]).

#### **IV.4.2. VCP proteinopathy**

Autosomal-dominant VCP proteinopathy is a rare multisystem proteinopathy with variable penetrance caused by mutations in the valosin-containing protein (*VCP*) gene [272]. The *VCP* gene (*VCP*; OMIM 601023), located at locus 9p13.3, codes for a cytosolic AAA class of ATPase

of the endoplasmic reticulum associated degradation system. It is involved in many different cellular functions and signaling pathways, including cell cycle control, membrane fusion, ubiquitin-proteasome degradation pathway of misfolded polypeptides and autophagosome control. It is heavily dependent on binding of co-factors [272-276]. Muscular biopsies of patients with *VCP* mutations feature rimmed vacuoles and nuclear and cytoplasmic inclusion positive for ubiquitin and TAR DNA binding protein-43 (TDP-43) [277]. TDP-43 aggregation is a common pathologic finding in frontotemporal dementia and ALS [278]. Therefore a disruption of normal protein homeostasis with accumulation of ubiquitinated and aggregated protein is thought to be causative for the clinical appearance of *VCP* proteinopathy, although the pathomechanism of the disease is mainly unknown [279]. *VCP* mutations affect several types of tissues, including skeletal muscle, nerves and bones.

Patients with *VCP* mutations display a broad variation of symptoms and genotype-phenotype correlation, even intrafamilial and interfamilial with identical genetic mutations and. In general, due to the small patient population, correlations are difficult to be established [277, 280, 281]. Mutations are frequently found to be causes of a symptom cluster of dominantly inherited Inclusion Body Myopathy (91 % of patients), with Paget's disease of the bone (51 %) and early-onset frontotemporal dementia with prominent neuropsychiatric symptoms (behavioral variant (bvFD), 30 %), called IBMPFD. Only 12 % feature the full trilogy of symptoms. Onset of myopathy lies typically in adulthood at a mean age of 43 years with progressive weakness of pelvic and shoulder girdle skeletal muscles, bearing similarities to the phenotype of limb-girdle muscle dystrophy or facioscapulohumeral muscular dystrophy. The onset of Paget's disease of the bone, usually lies at 40 years. Frontotemporal dementia is often diagnosed later at a mean age of 55 years. With a mean survival time of 62 years, *VCP* patients showed a reduced life span with death by respiratory failure, cardiomyopathy or cardiac failure [277, 279, 282]. Other regular symptoms include parkinsonism (3 %), familial amyotrophic lateral sclerosis (fALS; 9 %) and single cases of Alzheimer's disease, as well as other symptoms [277]. fALS constitutes 5 % of all ALS cases [283]. 1 to 2 % of hereditary fALS are found to be caused by *VCP* gene mutations, making it a rather rare cause [284, 285]. Additionally, neurogenic changes in electromyography were found in 24 % of patients, although presenting normal nerve conduction studies [277]. Apart from symptomatic treatment, there is currently no causal therapy available.

### **IV.5. Immortalization of cell lines**

Proliferative primary cells exhibit a finite limit of cultivation [286]. After reaching the limit, a non-dividing state, called replicative senescence, is entered [287]. This leads to a lack of stable cell cultures after the first generations [288]. Immortalized cell lines provide a solution for utilizing stable, comparable conditions for scientific research. Ideally, immortalized cell lines exhibit an

unlimited proliferation capacity and retain the typical properties of the original primary cells [289]. Immortalization of cells can occur spontaneously or can be created by specifically altering the cell line using viral or genetic material.

First unlimited proliferating cell lines were obtained from spontaneously immortalized cell clones or from cancer tissue. The oldest strain, HeLa cells, is derived from epidermoid cervix cancer of a female patient called Henrietta Lacks on February 8<sup>th</sup>, 1951. They showed no senescence and no cessation of proliferation [288], with cultivation ever since. As of November 2021, more than 115'000 articles and reviews about research using HeLa cells are listed in the MEDLINE online database. Other spontaneously immortalized cells are NIH 3T3, which stem from embryonic mouse fibroblasts. Cultivation according to rigid schedule of transfer every three days and inoculation at a defined cell density led to establishment of stable, ever-proliferating cell lines [290]. A line of immortalized myogenic cells was obtained by isolation and subsequent passaging of myoblast colonies derived from the thigh muscle of two-month-old mice. The so called C2C12 cells retain myogenic properties and fusion capacity [291]. Dozens of other spontaneously immortalized cell lines have been reported in different benign and malignant tissues.

Apart from selection of spontaneously immortalized cell clones from cultures to establish ever-proliferative cell lines, specific modifications can induce an increased proliferative capacity. One approach includes introduction of viral genes into the cell line. A viral gene commonly used is the large T-antigen, a double-stranded DNA binding protein of the simian virus 40 (SV-40), a member of the polyomaviridae. Its interactions with heat shock chaperone hsc70 and the two tumor suppressors retinoblastoma (pRB) and p53 protein facilitate transformation of cells to immortality [292]. Introduction of E6 and E7, proteins of human papillomaviruses (HPV), lead to inhibition of cell cycle arrest and cellular apoptosis through perturbation of tumor suppressor protein function. E6 degrades p53 protein and E7 affects retinoblastoma protein, which result in reduced DNA mutation repairs and disrupted, unphysiological cellular processes. Therefore, integration of these proteins can result in malignant transformation [293]. The use of human adenovirus type 5 E1A/E1B or E4 proteins constitute another possible path to avoid cellular senescence, although only few human cells have been successfully targeted e. g. human embryonic kidney cells (HEK) [294, 295].

Apart from viral genes, transduction with genes expressing cell cycle controlling proteins is a possible path to immortality. Two frequently used genes include human telomerase reverse transcriptase (*hTERT*; OMIM 187270) and cyclin-dependent kinase 4 (*CDK4*; OMIM 123829), targeting two pathways to replicative senescence. This approach has been used for design of many immortalized cells lines, e. g. for human myoblasts [289, 296].

Expression of human telomerase reverse transcriptase (hTERT), the catalytic subunit of the telomerase, leads to an elongation of the telomeres. These are capping ends of the chromosomes with a repeating sequence of 5'-TTAGGG-3' in humans, acting as a protection for the chromosomes. Replication of double-strand DNA is carried out using a semi-conservative mechanism, where each DNA strand is replicated and forms a new double-strand with its own copy [297, 298]. In cells each replication leads to a loss of base sequences at the 5'- end of the telomere, called end replication problem, resulting in a gradual shortening of 50-100 bp per population doubling [299-301]. Additionally, oxidative damage and other processes at chromosome ends lead to further shortening [302, 303]. The telomeres are believed to be a mitotic clock of the cell, and that the shortest and not the average telomere length determines cellular viability [304, 305]. After gradual shortening, telomere length reaches a critical level which results in activation of DNA damage signaling pathways, including activation of p53 pathway or induction of cyclin-dependent kinase inhibitors p21 and p16 [306].

The human ribonucleoprotein enzyme complex telomerase is composed of reverse transcriptase (hTERT) as catalytic subunit, telomerase RNA (hTR) as template and dyskerin, stabilizing hTR and pseudouridylating ncRNA [307, 308]. Telomeres develop a secondary t-loop structure containing the shelterin multiunit complex with at least six subunits, which binds to the specific telomere base sequence. Deletion of the TRF2 subunit led to a loss of 3'-telomeric overhang, activation of the p53-pathway and increased end-to-end-chromosome fusions, indicating deprotection of chromosome ends [309-311]. Telomerase has been shown to fulfill more than just telomere-elongation functions. Other putative roles include protection against DNA-damaging agents, mitochondrial stress and increase in DNA repair, elevated expression of cell growth genes and transcriptional modulation of the Wnt/beta-catenin signaling pathway by association with target gene chromatin [312-314].

Independently from telomerase activity, a mechanism called alternative lengthening of telomeres (ALT) leads to elongation of chromosomal ends. Telomerase activity is present in most of the carcinoma tissue, in contrast to its absence in somatic tissue. There are immortalized cell lines or tumor cells, which feature exceptionally long telomeres and a typical telomere length heterogeneity but show no signs of telomerase activity. The mechanism is based on homology-directed telomere synthesis [315-317]. Excessive elongation causes instability of the chromosomal ends and increases probability of carcinogenesis. Therefore, in human embryonic and induced pluripotent stem cells or other telomerase-positive cells, e. g. activated lymphocytes, mechanisms by homologous recombination proteins XRCC3 and Nbs1 for trimming of telomeres are active [318, 319].

The repeating nature of telomeres was first discovered in the ciliate *Tetrahymena* in 1978 with its recurring hexanucleotide sequence repeats (5'-CCCAA-3'), although their existence has been assumed earlier before, e. g. in works of later Nobel Prize recipients McClintock and Muller [320-323]. Their protective nature as a guardian against degradation of chromosome ends was first proven in yeast cells in 1982 [324]. The telomerase enzyme was detected shortly afterwards in *Tetrahymena* and subsequently further described [325-328]. For their discoveries Blackburn, Greider and Szostak jointly received the Nobel Prize in Physiology or Medicine in 2009 [329].

It was shown that elongation of cell telomeres using hTERT leads to significantly extended life spans of cells, e. g. in human retinal pigment epithelial cells and foreskin fibroblasts [287]. In human myoblasts, hTERT was not sufficient for full immortalization of cell lines [330].

Therefore, an additional second gene, cyclin-dependent kinase 4, is used. It codes for a serine/threonine kinase acting as a major checkpoint of the cell cycle at G/S1 transition. As catalytic subunit, CDK4 requires binding of a regulatory subunit called cyclin D for activation. After binding of the cyclin, activated CDK4 phosphorylates the retinoblastoma protein (Rb) and overrides its growth-inhibitory capacities. Dissolution of E2F transcription factor and its activation lead to progression of the cell cycle into S phase and subsequent initiation of DNA synthesis [331-333]. Humans feature a wide array of 20 CDKs, depending on 30 cyclins [334]. Apart from cell-cycle dependent functions, several CDKs and their cyclins exercise roles in different cell processes (reviewed in [335]).

CDK4 activity is subject to inhibitors of CDK4 (INK4). These include p16<sup>INK4a</sup>, p15<sup>INK4b</sup>, p18<sup>INK4c</sup> and p19<sup>INK4d</sup> [336-338]. Initially identified in human melanoma tissue, the *CDK4* gene mutation R24C, an exchange of arginine to cysteine, leads to inhibition of p16<sup>INK4a</sup> and other INK4 and disruption of cell cycle regulation [339]. In mice studies this mutation increased susceptibility of tissues for development of tumors [340]. Other inhibitory proteins of G1/S cell cycle progression, p21<sup>Cip1</sup>, p27<sup>Kip1</sup> and p57<sup>Kip2</sup>, are members of the Cip/Kip protein family [341, 342]. Arrest at G1/S boundary of the cell cycle is a common reason for replicative senescence of cells [343]. Overexpression of CDK4 resulted in bypass of telomere-dependent replicative senescence in human epithelial cells [344]. Transduction of *CDK4* gene into human myoblasts was shown to lead to an increased proliferation capability by prevention of a telomere-independent growth arrest with simultaneously retained myogenic properties [345].

Human myoblasts, either wild-type or with different pathogenic mutations, e. g. DMD, FSHD or congenital muscular dystrophy type 1A, have been successfully turned into immortalized cell lines with extended proliferation capabilities with retained myogenic properties by transducing

both described genes, *hTERT* and *CDK4*, and could serve as a tool for further research of the related neuromuscular diseases [289, 296].

## V. Aim of the project

The Duchenne muscular dystrophy (DMD) is an X-linked lethal myopathy. Symptomatic therapy has improved survival and quality of life for patients affected by DMD, but causal therapies have started to emerge. Every new therapy requires thorough testing *in vitro* and *in vivo* in animal models and subsequently in clinical trials to assess efficacy and safety of new drugs. DMD is the most common form of hereditary myopathies, but due to new drugs targeting single or small clusters of mutations, the number of patients eligible for each clinical trial is limited. Currently every new DMD drug must pass through the complete process of certification required by the national authorities, creating a time-consuming and costly bottleneck for further progress.

Animal models pose an important tool for *in vivo* evaluation of new treatments but small animal models, e. g. mice, do not imitate the human phenotype in terms of severity and feature large differences in physiology. Larger animals are far better suited. Pigs share many similarities in physiology and size with humans. A new DMD pig with an exon 52 deletion, developed by Wolf et al., represents an excellent model for DMD. Apart from the model's *in vivo* advantages, laboratory use of the porcine myoblasts has the potential to become a standard tool for *in vitro* high throughput testing of new therapies. This is especially important as the amount of available primary human DMD cell material for laboratory use is declining because of a sharp reduction in muscle biopsies due to first-line genetic diagnostic testing of patients.

Additionally, primary cells generated from these biopsies or animal models have limited proliferative capabilities. Immortalization provides a promising path for cultivating large amounts of cell material to ensure comparable and stable *in vitro* testing conditions. Stable integration of two cell cycle active genes, human telomerase reverse transcriptase (*hTERT*) and cyclin-dependent kinase 4 (*CDK4*) using a retroviral delivery system based on the Moloney murine leukemia virus, overcomes replicative senescence and induces extended proliferative capabilities in primary myoblasts. Importantly, the new immortalized cell line should feature comparable cellular characteristics and retain its myogenic potential. As of November 2021, this is the first reported immortalization approach using porcine myoblasts.

Immortalized porcine myoblasts have the potential to become a new powerful tool for high throughput screening and *in vitro* validation of new DMD therapies. Combination of an excellent large animal model and its cells' stable *in vitro* cultivation can be a great tool for efficient and fast pre-clinical assessment of new emerging therapies.

## VI. Materials and methods

### VI.1. Cell lines

#### VI.1.1. Pigs (*Sus scrofa*)

The cells used for immortalization originate from the Duchenne porcine animal model established by the working groups of Maggie C. Walter at Friedrich-Baur-Institute and Eckhard Wolf, Chair of Animal Breeding and Biotechnology of LMU [237]. The pigs feature a dystrophin-deficient phenotype similar to the human disease. The pigs 6212 and 6216, used for most of the experiments, are descendants of a carrier gilt and a healthy boar and therefore non-cloned.

We used cells of pigs with different life span and time of storage in order to optimize the experimental setting.

Cell/ animal number	Mutation	Sex	Date of birth and death, method of death	Age	Muscle
P352/15 730/15	DMD $\Delta$ 52	♂	*07.06.2015 †30.09.2015, euthanized (frozen at P2 12.10.2015)	23 days	M. semitendinosus
P362/15 731/15	none, wild type	♂	*08.06.2015 †30.09.2015, euthanized (frozen at P2 12.10.2015)	22 days	M. semitendinosus
P507/18 6212	DMD $\Delta$ 52	♂	*03.08.2018 †08.08.2018, euthanized	5 days	M. semitendinosus
P515/18 6216	none, wild type	♂	*03.08.2018 †10.08.2018, euthanized	7 days	M. semitendinosus

**Figure 9: Pigs used for porcine cell lines**

Isolation of porcine myoblasts from piglets of the porcine DMD animal model was carried out using a modified protocol originally established by Claudia Kalbe (Leibniz-Institut, Dummerstorf, Germany).

#### VI.1.2. Patients

Patients for molecular genetic analysis of hereditary degenerative neuromuscular diseases and clinical investigation were provided by physicians at the Friedrich-Baur-Institute, Munich, Germany, and collaborators at Eginition Hospital, Athens, Greece. After informed consent, blood samples were sent to the Friedrich-Baur-Institute for routine diagnostics and genomic DNA was isolated using the Wizard® Genomic DNA Purification Kit (Promega, Walldorf, Germany, Ref: A1120) according to instructions provided by the manufacturer.

### VI.1.3. Additional cell lines

Additionally, as control cell lines with myogenic properties, C2C12 cells and human immortalized myoblasts (0208ct7), were used. C2C12 is a spontaneously immortalized murine myoblast cell line. After informed consent, the 0208ct7 myoblast line was derived from a 36-year-old, healthy male donor and was transduced using pBABE-hTERT and pBABE-CDK4 vectors by a retroviral system kindly provided by Peter Schneiderat [296].

NIH 3T3 cells, spontaneously immortalized mouse fibroblasts, were utilized for proof-of-principle experiments and determination of colony forming units to assess the virus titer.

For transduction of vectors we used a helper virus-free retroviral delivery system. Phoenix-AMPHO (ATCC, Manassas, USA; ATCC® CRL-3213, Lot: 62346785) is a producer cell line for amphotropic retroviruses. The cells are based on a human embryonic kidney cell line transformed with Adenovirus E1a and a temperature sensitive T antigen co-selected with neomycin. The vectors are based on the Moloney Murine Leukemia Virus (MMLV) which allows gene delivery to most dividing cells. In order to minimize recombination potential, gag-pol and env have different, non-MMLV promoters. The envelope proteins can be co-selected with diphtheria toxin. Gag-pol carries a hygromycin co-resistance. The cell line is suitable for stable virus production in just a few days [346, 347].

## VI.2. Basics of cell cultivation

All cell cultivation took place at 37 °C using a humidified incubator at 5 % CO<sub>2</sub> (Binder, Tuttlingen, Germany; Ref.: CB-53). All cell culture works were carried out in a laminar flow hood (Heraeus, HS15). Microscopic imaging was conducted using an Olympus CKX53 microscope and an Olympus UC 90 camera (Olympus, Hamburg, Germany) connected to a desktop computer to power the provided Olympus cellSense Entry imaging software. Fluorescence imaging of in-vitro cultures was carried out using a fluorescence lamp (Lumen Dynamics, Mississauga, Ontario, Canada; Model: XI-120Q). A pipet aid (Drummond, Broomall, PA, USA; Ref.: 4-000-201) and sterile, nonpyrogenic and RNase/DNase-free serological pipets with volumes from 1 to 10 ml (Corning, Corning, NY, USA; Ref.: 4485 to 4488) and 25 ml to 50 ml (Greiner Bio One, Frickenhausen, Germany; Ref.: 768 180) were used. Culture plates were used in different sizes: 100 mm x 20 mm (Corning, Corning, NY, USA; Ref.: 430167), 150 mm x 25 mm (Corning; Ref.: 430599) and six-well tissue culture plates (Corning; Ref.: 353224). Tubes of 15 ml and 50 ml (Greiner Bio One; Ref.: 188 271 or 227 261) and 1.5 ml and 2 ml safe-lock tubes (Eppendorf, Hamburg, Germany; Ref.: 0030 120.086 and 0030 120.094) were utilized. A range of Pipetman® (Gilson, Middleton, WI, USA) and Research® plus pipets

(Eppendorf) were used with filter tips ranging from 10  $\mu$ l to 1.250  $\mu$ l (Biozym, Hessisch Oldendorf, Germany).

Depending on the type of cell different growth mediums were deployed. For the cultivation of porcine myoblasts we used MEM alpha (Gibco; Ref.: 12561-056) with 10 % fetal bovine serum (FBS) (PeloBiotech, Planegg, Germany, Ref.: PB-FCS-EU-0500) and 2 mM glutamine (GlutaMAX™-I (100X), Gibco/life technologies, Paisley, UK; Ref.: 35050-061) and antibiotic agents containing 0.5 ml gentamycin (Gibco, Ref.: #15750-037) and 0.5 ml amphotericin B (Gibco, Ref.: #15290018). Selection was carried out using antibiotic agents according to the established resistance gene of the plasmids. These are G418 Geneticin® 50 mg/ml (Gibco; Ref.: 10131-035), Hygromycin B Gold 100 mg/ml (Invivogen, Toulouse, France; Ref.: #ant-hg) and Puromycin 10 mg/ml (Gibco; Ref.: A11138-02).

Cultivation of 3T3 fibroblasts, Phoenix amphi cells and C2C12 myoblasts took place in DMEM (Gibco, #41966-029) with 10 % fetal bovine serum and 2 mM glutamine and antibiotic agents containing 10 units/ml penicillin and 10  $\mu$ g/ml streptomycin (Gibco, #15070063). Human myoblasts were cultured using skeletal muscle cell basal medium (PeloBiotech; Ref.: PB-BH-272-0090), prepared according to the manufacturer's instructions.

Rinsing of cell cultures was completed using Dulbecco's Phosphat Buffered Saline (PBS) (Sigma-Aldrich, Steinheim, Germany; Ref.: D8537-500ML). Splitting of cells was carried out rinsing the cells two times with PBS and using 0.05 % Trypsin-EDTA (1X) (Gibco/Life technologies, Paisley, UK; Ref.: 25300-054). Trypsinizing for the BioRad TC20™ automated cell counter (BioRad, Feldkirchen, Germany) was facilitated using TrypsinLE™ Express (Gibco; Ref.: 12604-013). For cell counting with the Neubauer chamber (Paul Marienfeld, Lauda Königshofen, Germany; Ref.: 0640030) Accutase® (Innovative Cell Technologies, San Diego, CA, USA; Ref.: A6964) was used.

Cryostocks were prepared by rinsing cells two times with PBS and trypsinizing. Cells were centrifuged using a high-speed refrigerated bench centrifuge (Sigma Zentrifugen, Osterode am Harz, Germany; Sigma 6K15) for 10 min at 11'000 x g and 4 °C. Supernatant was discarded and the pellet was resuspended using cryo medium. As of 2017, cryo medium consisted of 90 % FBS and 10 % dimethyl sulfoxide (DMSO; Carl Roth, Karlsruhe, Germany; Ref.: A994.1). Previously, a mixture of 70 % DMEM, 20 % FBS and 10 % DMSO was used. 1 ml aliquots were placed in cryotubes (Nunc, Langenselbold, Germany) and stored at -80 °C in a laboratory freezer (New Brunswick Scientific, Edison, NJ, USA; U41085).

### VI.3. Plasmids

Previously published plasmids, carrying the pBABE backbone and including an ampicillin resistance cassette, were used for this first approach of immortalization of porcine myoblasts. They differ in different distinct selectable markers for each vector.

pBABE-puro-hTERT features a 3'500 bp insert containing the *TERT* cDNA of *Homo sapiens* and a puromycin-resistance as selectable marker (Figure 80).

*CDK4* cDNA with the R24C mutation was introduced using the pBABE-hygro CDK4 R24C plasmid. It features a 1'000 bp insert with the *CDK4* cDNA of *Homo sapiens* and a hygromycin resistance gene as a selectable marker (Figure 81).

For monitoring purposes of transfection and transduction steps, two different GFP-variants were used (Figure 82 and Figure 83). pBABE-neo-IRES-eGFP features a 1.331 bp sized insert with the enhanced *GFP* cDNA of crystal jelly (*Aequorea victoria*) with an internal ribosome entry site and a neomycin resistance gene as a selectable marker. The commercial control vector pmaxGFP® is included in the Amaxa® Cell Line Nucleofector® Kit V (Lonza; Ref.: VCA-1003). It is designed to monitor transfection efficacy using fluorescence microscopy by featuring a green fluorescent protein (GFP) gene derived from the copepod (*Pontellina plumata*). It came at a determined concentration (0.5 µg/µl in 10 mM Tris pH 8.0).

Full gene sequences and sequence maps are available in the annex.

Plasmids with the pBABE backbone (high-copy vector) were delivered transfected into DH5alpha *E. coli* bacteria with an ampicillin bacterial resistance gene. A bacterial streak was performed using culture plates with lysogeny growth (LB) medium with 0.29 µM ampicillin. Plates were cultured at 37 °C under normoxic conditions overnight using a heated oven (Heraeus Instruments, Hanau, Germany).

A preparatory culture was generated using a single bacterial colony which was suspended in 5 ml LB medium with 0.29 mM (1 µl/ml) ampicillin in a push-cap tube and cultured at 37 °C under normoxic conditions in an incubator orbital shaker at a shaking speed of 150/min (Certomat, B. Braun, Melsungen, Germany) overnight.

A main culture was generated using 0.5 ml of the preparatory culture adding 150 ml LB medium and 0.29 mM (1 µl/ml) ampicillin. Cultivation took place in an incubator orbital shaker overnight, applying the same conditions. The main culture was stored at +4 °C before further preparation.

A stock solution made from 700 µl of preparatory culture and 700 µl 80 % glycerol, was stored at -80 °C.

For further preparation of plasmid DNA, the Nucleobond® PC 500 kit (Macherey-Nagel, Düren, Germany, Ref: 740574) and the provided protocol were used. If not indicated otherwise, all materials and agents utilized were part of that kit. The main culture was centrifuged (Hettich; Rotina 420R, 4'500 x g, + 4 °C) for 15 min. The supernatant was discarded. For cell lysis, 12 ml of the provided S1 buffer S1 at + 4 °C were used to resuspend the cell pellet by gentle inverting the flask. 12 ml of S2 buffer were added at room temperature and incubated for 5 min before 12 ml of S3 buffer were added at + 4 °C. The mixture was kept on ice for 30 min. Binding columns were equilibrated using 6 ml of N2 buffer. For clarification of the lysate, it was poured into folded filters, which were placed in the columns and had been humidified using 2 ml of N2 buffer. After emptying of the filters by gravity flow, washing was carried out using 32 ml of N3 buffer. For elution of DNA columns were placed on top of 2 ml tubes (Eppendorf) and 15 ml of buffer N5 were inserted. 11 ml of iso-propanol were used to precipitate the DNA. The mixture was left on ice for 30 min and then centrifuged for another 30 min (Eppendorf centrifuge 5417, 15'000 x g, + 4 °C). Supernatant was discarded and 5 ml of 70 % Ethanol were added. For washing mixture was centrifuged (device, 15'000 x g, room temperature) for 5-10 min. Ethanol was removed and the pellet was left to dry for 20 min until it was visibly opaque. The DNA pellet was resuspended using 200 µl of TE buffer.

The concentration of plasmid DNA was determined using a Nano-Drop® 1000 (ThermoFisher, Wilmington, DE, USA) with 1.5 µl sample volume for measuring as specified by the manufacturer.

### **VI.4. Use of genetically modified organisms (GMOs)**

All works were carried out in compliance with the applicable laws and rules of the European Union, Federal Republic of Germany and Free State of Bavaria. The use of GMOs was approved by the government of Upper Bavaria (Regierung von Oberbayern) as responsible supervisory authority (Ref.: AZ.8791.GT\_2\_722-7-3).

### **VI.5. Test of antibiotic resistance**

Testing of antibiotic resistance was carried out in order to specify intrinsic antibiotic resistance of the cell lines used and be able to conduct a reliable and efficient selection by antibiotic selection agents.

Cells were plated in high density in six-well plates and cultured in 2.5 ml of normal cell culture medium per six-well with added antibiotic agents. Duplicates were seeded for every antibiotic

drug and cell line used. For each combination of cell line and drug six different concentrations were tested. Antibiotic agents used include puromycin, hygromycin and G418. A positive control duplicate without antibiotic agents was seeded and cultured accordingly. All cells were monitored for surviving and growing cell colonies.

P507/18 and P515/18 myoblasts' antibiotic resistance was tested for three different agents and one combination of them (Figure 10).

	Concentrations used (in µg/ml)					
<b>Puromycin</b>	0.50 µg/ml	1.00 µg/ml	1.50 µg/ml	2.00 µg/ml	3.00 µg/ml	4.00 µg/ml
<b>Hygromycin</b>	50 µg/ml	75 µg/ml	100 µg/ml	200 µg/ml	300 µg/ml	400 µg/ml
<b>G418</b>	100 µg/ml	200 µg/ml	300 µg/ml	400 µg/ml	500 µg/ml	600 µg/ml
<b>Puromycin &amp; hygromycin</b>	0.05 µg/ml + 5 µg/ml	0.10 µg/ml + 1 µg/ml	0.20 µg/ml + 20 µg/ml	0.30 µg/ml + 30 µg/ml	0.40 µg/ml + 40 µg/ml	0.50 µg/ml + 50 µg/ml

Figure 10: Antibiotic concentrations used on P507/18 and P515/18

P352/15 and P362/15 myoblasts were tested for two antibiotic agents and one combination of them (Figure 11).

	Concentrations used (in µg/ml)				
<b>Puromycin</b>	0.50 µg/ml		0.75 µg/ml		1.00 µg/ml
<b>Hygromycin</b>	50 µg/ml		75 µg/ml		100 µg/ml
<b>Puromycin + hygromycin</b>	0.10 µg/ml + 10 µg/ml	0.25 µg/ml + 25 µg/ml	0.50 µg/ml + 50 µg/ml	0.75 µg/ml + 75 µg/ml	1.00 µg/ml + 100 µg/ml

Figure 11: Antibiotic concentrations used on P352/15 and P362/15

The Phoenix amphi producer cell line's resistance was tested for three antibiotic agents (Figure 12). Hygromycin concentrations of 50 and 100 µg/ml were eventually increased to 1'400 and 2'000 µg/ml to assess antibiotic resistance.

	Concentrations used (in µg/ml)					
<b>Puromycin</b>	0.50 µg/ml	0.75 µg/ml	1.00 µg/ml	1.50 µg/ml	2.00 µg/ml	3.00 µg/ml
<b>Hygromycin</b>	50 µg/ml/ 1'400 µg/ml	100 µg/ml/ 2'000 µg/ml	200 µg/ml	400 µg/ml	600 µg/ml	800 µg/ml
<b>G418</b>	200 µg/ml	300 µg/ml	400 µg/ml	600 µg/ml	800 µg/ml	1'000 µg/ml

Figure 12: Antibiotic concentrations used on Phoenix amphi producer cell line

The 3T3 cell line's resistance was tested for three antibiotic agents (Figure 13).

	Concentrations used (in µg/ml)				
<b>Puromycin</b>	0.50 µg/ml	1.00 µg/ml	1.50 µg/ml	2.00 µg/ml	2.50 µg/ml
<b>Hygromycin</b>	50 µg/ml	100 µg/ml	150 µg/ml	200 µg/ml	250 µg/ml
<b>G418</b>	200 µg/ml	300 µg/ml	400 µg/ml	500 µg/ml	1'000 µg/ml

Figure 13: Antibiotic concentrations used on 3T3

## VI.6. Transfection of producer cell line

Transfection of the Phoenix amphi producer cell line was carried out using the Amaxa Nucleofector® II device (Lonza, Cologne, Germany) and the Amaxa® Cell Line Nucleofector® Kit V (Lonza; Ref.: VCA-1003). The transfection of HEK-293 cells was carried out accordingly to the protocol provided by Lonza.

The Amaxa Nucleofector® II device's function is based on electroporation with added special solutions for transfection of cell lines. As advised, the producer cell line was cultured in normal growth medium before being trypsinized and centrifuged at 300 x g for 10 min. Supernatant was completely removed and the cell pellet was resuspended in 100 µl of the provided Nucleofector® Solution V. A corresponding amount of DNA ranging between 1 - 5 µg from stock or pmaxGFP®-vector as positive control was added to the mixture. A mock approach without addition of DNA was carried out as negative control (Figure 14).

Plasmid	DNA concentration	Volume added to mixture	Amount of DNA added
pBABE-puro-hTERT	1'595.2 ng/µl	2.66 µl	4.24 µg
pBABE-hygro-CDK4 R24C	847.1 ng/µl	5.00 µl	4.24 µg
pBABE-neo-IRES-eGFP	346.3 ng/µl	5.00 µl	1.73 µg
pmaxGFP®	0.5 µg/µl (according to manufacturer)	4.00 µl	2.00 µg

**Figure 14: Plasmid volumes and amounts of DNA used**

After transfer of the mixture into cuvettes and placing them into the Amaxa device, Nucleofector® program Q-001 was carried out. Immediately after completion, 500 µl of pre-heated (37 °C) growth medium was added to every sample before being seeded into culture plates.

The transfected Phoenix amphi cells were selected immediately after transfection in normal growth medium with added antibiotic selection agent according to the induced antibiotic resistance. The Phoenix cell line carries two co-selective markers, diphtheria toxin and hygromycin.

The cells used as mock approach for transfection were split into three plates and treated accordingly with selective agents. Cells transfected with pmaxGFP® were not selected and only used for determination of transfection efficacy. After transfection, these cells were seeded into four chamber glass slides and stained with DAPI. Cells were counted using a fluorescence microscope with attached camera (Hamatsu; Ref.: A3472-06 or AxioCam HRc, Zeiss).

Plasmid	Induced antibiotic resistance	maximum antibiotic concentration	minimum antibiotic concentration
pBABE-puro-hTERT	Puromycin	1.50 µg/ml	1.50 µg/ml
pBABE-hygro-CDK4	Hygromycin	800 µg/ml	400 µg/ml
pBABE-neo-IRES-eGFP	G418	1'000 µg/ml	400 µg/ml

**Figure 15: Induced resistance by transfected plasmids and maximum selection agent concentration**

Cell lines were cultured for at least 28 days using an antibiotic resistance up to the indicated maximum and at least the indicated minimum concentration of the selection agent. The cells were repeatedly trypsinized and split up to a 1:8 ratio in order to gain a pure, selected culture.

### Production of virus

The production of virus was carried out after a repeated cycle of trypsinizing and splitting the cells in order to get the highest ratio of resistant and therefore transfected cells.

Once the desired confluency of more than 80 % was achieved, cells were rinsed with PBS two times and culture medium was changed to production medium, made from DMEM + 2 % Ultrosor G (Pall life sciences, Cergy-Sainte-Christophe, France; Ref.: 15950-017) + 2 mM glutamine using 8 ml for a 13.5 cm culture plate followed by incubation for 24 h at 37 °C.

Supernatant was harvested using a 10 ml syringe (Becton Dickinson S.A., Fraga, Spain) and filtered by using a 0.45 µm filter (Merck Millipore, Darmstadt, Germany). Cryo stocks of 1 ml were placed in 1.5 ml tubes and stored at - 80 °C.

### Viral titers

Viral titers were validated by transducing 3T3 cells and selected with the corresponding antibiotic agent. 3T3 cells were plated in duplicates in six-well-plates and cultured using normal growth medium. Once the density was over 60 %, they were rinsed two times with PBS and prepared for transduction. A mock control duplicate was seeded and cultured with selection agent accordingly without being transduced.

Transduction was facilitated using viral supernatant from transfected Phoenix amphi cell lines and hexadimethrine bromide/polybrene (Sigma-Aldrich, H9268). A titration was carried out to determine colony forming units. 1 ml of fresh or frozen supernatant per virus were used and allocated according to the following diagram (Figure 16). Working concentration of polybrene was 4.0 µg/ml for all wells. Growth medium used was made of DMEM, 2 mM glutamine and 10 % FBS with added penicillin/streptomycin.

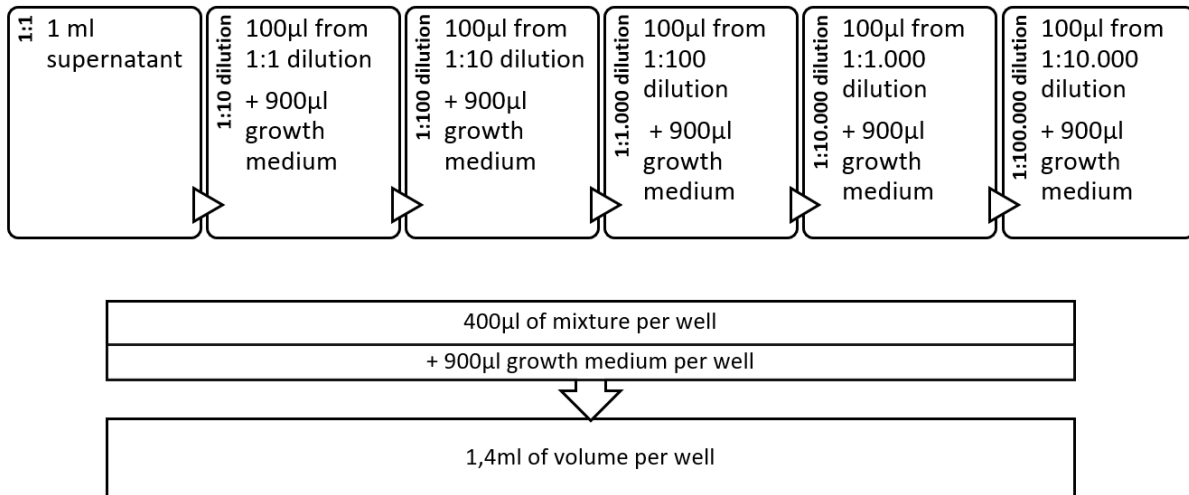


**Figure 16: Titration of virus scheme**

Selection was carried out using the respective agent for the induced antibiotic resistance and slowly titrated to maximum concentration in order to let cells recover from stress of transduction. Minimal and maximal antibiotic concentrations are indicated below (Figure 17).

Transduced plasmid	Resistance gene	Maximum/ minimal antibiotic concentration
pBABE-puro-hTERT	puromycin	0.75 µg/ml / 0.75 µg/ml
pBABE-hygro-CDK4 R24C	hygromycin	400 µg/ml / 150 µg/ml
pBABE-neo-IRES-eGFP	neomycin/ G418	1'000 µg/ml / 400 µg/ml

**Figure 17: Overview of antibiotic selection**

As proof of tropism of the produced virus containing CDK4, an antibiotic titration with lower concentrations (150, 200 and 300 µg/ml hygromycin) and undiluted viral supernatant with infection on two consecutive days was carried out. Additionally, existence of GFP-positive cells was monitored for retroviral transduction containing pBABE-neo-IRES-eGFP, with use of C2C12 and 3T3 cell lines and consecutive transductions.

Colonies were cultured for at least 14 days well after death of mock control duplicate and stained with a mixture of 2.1 ml 0.5% methylene blue (M9140, Sigma Aldrich) and 4.9 ml distilled water (B. Braun, Melsungen, Germany). Wells were left to dry for a day before being photographically documented.

Colony forming units (CFU) were calculated using the formula:

$$CFU = \frac{\text{number of colonies} \times \text{dilution}}{\text{volume of original well}}$$

## VI.7. Porcine myoblasts

### VI.7.1. Transduction of myoblasts

In total, three transduction approaches were carried out. For all of them, primary myoblasts were seeded in wells and cultured in growth medium to a confluency of 90 %. Once the cells reached the desired confluency, transduction was carried out. Cells were rinsed two times using PBS, and fresh growth medium was added. Depending on the approach, 1 ml fresh or frozen supernatant of producer cell cultures per culture plate were used. 4 µg/ml of hexadimethrine bromide/polybrene (f. c. Sigma-Aldrich; H9268) was also added.

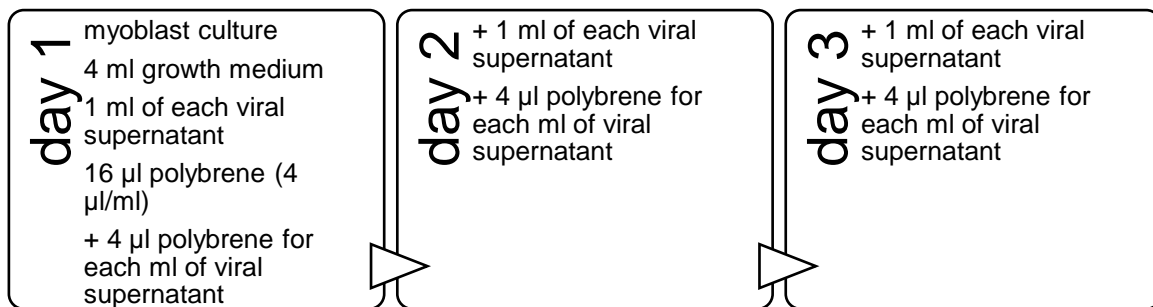


**Figure 18: Protocol for transduction of myoblasts**

Depending on the approach, cells were transduced on consecutive days as indicated in the following tables. A mock approach for each series was prepared in order to monitor resistance of transduced cells to the appropriate antibiotic agent as a negative control. pBABE-neo-IRES-eGFP was used as a positive control.

#### First approach

The first approach with myoblasts included transduction of P352/15 (DMD) and P362/15 (WT) with thawed viral supernatant on three consecutive days immediately after defrosting and culturing of frozen myoblasts. In the initial approach, only viral supernatant containing pBABE-puro-hTERT were used. After three days of transduction, an immediate antibiotic selection with 1.50 µg/ml puromycin was started, before altering the concentration between 0.50 and 3.00 µg/ml in the course of the experiment. A negative control (mock approach) was cultured accordingly. Non-transduced myoblasts from the same passage were cultured in parallel.

day of growth	P352/15	P362/15
1	hTERT	hTERT
2	hTERT	hTERT
3	hTERT	hTERT

**Figure 19: Transduction scheme first approach P352/15 and P562/15**

	<b>hTERT</b>		
<b>maximal concentration</b>	1.5 µg/ml, since day 26: 3.0 µg/ml puromycin		
<b>minimal concentration</b>	none		

Figure 20: Range of antibiotic concentrations used in first approach

### Second approach

A second approach using the same frozen myoblasts encompassed different combinations of thawed viral supernatant with pBABE-puro-hTERT or pBABE-hygro-CDK4 R24C and subsequent corresponding antibiotic selection (Figure 21). As usual, a negative control mock approach and non-transduced myoblasts of the same passage were cultured in parallel.

growth day	P362/15 hTERT			P362/15 CDK4	P362/15 hTERT + CDK4	
1	hTERT			CDK4	hTERT + CDK4	
4	hTERT			CDK4	hTERT + CDK4	
6	hTERT			CDK4	hTERT + CDK4	
8 - 27	1.0 µg/ml puromycin			100 µg/ml hygromycin	1.0 µg/ml puromycin + 100 µg/ml hygromycin	
27	<b>P362/15 hTERT I</b>	<b>P362/15 hTERT II</b>	<b>P362/15 hTERT III</b>	<b>P362/15 hTERT IV</b>	<b>P362/15 hTERT V</b>	<b>P362/15 hTERT VI</b>
27	CDK4	1.0 µg/ml puromycin		CDK4	1.0 µg/ml puromycin	
29	CDK4			CDK4		
32	0.5 µg/ml puromycin + 50 mg/ml hygromycin	CDK4	1.0 µg/ml puromycin	0.3 µg/ml puromycin + 30 mg/ml hygromycin		
34		CDK4				
37		0.25 µg/ml puromycin + 25 mg/ml hygromycin				
43	0.25 µg/ml puromycin + 25 mg/ml hygromycin			0.25 µg/ml puromycin + 25 mg/ml hygromycin		

Figure 21: Overview of transduction and antibiotic selection of P362/15 cell approaches in second approach

### Third approach

The third approach was conducted using fresh P515/18 cells (WT) and thawed P507/18 (DMD) cells, which had been frozen for a duration of only three days. Cells were cultured before transduction for 12 days. Viral supernatant, produced freshly in parallel and containing pBABE-puro-hTERT or pBABE-hygro-CDK4 R24C, was used immediately without freezing for the various transductions with subsequent antibiotic selection (Figure 22 and Figure 23). For each cell culture, a negative control mock approach was cultured accordingly. A non-transduced myoblast culture was maintained for each cell line (DMD VI and WT VI).

growth day	DMD/WT I	DMD/WT II	DMD/WT III	DMD/WT IV	DMD/WT V	DMD/WT VI	DMD/WT VII
12	hTERT	CDK4	eGFP	hTERT	CDK4	none	hTERT + CDK4
13	hTERT	CDK4	eGFP	hTERT	CDK4	none	hTERT + CDK4
14	hTERT	CDK4	eGFP	hTERT	CDK4	none	hTERT + CDK4
...							
23	CDK4	hTERT	eGFP	-	-	-	-
24	CDK4	hTERT	eGFP	-	-	-	-

Figure 22: Transduction scheme third approach P507/18 and P515/18

growth day	DMD/WT I	DMD/WT II	DMD/WT III	DMD/WT IV	DMD/WT V	DMD/WT VI	DMD/WT VII
15	0.5 µg/ml puromycin	50 µg/ml hygromycin	40 µg/ml G418	0.5 µg/ml puromycin	50 µg/ml hygromycin	none	0.05 µg/ml puromycin + 5 µg/ml hygromycin
19	0.75 µg/ml puromycin	75 µg/ml hygromycin	80 µg/ml G418	0.75 µg/ml puromycin	75 µg/ml hygromycin		0.075 µg/ml puromycin + 7.5 µg/ml hygromycin
21			120 µg/ml G418				
22	new transduction on day 23 and 24			1.00 µg/ml puromycin	100 µg/ml hygromycin		0.1 µg/ml puromycin + 10 µg/ml hygromycin
25	0.0625 µg/ml puromycin + 6.25 µg/ml hygromycin		200 µg/ml G418	1.25 µg/ml puromycin	125 µg/ml hygromycin		0.125 µg/ml puromycin + 12.5 µg/ml hygromycin
28	0.15 µg/ml puromycin + 15 µg/ml hygromycin		275 µg/ml G418	1.5 µg/ml puromycin	150 µg/ml hygromycin		0.15 µg/ml puromycin + 15 µg/ml hygromycin
31	0.2 µg/ml puromycin + 20 µg/ml hygromycin		350 µg/ml G418	2.0 µg/ml puromycin	200 µg/ml hygromycin		0.2 µg/ml puromycin + 20 µg/ml hygromycin
34	0.25 µg/ml puromycin + 25 µg/ml hygromycin		500 µg/ml G418	2.5 µg/ml puromycin	250 µg/ml hygromycin		0.25 µg/ml puromycin + 25 µg/ml hygromycin
38	0.30 µg/ml puromycin + 30 µg/ml hygromycin			3.0 µg/ml puromycin	300 µg/ml hygromycin		0.30 µg/ml puromycin + 30 µg/ml hygromycin
43	<b>DMD/WT VI</b>		<b>DMD/WT VIIa</b>				<b>DMD/WT VIIb</b>
	none		0.2 µg/ml puromycin + 20 µg/ml hygromycin until day 59			none	

Figure 23: Overview of antibiotic selection of different cell approaches in third approach

Further cultivation of myoblasts was carried out using normal growth medium without antibiotic selection starting at day 59 for DMD/WT VIIa or day 43 for DMD/WT VIIb cell lines.

Transduction efficacy was measured as ratio of GFP-positive cells using the DMD III and WT III cell lines. Cells were cultured in selection medium with added concentration of G418 up to 400 µg/ml for at least 46 days after last transduction.

### VI.7.2. Cell doublings and cell counting

Cell counting was carried out using a Neubauer cell counting chamber (Paul Marienfeld, Lauda Königshofen, Germany; Ref.: 0640030). Cells were rinsed with PBS twice and detached using Accutase® (Innovative Cell Technologies, San Diego, CA, USA; Ref.: A6964). 400 µl per six-well or 1.5 ml per 10 cm plate of Accutase were used. A total of 30 µl of cell suspension for each cell line, diluted with the same amount of 0.4% trypan blue, was utilized for viable cell counting (dye exclusion method). Determination of cell number took place up to four times, counting the four corners and the middle square of the chamber, i. e. five squares. Counting was carried out once a week for a duration of 21 days. Additionally, parallel automatic cell counting was carried out using the TC20 Automated Cell Counter (BioRad, Feldkirchen, Germany). Mean population doublings were calculated using the following formula (after [348]):

$$\text{mean population doublings} = \frac{\log \frac{\text{number of cells counted}}{\text{number of cells seeded}}}{\log 2}$$

Estimated mean population doublings were determined using the documented confluency of cells in culture and splitting intervals during the whole period of cultivation.

### VI.7.3. Limited dilution

To validate colony forming ability of transduced myoblasts, limited dilution experiments were carried out. Cell concentration was measured using the Neubauer chamber. To dilute cells properly into a 96 well plate, we used the following formula.

$$\text{necessary volume for transfer} = \frac{50 \text{ cells}}{\text{concentration of cells per ml}}$$

In case of too small volumes for transfer, a pre-dilution was carried out, e. g. 10 µl of cell suspension in 990 µl of growth medium. The appropriate volume of cell suspension or pre-dilution was added to 10 ml of growth medium. 105 µl of the mixture was added to each well. Cells were cultured as usual with transfer into larger culture plates when reaching a sufficient confluency.

### VI.7.4. Fusion of myoblasts

Fusion of myoblasts was done by rinsing cells with PBS and adding a fusion medium made of DMEM and 2% horse serum (Gibco). Cells were fused on different culture surfaces including unmodified plastic culture plates and glass slides. Another approach was modified after a published method [349] using a 1:1 mixture of 1 % growth factor reduced Matrigel (Corning Matrigel GFR Basement Membrane Matrix; Ref.: #354230) and 2 % rat type I collagen solution

(Sigma; Ref.: C3867). Glass slides (Labtek II Chamber Slide; NUNC, Rochester, NY, USA; Ref.: 154526 and 154534) were briefly rinsed with 1 N KOH and rinsed with ddH<sub>2</sub>O or PBS afterwards.

### **VI.7.5. Immunofluorescence staining**

Immunofluorescence staining of myoblasts was carried out using two methods depending on the way of cultivation.

Cells cultured on coated glass slides or plastic plates were stained using the following standard protocol. Growth medium was removed, and cells were rinsed with PBS. Fixation was carried out by incubating cells for 10 min with 3.7 % paraformaldehyde (PFA) in 1 x CSK buffer. Solution was removed and permeabilization was conducted by using 0.1 % Triton-X 100 (ICN Biochemicals, Aurora, OH, USA; Ref.: 807426) for 15 min. Subsequently, the supernatant was removed and a washing step with PBS + 0.1 % Tween-20 (Sigma; Ref.: P1379-500ML) was carried out three times for 5 min each. Blocking took place by adding PBS + 5 % horse serum for at least 1 hour or overnight at + 4 °C. The selected primary antibody was added at desired concentration in PBS + 5 % horse serum for at least 1 h. Another three times washing step with PBS + 0.05 % Tween-20 with 5 min each followed. The secondary antibody was diluted in PBS + 5 % horse serum and incubated for 1 h. Finally, two washing step with PBS + 0.1 % Tween-20 and a final one just with PBS with 5 min each followed and mounting medium with DAPI (Vectashield, Ref.: H1200) was put onto a clean slide and mounted gently without air bubbles onto the cells. The slide was left to dry overnight and was sealed using nail polish. For cultures on plastic plates no glass slide was added.

Alternatively, cells grown on 11 mm glass coverslips were picked up from the culture plate using tweezers and gently washed in PBS before placing in - 20 °C cold methanol (Roth; Ref.: CP43.4). Samples were kept at - 20 °C in a freezer. For further processing samples were rinsed three times with PBS for 5 min. Blocking solution, made of 90 % PBS + 0,1 % Tween-20 and 10 % fish gelatin, was pipetted onto a water-repellent surface and cover slips were gently inverted and placed on top of the drop of blocking solution and incubated for 20 min. Primary antibodies were prepared in the desired concentration with the blocking solution and added onto the cover slip. The primary antibody was incubated for at least one hour or overnight at + 4 °C. A series of three washing steps with PBS + 0,1 % Tween-20 with 5 min each followed. The secondary antibody was diluted to the desired concentration in blocking solution and incubated for 1 h on the sample. Finally, the sample was washed two times with PBS + 0,1 % Tween-20 and one time with PBS for 5 min each, before mounting on a glass slide using 10 µl of mounting medium with DAPI. After drying and removal of excessive mounting medium, the coverslips were sealed using nail polish.

If not indicated otherwise, all experiments took place at room temperature. Samples were stored at - 20 °C in a freezer. Antibodies are shown below (Figure 24).

Primary antibody (dilution)					
Desmin (1:50)	monoclonal anti-human D33	mouse Desmin	DAKO	Ref.: M0760	Lot: 20069184
Secondary antibody (dilution)					
Alexa Fluor plus 488 IgG (H+L) (1:500)			ThermoFisher Scientific	Ref.: A32766	Lot: TF271737

Figure 24: List of antibodies

## VI.8. Further molecular genetic analyses

### VI.8.1. Sequence analysis in myoblasts

To ensure absence of recombinant retroviruses capable of replication in the myoblast cell culture for safety reasons, further sequence analyses of DMD VII and WT VII by PCR for existence of the gag-pol- and env-genes were carried out. Additionally, further PCR and RT-PCR testing for verification of successful integration of *hTERT* and *CDK4* genes and their loci were conducted.

### VI.8.2. Sequencing of *CDK4* and *hTERT* genes in producer cell line

To detect correct integration of plasmid DNA in the Phoenix amphi producer cell line a polymerase chain reaction protocol and sequencing was carried out. DNA extraction was conducted using the Wizard Genomic DNA Purification Kit (Promega: Ref.: A1120) according to the manufacturer's instructions. A PCR protocol was carried out using pBABE-3' and pBABE-5' primers (Figure 25 and Figure 26). Full primer sequences targeting sequences of the pBABE-backbone can be found in the annex.

<i>hTERT</i> and <i>CDK4</i> cDNA-sequence	Volumes per test
25 µl	Hot Start Green Mix (Thermo Fisher; Ref.: #K1061)
5.0 µl	gDNA
23 µl	nuclease-free water
0.5 µl	sense primer
0.5 µl	anti-sense primer
<b>50 µl</b>	<b>total volume per test</b>

Figure 25: PCR mixture for *hTERT* and *CDK4* cDNA sequence

<i>hTERT</i> and <i>CDK4</i> cDNA sequence		
temperature	time	
95 °C	4 min	

95 °C	30 sec	40 repeats
55 °C	30 sec	
72 °C	90 sec	
72 °C	7 min	

Figure 26: PCR protocol for *hTERT* and *CDK4* cDNA sequence

Gel electrophoresis, DNA sequencing and sequence analyses were carried out as described below for patients' samples.

## VI.9. Molecular genetic analyses of hereditary degenerative neuromuscular diseases

Molecular analyses were conducted on genomic DNA of patients. From the clinical presentation, these patients were suspected to feature a mutation in the *GNE* gene or *VCP* gene respectively.

### VI.9.1. Primers

Routine testing included exons 2-12 for the *GNE* gene and 1-17 for the *VCP* gene. The full primer sequences are listed in the annex.

### VI.9.2. Polymerase chain reaction protocol

For each gene a different polymerase chain reaction protocol was used established in routine testing. Details of the PCR protocol are indicated in the tables below.

For PCR, a Mastercycler personal (Eppendorf) was used. The PCR product was stored in a cooler at + 4 °C.

<i>VCP</i> gene exon 1-17	Volumes per exon	<i>GNE</i> gene exon 2-12
25 µl	Hot Start Green Mix (Thermo Fisher; Ref.: #K1061)	25 µl
1.0 µl	DNA	1.0 µl
23 µl	nuclease-free water	22 µl
0.5 µl	sense primer	1.0 µl
0.5 µl	antisense primer	1.0 µl
1.0 µl	only for <i>VCP</i> exon 1 + 10: 7-deaza dGTP	-
<b>50 µl / 51 µl for exon 1 + 10</b>	<b>total volume per exon</b>	<b>50 µl</b>

Figure 27: PCR mixture for *VCP* and *GNE* gene

<i>VCP</i> gene		<i>GNE</i> gene	
temperature	time	temperature	time
95 °C	4 min	95 °C	4 min

95 °C	30 sec	40 repeats		95 °C	30 sec	40 repeats
56 °C	30 sec			56 °C	30 sec	
72 °C	1 min			72 °C	1 min	
72 °C	7 min			72 °C	7 min	

Figure 28: PCR protocols for the *VCP* and the *GNE* gene

### VI.9.3. Gel electrophoresis

A standard 1 % agarose gel was made using agarose (VWR life sciences, Leuven, Belgium; Ref.: 35-1020) and TAE buffer. Staining was carried out with with 0,01 % ethidium bromide (10 mg/ml, Sigma Aldrich). 40 µl of PCR product for each exon was added per lane containing tracking dyes and a density reagent. 10 µl of each 1 kbp and 100 bp ladder (N3232S and N0467S, NEB, Ipswich, MA, USA) were in a separate lane for correlation of fragment size. A voltage of 130 V was applied for 60 min using a flatbed electrophoresis system (Hofer HE 99X Max Submarine Electrophoresis Unit, Thermo Fisher Scientific, Waltham, MA, USA). Gels were documented using a UV-table and camera (Intas, Göttingen, Germany). Bands were cut out and stored at + 4 °C.

The amplified DNA fragments were extracted using the NucleoSpin® gel and PCR clean-up system (Macherey-Nagel, Düren, Germany) according to the manufacturer's specifications.

### VI.9.4. DNA-sequencing and analysis of data

15 µl of eluted DNA (60-120 ng total) and 2 µl of 1:20 diluted sense primer (2 pmol total) were applied to a 96-well plate for sequencing. Sequencing was conducted by Eurofins Genomics Germany GmbH (Ebersberg, Germany) using Sanger sequencing. Raw sequencing data was received in .ab1 and .pdf format for further investigations. Further analyses were carried out using Chromas software (Technelysium, South Brisbane, Australia) for electropherogram visualization and the online Basic Local Alignment Search Tool (BLAST) provided by the National Center for Biotechnology Information (U.S. National Library of Medicine, Bethesda, MD, USA). Identified sequence alterations were checked for previous reporting using the online MEDLINE database.

## VII. Results

### VII.1. Concentration of prepared plasmids

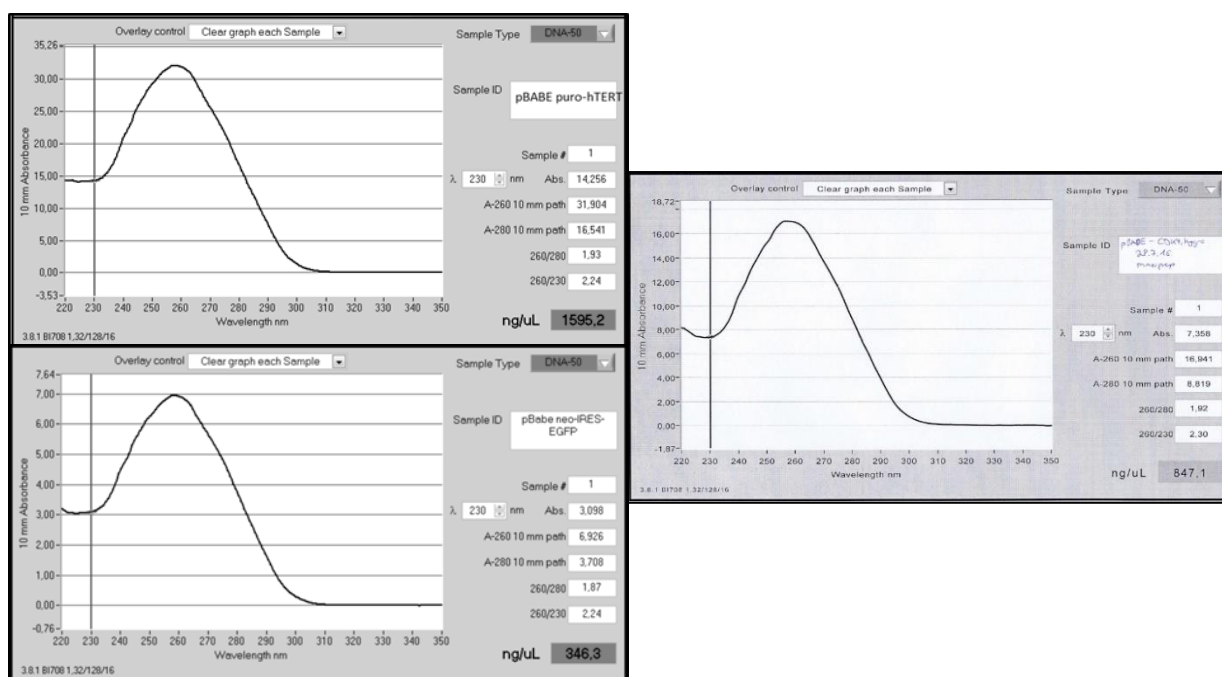


**Figure 29: Visualization of DNA measurement of pBABE-puro-hTERT (top left), pBABE-hygro-CDK4 R24C (right), pBABE-neo-IRES-eGFP (bottom)**

Using the NanoDrop® system the concentration of DNA was determined after conduction of the described preparatory works for the plasmids. pBABE-puro-hTERT showed the highest concentration of 1595.2 ng/μl with a 260/280 ratio of 1.93. pBABE-hygro-CDK4 R24C was at a concentration of 847.1 ng/μl with a 260/280 ratio of 1.92. pBABE-neo-IRES-eGFP was measured at a concentration of 346.3 ng/μl with a 260/280 ratio of 1.87.

All plasmids were eluted, as specified, in 200 μl TE buffer, resulting in the following total DNA amounts (Figure 30).

Plasmid	DNA concentration of stock as determined by Nanodrop	Amount of DNA in 200 μl TE buffer
pBABE-puro-hTERT	1'595.2 ng/μl	319.04 μg
pBABE-hygro-CDK4 R24C	847.1 ng/μl	169.42 μg
pBABE-neo-IRES-eGFP	346.3 ng/μl	69.26 μg

**Figure 30: Amount of plasmid DNA**

## VII.2. Testing of antibiotic resistance

### Myoblasts

P507/18 and P515/18 cells grew in selection medium with a puromycin concentration up to 1.0  $\mu\text{g/ml}$ , with a decisive decline in cell confluency compared to the lowest tested concentration of 0.5  $\mu\text{g/ml}$  after 24 days. A concentration of 1.5  $\mu\text{g/ml}$  resulted in detachment of all cells.

The addition of hygromycin led to a loss of all cells in both lines even at the lowest concentration of 50  $\mu\text{g/ml}$  within a week.

No proliferative P515/18 cells were visible under selection with G418 after 16 days. P507/18 cells showed signs of proliferation even after 20 days in all concentrations up to 600  $\mu\text{g/ml}$  G418, although in considerably lower intensity and confluency in combination with more cell deaths. Cell morphology was visibly changed at G418 concentrations higher than 300  $\mu\text{g/ml}$ , probably due to cellular stress (Figure 31).

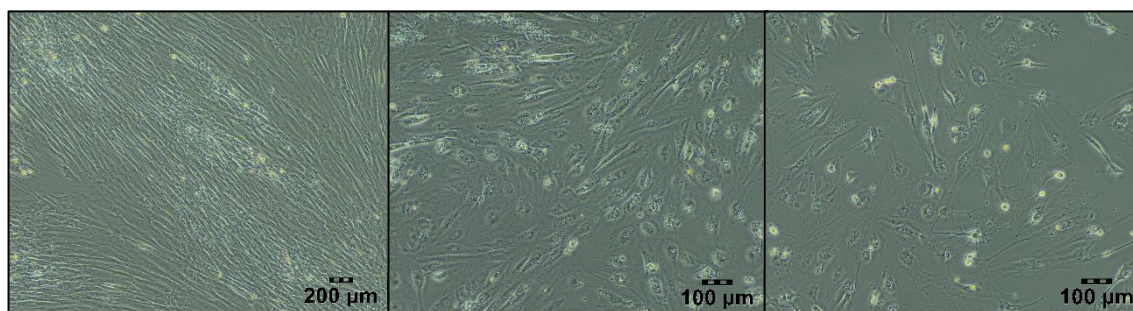


Figure 31: Comparison of P507/18 cells on day 20 of antibiotic selection: 200  $\mu\text{g/ml}$  G418 (left), 400  $\mu\text{g/ml}$  (middle), 600  $\mu\text{g/ml}$  (right)

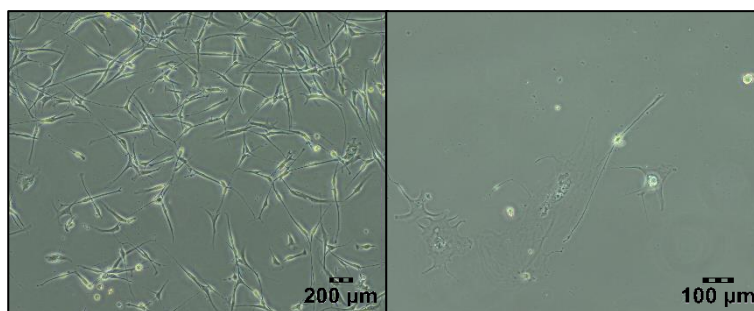


Figure 32: Example of myoblast growth (P507/18) under double selection day 20: 0.05  $\mu\text{g/ml}$  puromycin + 5  $\mu\text{g/ml}$  hygromycin (left), 0.1  $\mu\text{g/ml}$  puromycin + 10  $\mu\text{g/ml}$  hygromycin (right)

Simultaneous addition of puromycin and hygromycin led to growth in the lowest concentration of 0.05  $\mu\text{g/ml}$  puromycin and 5  $\mu\text{g/ml}$  hygromycin, although not reaching 100 % confluency and exhibiting only morphologically altered single cells in the double concentrations of 0.1  $\mu\text{g/ml}$  puromycin and 10  $\mu\text{g/ml}$  hygromycin (Figure 32). All higher tests resulted in complete cell

detachment. In comparison, P515/18 cells showed a better growth than P507/18 during double antibiotic selection testing.

Negative control cell cultures of P507/18 and P515/18 without addition of antibiotic selection agents showed intense growth throughout a period of 24 days, which required repeated splitting of the cell culture with subsequent stable regrowth.

P352/15 and P362/15 showed colony growth only for the smallest tested concentrations of puromycin (0.5 µg/ml), while single P362/15 cells grew at concentrations up to 0.75 µg/ml puromycin after 22 days of selection. Single, morphologically altered and non-proliferative cells did not detach at the next higher concentration of 1.0 µg/ml. Hygromycin addition led to detachment of all cells at all concentrations except for 50 and 75 µg/ml in P352/15 and 50 µg/ml in P362/15. In double selection titration, P352/15 and P362/15 only exhibited growth in 0.1 µg/ml puromycin and 10 µg/ml hygromycin. For all antibiotic agent and cell lines, duplicates of negative controls featured stable growth.

#### **Phoenix amphi producer cell line**

Addition of puromycin led to complete detachment of all cells at concentration higher than 0.5 µg/ml after 20 days.

These cells exhibited growth under selection with either G418 or hygromycin at all tested concentrations. Repeated splitting of cell cultures resulted in a slower regrowth rate at higher concentrations than lower ones, i. e. after an increase of hygromycin concentrations up to 1'400 µg/ml and 2'000 µg/ml.

Cellular growth was substantial in all negative control cultures, requiring repeated splitting with stable regrowth.

#### **NIH 3T3**

Only the sole addition of the lowest possible concentrations of puromycin (0.5 µg/ml) or hygromycin (50 µg/ml) resulted in growth of 3T3 cells after 17 days. All higher concentrations led to complete detachment of all cells. Colonies were formed under G418 selection up to a concentration of 300 µg/ml.

Negative controls without added antibiotic agents showed clear and stable growth.

### VII.3. Transfection of producer cell line

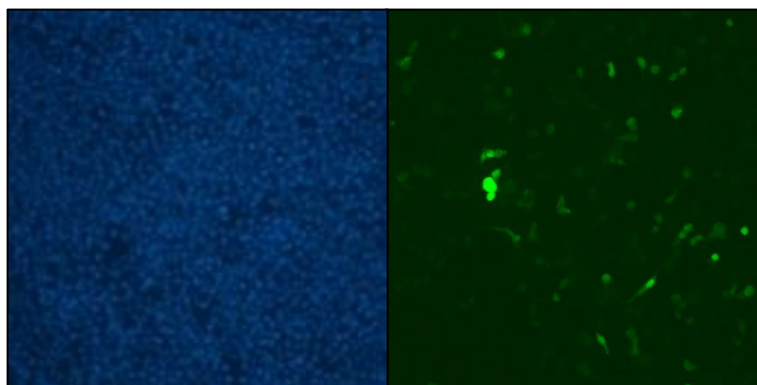


**Figure 33: left: Phoenix amphi cells, stained for DAPI, right: pmaxGFP® as positive control, day 1 after transfection**

Transfection was carried out according to the protocol indicated in the methods section. The positive control pmaxGFP® showed a transfection efficacy of 11.69 %, counted in duplicates, on the first day after transfection. Initially no green fluorescent producer cells transfected with plasmid pBABE-neo-IRES-eGFP were detected. After 17 days the first green fluorescent producer cells became visible. These GFP-positive cells usually appeared in clusters and continued to do so even after trypsinization (Figure 34).

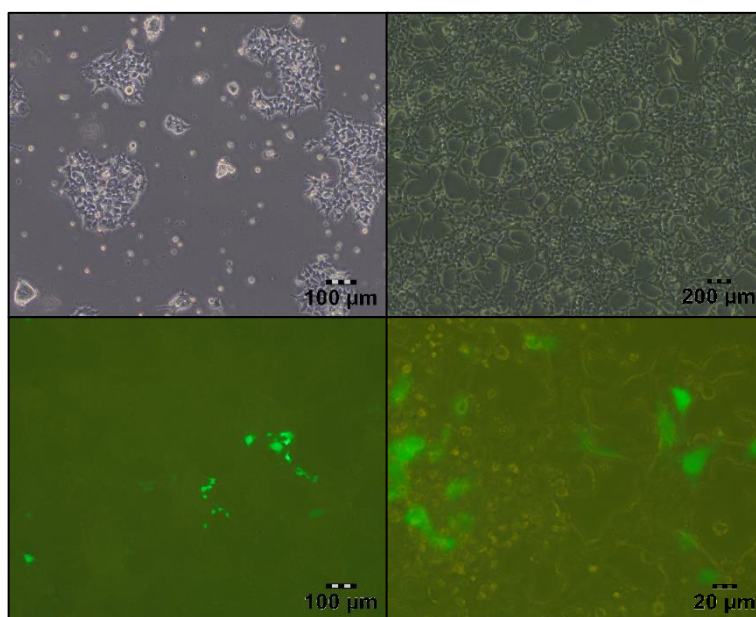


**Figure 34: Typical growth pattern of Phoenix amphi producer cell line in varying confluencies under antibiotic selection (top left & right), examples of expression of pBABE-neo-IRES-eGFP (bottom left & right)**

After transfection, Phoenix amphi producer cell lines were immediately cultured in growth medium with a suitable antibiotic selection agent. Concentration of the selection agent was increased or decreased over the selection period, depending on growth curve (Figure 35). All

transfected cells showed a significant loss of confluency immediately after start of selection. Regrowth occurred in small colonies despite antibiotic selection, indicating resistance towards the used selection agent.

plasmid	resistance gene	maximum concentration	minimal concentration
pBABE-puro-hTERT	puromycin	1.5 µg/ml	1.5 µg/ml
pBABE-hygro-CDK4	hygromycin	800 µg/ml	400 µg/ml
pBABE-neo-IRES-eGFP	neomycin	1'000 µg/ml	400 µg/ml

Figure 35: Selection of transfected producer cells

The negative control mock approach was cultured using the same growth medium with selection agent. There were no viable cells in the puromycin mock approach after three days and in the hygromycin approach after 17 days of selection. The Phoenix amphi producer cell line has an intrinsic neomycin and hygromycin resistance. Therefore, selection and mock approach using neomycin and hygromycin could not be carried out efficiently. The Phoenix amphi cells exhibited the pre-described clustered, pile-like growth behaviour, which were hardly separated by trypsinization. Therefore, regular well-timed splitting of the cell line was crucial.

#### VII.4. Viral titers

Viral titers were determined using a titration assay based on 3T3 cells as described in the methods section.

The use of thawed supernatant, containing pBABE-puro-hTERT, led to a calculated mean viral titer of  $3.18 \times 10^4$  U/ml, determined in two separate approaches with duplicates each. Fresh supernatant resulted in a significantly higher mean viral titer of  $6.43 \times 10^5$  U/ml, measured in duplicate (Figure 36).

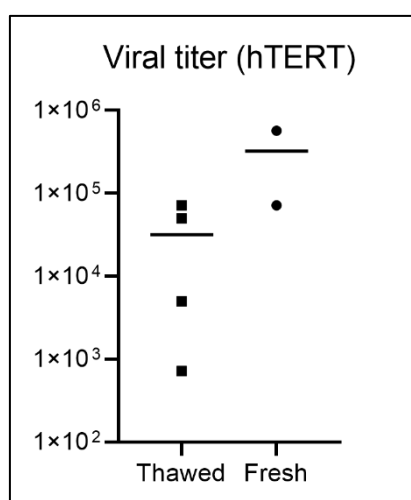
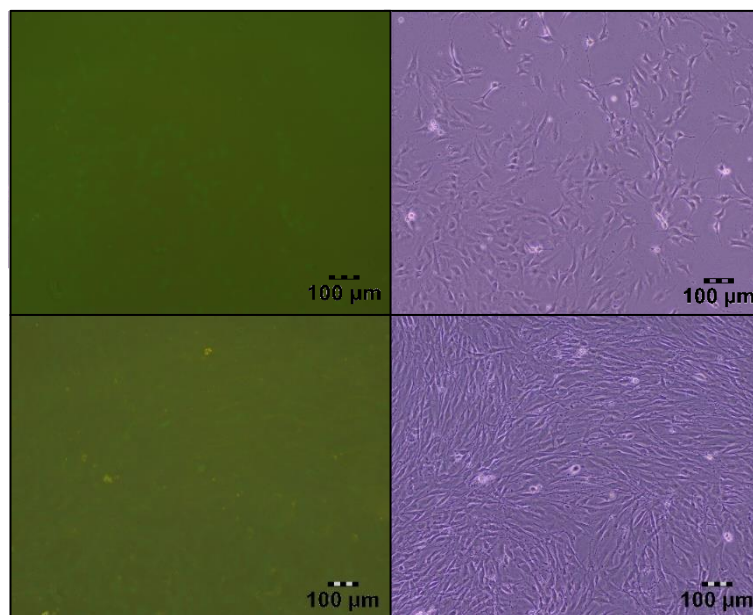


Figure 36: Mean viral titer (hTERT)

Thawed and fresh viral supernatant containing pBABE-hygro-CDK4 R24C did not lead to colony growth under selection with 400 µg/ml hygromycin. An approach with non-diluted transduction of thawed supernatant on two consecutive days, resulted in visible colony formation in both duplicates under 150 µg/ml and one duplicate of 200 µg/ml hygromycin selection. A single transduction approach, using pBABE-hygro-CDK4 R24C containing viral supernatant, with initial antibiotic selection of 400 µg/ml hygromycin for two weeks, which was subsequently decreased to 150 µg/ml hygromycin, led to formation of colonies in both wells. Technically, this corresponds to a viral titer of 3.93 U/ml.

Use of fresh or thawed viral supernatant containing pBABE-neo-IRES-eGFP did not lead to consistent findings in various dilutions, e. g. as single colonies were formed in 1:10 dilution but not in 1:1. A similar approach to the one used with pBABE-hygro-CDK4 R24C, with lowering of antibiotic selection from 1'000 to 400 µg/ml G418, resulted in formation of single colonies in the first two dilutions. Consecutive transduction of C2C12 and 3T3 cells on two days with fresh supernatant resulted in GFP-positive cells, which were resistant to G418 selection up to 500 µg/ml for more than two weeks and featured strong growth.



**Figure 37: GFP-positive C2C12 cells (top left) and growth pattern top right) 17 days and GFP-positive 3T3 cells (bottom left) and growth pattern (bottom left) 14 days after transduction with pBABE-neo-IRES-eGFP containing viral supernatant and subsequent antibiotic selection up to 500 µg/ml G418**

In all approaches, the negative mock controls featured completely detached cells in all wells under appropriate antibiotic selection during the observation period.

## VII.5. Porcine myoblasts

### VII.5.1. Transduction of primary myoblasts

In total three approaches of porcine myoblast transduction were carried out.

#### First approach

In the first approach, myoblasts of P352/15 and P362/15 cell lines were transduced with thawed pBABE-puro-hTERT viral supernatant on three consecutive days.

In both transduced DMD and WT approaches and their applicable negative mock control, selection with 1.5 µg/ml puromycin was initiated immediately after transduction. After initial loss of confluence in transduced cells (called P352/15 hTERT and P362/15 hTERT), regrowth occurred under maintained selection pressure. 23 days after last transduction, the cell lines were split and selected with different antibiotic concentrations.

P362/15 hTERT were selected with either 1.5 µg/ml or 3.0 µg/ml puromycin. Higher concentrations seemed to result in slower growth and lower confluency. On day 53 a split of 1:6 resulted in a confluency of 25 respectively 15 %. Afterwards, confluency did not recover, even after relocation into smaller wells and clusters of large, irregularly formed cells appeared. On day 100 no vital P362/15 hTERT cells were detected.

P352/15 hTERT cells featured a slower growth compared to P362/15 hTERT. After splitting on day 23 after transduction, selection was lowered from 1.5 µg/ml puromycin to either 0.75, 0.5 µg/ml or no puromycin. The two higher concentrations resulted in culture of only single cells and lacked any noteworthy colony formation. The removal of puromycin in P352 hTERT I on day 26 led to increased proliferation, colony formation and restoration of confluency well beyond day 116. Re-introduction of antibiotic selection with 1.0 µg/ml puromycin on these cells (P352 hTERT Ib) on day 95 resulted in decrease of confluency without colony forming. Age-matched cells (P352 hTERT Ia) without puromycin selection did not decrease in growth.

The negative mock approach with appropriate antibiotic selection did not show any signs of growth on day 26. Non-transduced P362/15 cells served as control cells from day 26 onward and featured stable growth for more than 80 days.

#### Second approach

In the second approach, myoblasts of P352/15 and P362/15 cell lines were cultured with thawed viral supernatant containing only pBABE-puro-hTERT (called P352/15 hTERT or P362/15 hTERT) or pBABE-hygro-CDK4 R24C (called P352/15 CDK4 or P362/15 CDK4) or a

combination of both (called P352/15 hTERT & CDK4 or P362/15 hTERT & CDK4) for three days, as indicated in Figure 21.

P352/15 hTERT and P362/15 hTERT featured growth under initial selection with 1.0 µg/ml puromycin, before a splitting of the cell line into six different approaches was carried out on day 27. Three approaches per cell line were co-transduced with thawed supernatant containing pBABE-hygro-CDK4 R24C on days 27 and 29 respectively 32 and 34. A co-selection with puromycin and hygromycin, ranging from 0.25 µg/ml puromycin and 25 µg/ml hygromycin to the double amount was carried out after co-transduction. By day 43 only P362/15 hTERT & CDK4 II with transduction of pBABE-hygro-CDK4 R24C on days 32 and 34 and co-selection with the lowest dose of 0.25 µg/ml puromycin and 25 µg/ml hygromycin, featured a high confluency. All other co-transfected cell lines were only present in form of single, non-proliferative cells or none at all, after showing a steep decline in confluency after introduction of pBABE-hygro-CDK4 R24C and beginning of co-selection with puromycin and hygromycin.

Selection of P352/15 CDK4 and P362/15 CDK4 with a selection medium containing 100 µg/ml hygromycin resulted in complete cell detachment in both cultures until day 27. P352/15 hTERT & CDK4 and P362/15 hTERT & CDK4 encountered the same fate after selection with 1.0 µg/ml puromycin and 100 µg/ml hygromycin after 27 days.

All negative mock approaches with appropriate antibiotic selection featured completely detached cells by 17 to 27 days of culture. During the duration of the experiment of 43 days, non-transduced P352/15 and P362/15 were cultured as control cell lines and exhibited stable growth.

### **Third approach**

The third approach was carried out with the knowledge acquired in the first two rounds. Different myoblast cell lines were used, which were derived from younger pigs than P352/15 and P362/15 and had only been cultivated for three days before freezing (P515/18) or not been frozen at all (P507/18). Additionally, freshly harvested viral supernatant from parallelly cultured Phoenix amphi producer cells was utilized in contrast to thawed supernatant samples in previous approaches. Transduction was carried out for three or two consecutive days (Figure 22). Seven different approaches have been conducted with subsequent various antibiotic selection and a smoother increase in concentration (Figure 23).

The first transduction was carried out on day 12 of cultivation with preparation of seven culture plates per cell line. Confluency of P507/18 cells was 50 – 60 %, while P515/18 were slightly more confluent at 60 - 70 %. This value decreased after the indicated consecutive viral transductions and subsequent initiation of appropriate antibiotic selection. Observation of

previous approaches indicated a growth retarding effect of frequent complete medium exchange. Therefore, the culture plates were not rinsed with PBS before photographic documentation leading to appearance of detritus and detached cells in the documentation.

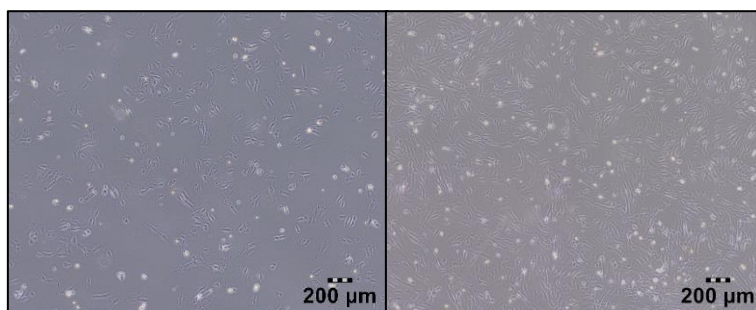


**Figure 38: Cell culture at day 12 before transduction, P507/18 (left) and P515/18 (right)**

Three approaches per cell line were subject to a second transduction for another two days and subsequent alteration in the antibiotic selection scheme. The results of the different cell lines are reported in the following sections.

### **hTERT-transduction**

P507/18 and 515/18 were transduced with pBABE-puro-hTERT-containing viral supernatant on day 12, 13, and 14. These were designated as DMD I or IV and WT I or IV. DMD I and WT I would later be subject to a second transduction with viral supernatant containing pBABE-hygro-CDK4 R24C on days 23 and 24 (Figure 22).

After the first transduction both cell lines experienced a decline in cellular confluency with appearance of detritus and even large-scale delamination. Detachment of the cell layer did not occur in any other myoblast cell line (Figure 39). Despite the extensive cell loss, a steady regrowth under antibiotic selection with puromycin occurred with a gradual increase in the concentration from 0.5 µg/ml to 3.0 µg/ml by day 43 (Figure 40).

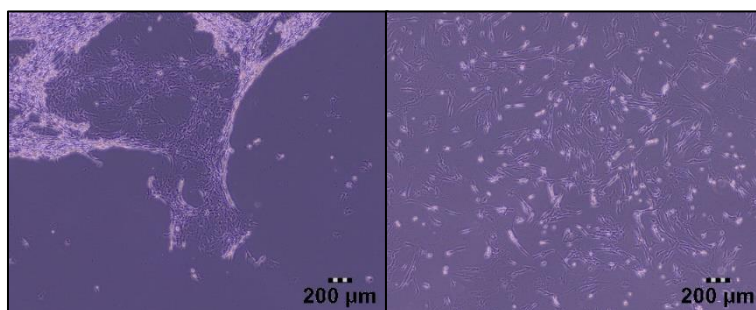


**Figure 39: P507/18 hTERT (DMD I) day 19, 5 days after antibiotic selection initiation (left), day 21, 7 days under antibiotic selection (right).**

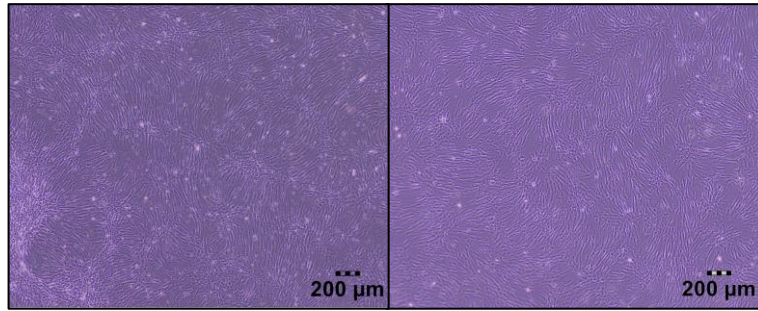


**Figure 40: DMD IV (left) and WT IV (right) on day 28 regained confluency under antibiotic selection with 1.5  $\mu\text{g}/\text{ml}$  puromycin.**

A negative control approach of non-transduced and equally antibiotic-selected myoblasts did not detect display any visible growth for both cell lines after addition of puromycin. Single, morphologically changed cells survived until day 25.

### **CDK4-transduction**

Equally, in each case two approaches of P507/18 and 515/18 were transduced with of pBABE-hygro-CDK4 R24C-containing viral supernatant on day 12, 13 and 14, called DMD II or V and WT II and V. DMD II and WT II would be additionally transduced with pBABE-puro-hTERT containing viral supernatant on days 23 and 24 (Figure 22).

The effect of antibiotic-induced cell detachment was most drastic in singly hygromycin-selected cultures, as already exhibited in antibiotic resistance testing experiments. Merely single vital cells survived the first days after initiation of antibiotic selection, leading a way to stable regrowth under antibiotic selection in gradually increasing concentrations of hygromycin up to 300  $\mu\text{g}/\text{ml}$  at day 43 (Figure 41 and Figure 42). This regrowth was visibly slower than in hTERT-transduced cultures.

A negative control approach of non-transduced and equally antibiotic-selected myoblasts showed the same marked drop in cell confluency and did not detect any visible growth for both cell lines after addition of hygromycin. Single, morphologically changed cells survived until day 38.

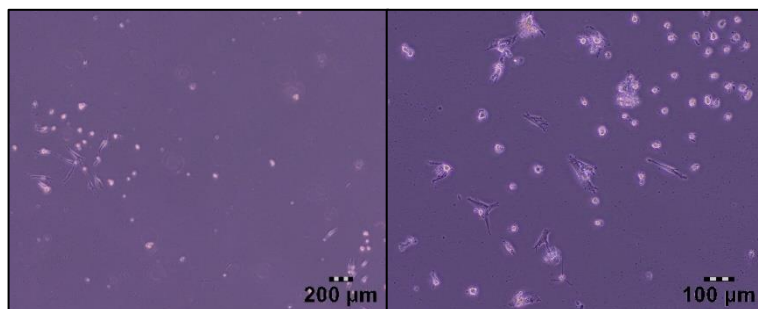


**Figure 41: Visualization of sharp decline in cell confluency on day 19, four days after addition of hygromycin, single cells with signs of colony-like growth (DMD II left; WT II right).**

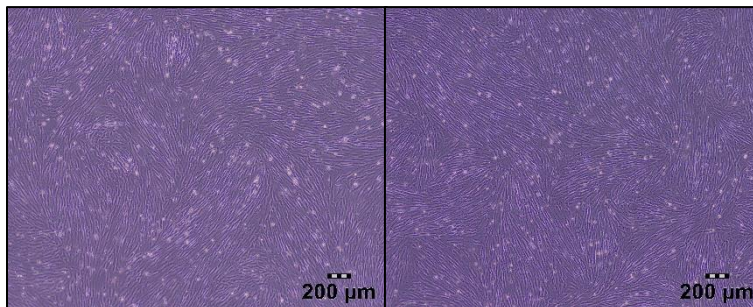


Figure 42: DMD V (left) and WT V (right) on day 28 regained confluency under antibiotic selection.

## Double transductions

### Simultaneous transduction of CDK4 and hTERT

One approach for each of P507/18 and P515/18 respectively was co-transfected on days 12, 13, and 14 with two viral supernatants containing both genes used for transduction. These were designated DMD VII and WT VII. Antibiotic selection was started immediately after transduction at a concentration of 0.05 µg/ml puromycin and 5 µg/ml hygromycin at day 15. Comparably to the other approaches, a major decline in confluency was visible (Figure 43). Regrowth occurred in form of insular-shaped colony formation (Figure 44). In spite of gradual increase in antibiotic concentrations up to a maximum amount of 0.3 µg/ml puromycin and 30 µg/ml hygromycin on day 38, DMD VII and WT VII expressed a stable growth which required not only expansion on several culture plates, but also repeated splitting that allowed additional storage of cryo-aliquots (Figure 45 and Figure 46).

Out of all transduced cell lines, DMD VII and WT VII showed the fastest proliferation for their respective basic cell line, which revealed that the DMD cells were comparatively slightly more proliferative.

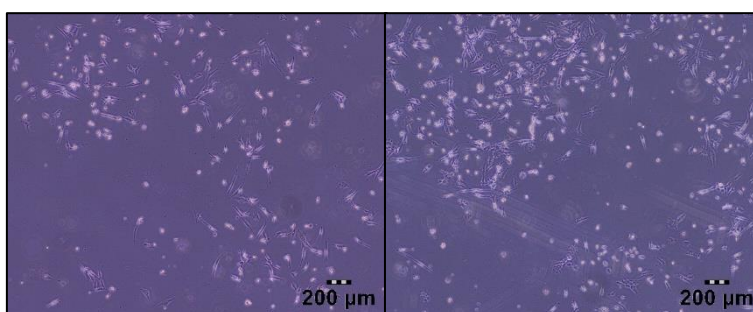


Figure 43: Insular-shaped regrowth pattern of DMD VII (left) and WT VII (right) on day 19.

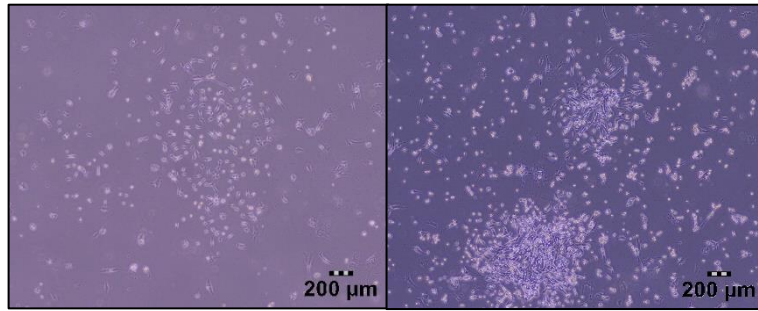


Figure 44: Growth pattern of DMD VII (left) and WT VII (right) on day 20.

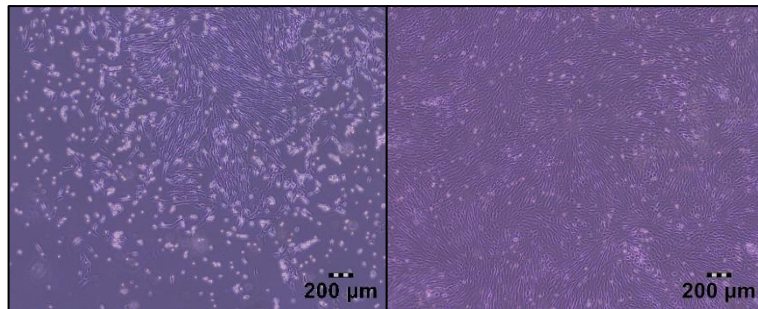


Figure 45: DMD VII (left) and WT VII (right) on day 28.

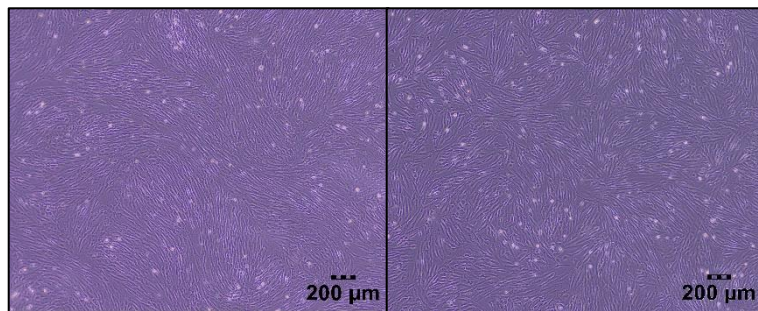
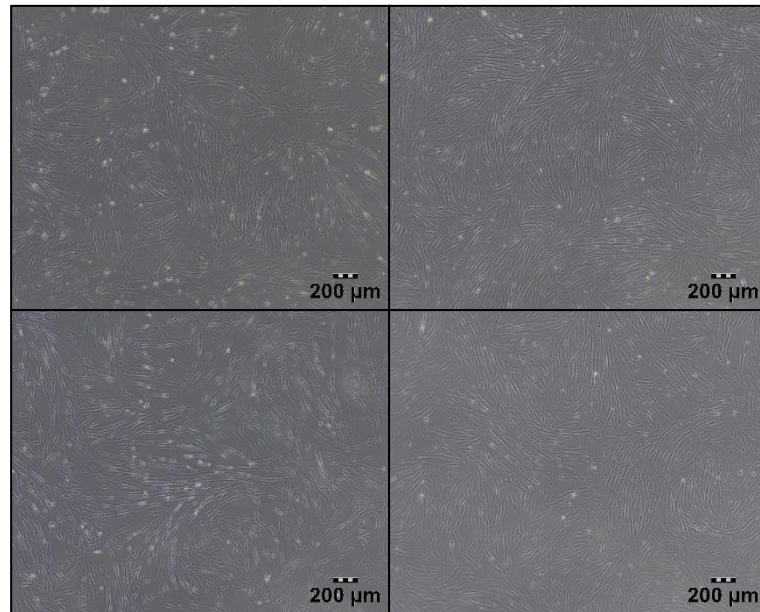
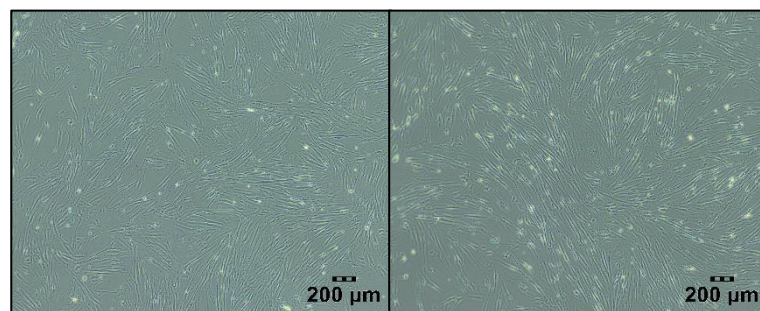


Figure 46: DMD VII (left) and WT VII (right) on day 38 under maximum antibiotic selection concentration (0.3 μg/ml puromycin and 30 μg/ml hygromycin).

As all other cell lines, DMD VII and WT VII were frozen as cryo-aliquots and stored at - 80 °C on day 42. Aliquots of DMD VII und WT VII were thawed at day 43 alongside age-matched controls of DMD VI and WT VI. Half of the cell population was further subjected to antibiotic selection with 0.2 µg/ml puromycin and 20 µg/ml hygromycin until day 59 (DMD VIIa and WT VIIa). The other half was cultured in normal growth medium without an added antibiotic selection agent (DMD VIIb and WT VIIb). These two approaches for each cell line exhibited a visibly faster growth of the DMD VIIb and WT VIIb, although all transduced cell lines seemed to have retained their potential for advanced, but slightly slower proliferation (Figure 47).



**Figure 47: Comparison of DMD VIIa (top left), DMD VIIb (top right), WT VIIa (bottom left) and WT VIIb (bottom right) on day 57, being under antibiotic selection with 0.2 µg/ml puromycin and 20 µg/ml hygromycin; DMD and WT VIIb were non-selected.**



**Figure 48: 9-DMD VII (left) and 9-WT VII (right) on day 206.**

During regular splitting of the cell culture, various daughter cultures were derived in different sized culture plates. Additionally, regular cryo-aliquots were stored at - 80 °C. The best proliferating cultures of DMD VII and WT VII originate from a culture derived from DMD VIIa and WT VIIa on day 74 and grown in a six-well. In general, cell confluency seemed to be a crucial variable for proliferation speed and capacity of the cell lines. In this approach, total cultivation

time for 9-DMD VII and 9-WT VII accumulated to more than 250 days with visible cell proliferation and overall comparability of morphologic appearance until the end of cell culture (Figure 48).

A negative control approach of non-transduced and equally antibiotic-selected myoblasts did not display any visible growth for both cell lines after initiation of double-selection. Single, morphologically altered cells survived until day 31 (P515/18) and 28 (P507/18).

### Iterative transduction

DMD I and WT I were subject to a second transduction with viral supernatant containing pBABE-hygro-CDK4 R24C. For DMD II and WT II a second transduction with pBABE-puro-hTERT took place. The detailed course before these second transductions on days 23 and 24 has been described above (Figure 22)

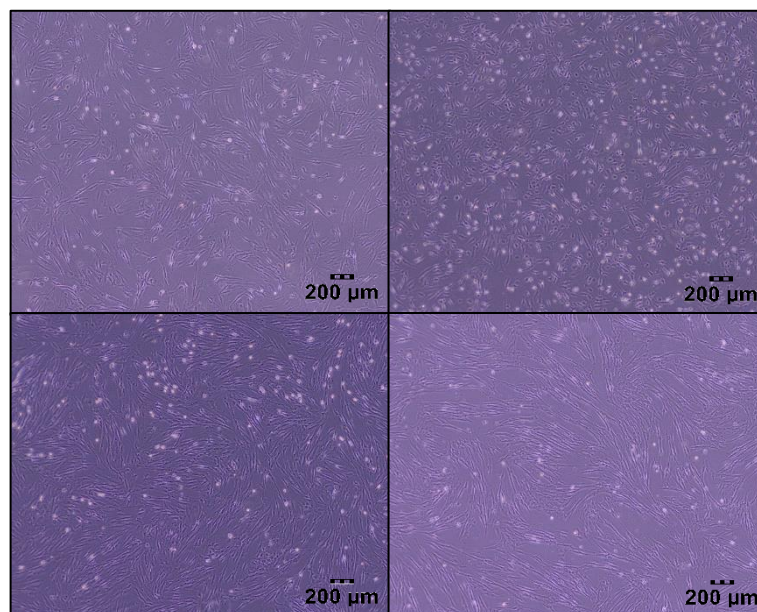


**Figure 49: DMD I (top left) and WT I (top right) and DMD II (bottom left) and WT II (bottom right), all on day 38 under selection with 0.3 µg/ml puromycin and 30 µg/ml hygromycin.**

In both cases the antibiotic selection was gently increased with every change of medium. In general, DMD I and WT I did feature a faster growth than DMD II and WT II. Interestingly, DMD I and WT I featured the same decline of cellular confluency with appearance of detritus and even more widespread detachment than after their first transduction with a different vector. After this loss of confluency, especially distinctive in WT I, a stable regrowth until freezing on day 42 occurred. In total, these iteratively transduced myoblasts featured a visibly slower expansion than DMD VII and WT VII (Figure 49).

Negative control approaches of non-transduced and equally antibiotic-selected myoblasts did not show any visible growth for all cell lines after initiation of double selection. Single, morphologically altered cells survived until day 34 (WT II) and 38 (DMD I, II and WT I).

### Control cells

One approach, each for P507/18 and P515/18, was performed without a selection agent, to serve as control cells for growth. Both, designated DMD VI and WT VI, showed stable and continuous growth over the first 43 days with more population doublings than DMD VII and WT VII, requiring splitting and storage of cryo-aliquots (Figure 58 and Figure 59).

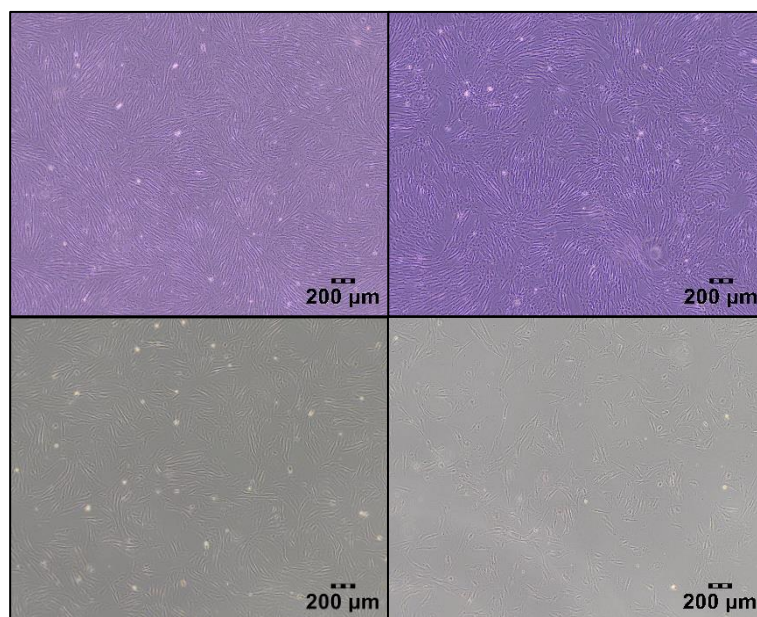


**Figure 50: DMD VI (top left) and WT VI (top right) on day 38, DMD VI (bottom left) and WT VI (bottom right) on day 53**

As all of the cell lines, DMD VI and WT VI were frozen on day 42. Regrowth was visible until day 59, whereafter a decrease in growth did not allow for reaching a high confluency anymore, although there was visible growth. Furthermore, the ratio of irregularly shaped cells with development of vesicles increased or cellular death was increasing. The last splitting of both cell lines, DMD VI and WT VI, took place on day 59.

These cell lines were continued to be cultured until day 221, where only single, morphologically disturbed cells without signs of proliferation remained (Figure 51).

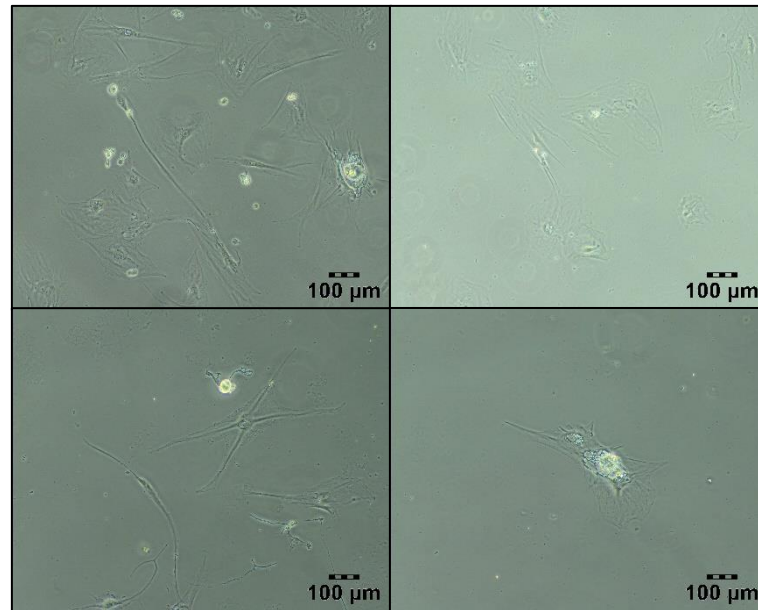


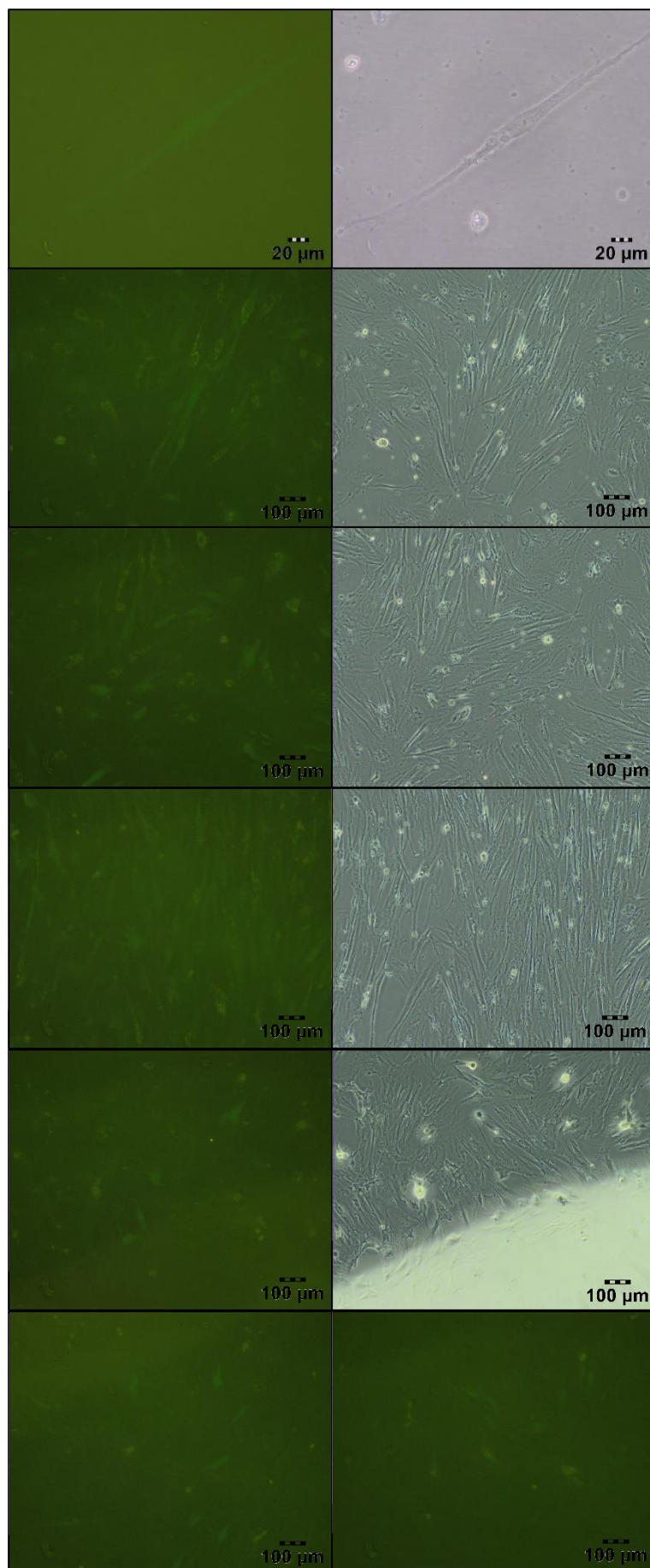
**Figure 51: Irregularly shaped cells on day 129; DMD VI (top left) and WT VI (top right); DMD VI (bottom left) and WT VI (bottom right) on day 221.**

### **eGFP-Transduction**

P507/18 and P515/18 were transduced with pBABE-neo-IRES-eGFP-containing viral supernatant as a positive control, called DMD III and WT III. Transduction took place on growth days 12, 13 and 14 with the above-mentioned viral supernatant and selection was increased in steps from 40 µg/ml G418 to 120 µg/ml G418 on day 21 (Figure 22).

Expressing the same growth characteristics as for the other cell lines, DMD III and WT III did also show an initial decrease of cellular confluency, albeit much lower in DMD III, most likely due to the intrinsic neomycin resistance cassette in P507/18 cells, before regrowth. Before the second round of viral transduction on days 23 and 24, DMD III and WT III were at a confluency of 50 % and 20 %, respectively. Antibiotic selection was tightened after the second round with increasing concentration of G418 up to 500 µg/ml on day 34, which led to only a slight decrease in confluency with continued expression of a stable cell population in both approaches, DMD III and WT III. Stable cellular expression of GFP was detected on day 48, i. e. 24 days after last transduction, in both cell lines. Before, single transient GFP-positive cells had appeared in WT III on day 23 (Figure 52).

**Figure 52: (next page): green fluorescent cells: 1. row: WT III on day 23; 2. row: WT III on day 53; 3. row: WT III on day 55; 4. row: WT III on day 82; 5. row: DMD III on day 48; 6. row: DMD III on day 53**



Some DMD III cells exhibited different morphologic characteristics under selection with G418, with larger cells and a spike-like structure of the exterior boundary of the cell, as visible in Figure 53.

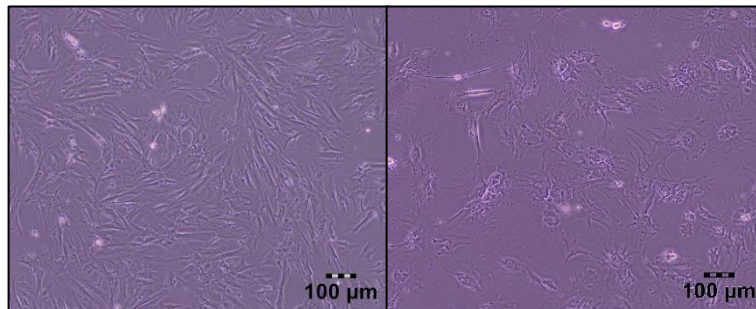


**Figure 53: Morphologic features of DMD III on day 14 (left) without selection and on day 28 (right) under selection with 275 µg/ml G418.**

A negative control approach of non-transduced and equally antibiotic-selected myoblasts did not reveal any visible growth for P515/18 cells after initiation of selection with G418. Single, morphologically changed cells survived until day 38. Due to the intrinsic neomycin resistance cassette, antibiotic selection of P507/18 could not be carried out effectively, resulting in a non-transduced culture with a confluency of more than 50 % under maximum antibiotic selection with a G418 concentration of 500 µg/ml on day 42. No GFP-positive cells were detected in this control culture.

### Transduction efficacy

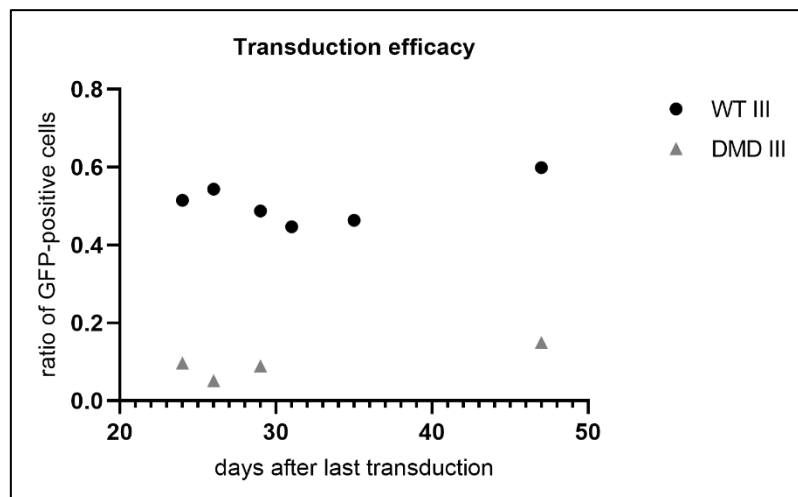


**Figure 54: Transduction efficacy measured by ratio of GFP-positive transduced porcine myoblasts under antibiotic selection. The timeline shows days after last transduction.**

Transduction efficacy was measured by the GFP-positive cell ratio in DMD III and WT III. Antibiotic selection was carried out to a maximum concentration of 400 µg/ml G418. Results showed that a significantly higher proportion of WT III cells was GFP-positive than of DMD III cells over the observed period.

### Morphological changes

In general, the morphology of transduced myoblasts did not differ from their non-transduced control group during the initial growth period. Younger cells tended to be smaller and more round shaped. Over time, their morphology changed to a slimmer appearance, most likely because of interaction with other cells. Nevertheless, in older cell cultures, cells with the morphology comparable to those of younger ones were still frequent.

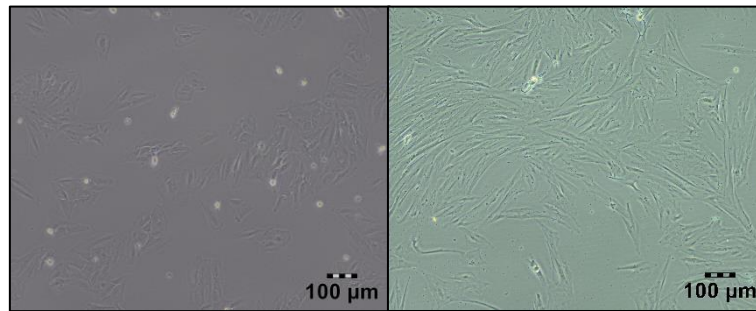


Figure 55: Comparison of cell morphology of P507/18 on day 9 (left) and 9-DMD VIIa on day 178 (right).

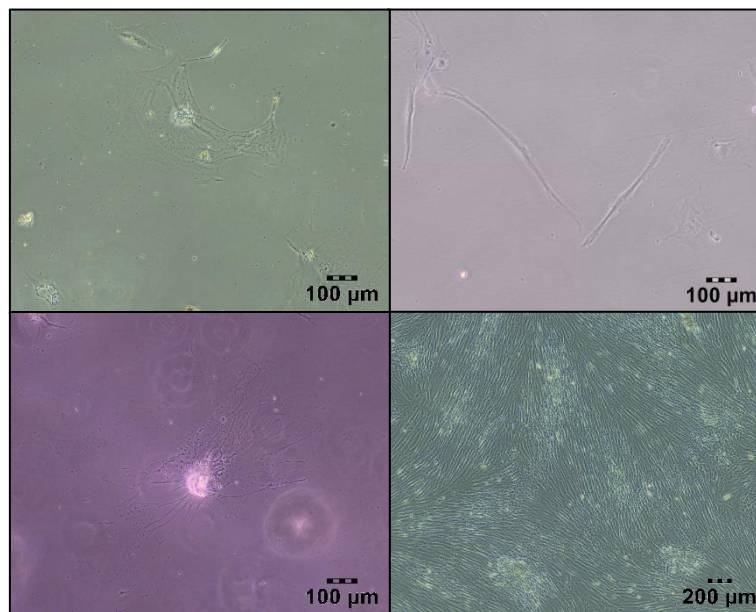


Figure 56: Typical apoptotic cells with a flat, irregularly shaped morphology on day 213 (upper left) and WT VIIb on day 95 (bottom left); spontaneous myotube-like formation and irregularly shaped P515/18 cells on day 67 (upper right); cluster formations of DMD VII on day 62 (bottom right).

With increasing duration of cultivation, some cells featured a larger cell body, progressively displaying vacuoles. These appeared in cell cultures of all ages, although the ratio seemed to increase with age. Furthermore, cell nuclei increased in size and were more roundly shaped (Figure 56). This transition can be seen as a sign of cellular senescence and was particularly common in cells with a more isolated location in the culture. Cells were also susceptible to

exterior factors, i. e. physical stress induced by removal of glass cover slips from a growing culture. Additionally, in some cultures spontaneous formation of myotube-like cells took place.

As visible above, the growth pattern of the myoblast cultures did not alter from the initial, younger P507/18 to 9-DMD VIIa cells well beyond day 250 of growth. At higher confluencies, cluster-like structures became visible.

### Specific challenges of porcine cell culture

Porcine myogenic cells are a cell type not frequently used for *in vitro* experiments. Perfect cultivation conditions for these cells have not been well established yet.

Proliferation speed and capacity varied widely on different parameters, including the choice of culture dishes. Porcine myoblasts required a longer period of trypsin application before splitting, i. e. more than the usual five minutes. Irregularly shaped myoblasts often did not detach at all. The usage of Accutase seemed to speed up the process, although still been markedly slower than comparable human myoblasts or fibroblasts as 3T3. To maximize efficacy of the used agent, extensive washing of the culture with PBS or a short rinsing of cells with trypsin was carried out before, leading to a decreased incubation time and amount of trypsin used and therefore limiting damage to the cells.

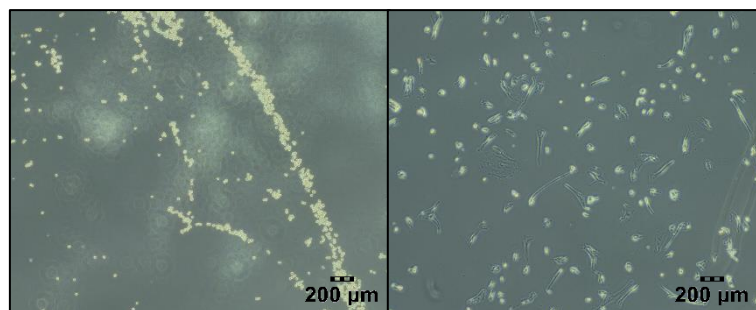


**Figure 57: DMD VII cells under trypsinization exhibiting trabecular-shaped formation of trypsinized cells (left), DMD VI cells after trypsin application with cell remnants (right).**

Additionally, growth seemed to slow down after trypsinization for a period of one to two days, especially in older cultures. Furthermore, porcine myoblast cultures seemed to be dependent on maintenance of appropriate cell confluency. Very low cell densities, e. g. up to 20 %, required a considerably longer period of time for visible growth than higher confluencies, e. g. more than 50 %. Single cells regularly showed signs of senescence and even apoptosis.

Another feature, highlighted in the porcine myoblast culture, is the sensitivity to frequent cycles of splitting, probably due to increased stress. In general, P507/18 seemed to have a larger resilience towards these stressors than P515/18 cells. A regular interval of splitting every three

to four days proved to be the best option. Longer intervals resulted in a visible slowdown of cell proliferation, although a return to the optimal growth regimen led to restoration of growth capability. Additionally, only partial removal and re-supplementation of growth medium, leading to a mixture of fresh and previous growth medium (in terms of a “conditioned” medium), seemed to promote the proliferation ability of the cells.

Another noteworthy observation is the different growth pattern and speed depending on size and material of the culture plates and their coatings. The best choice of size seemed to be culture plates with a diameter of 3.5 cm (area of 9.62 cm<sup>2</sup>) and 8.5 cm (area of 56.75 cm<sup>2</sup> in area). Larger and smaller plates were only used in the event of unusually large or small amounts of cells to maintain optimal confluency. Growth on glass cover slips, placed in plastic wells, did not show a visible difference to plastic but frequently led to detachment of cells during medium change or application of PBS for washing. Uncoated glass cover slips were frequently overgrown on both sides. Cell proliferation in glass chamber slides with and without coating in general lagged behind considerably.

### VII.5.1. Cell doublings and cell counting

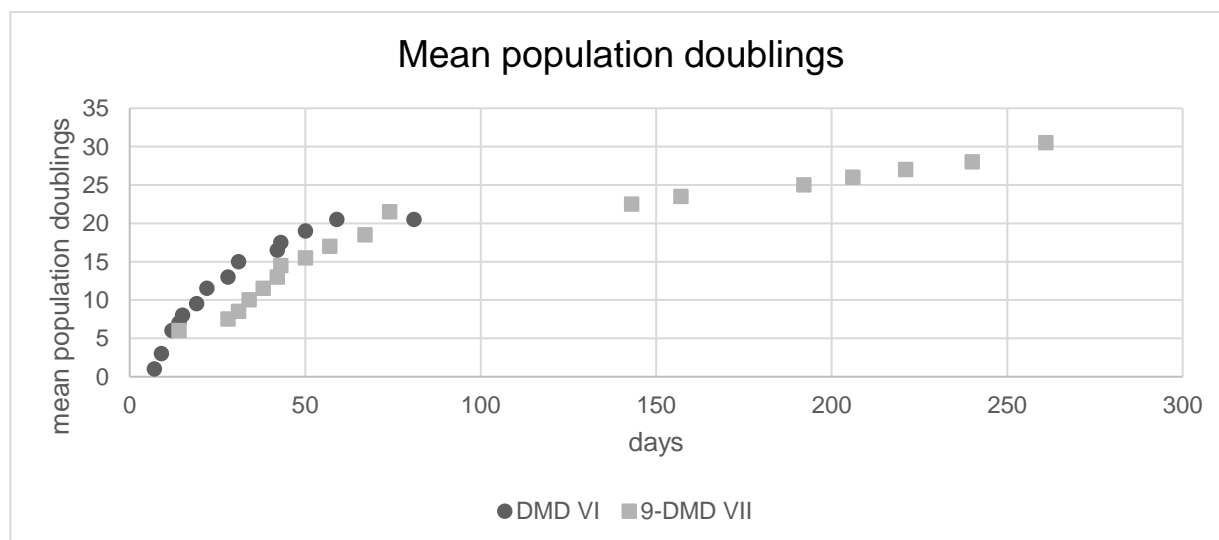


**Figure 58: Estimated mean population doublings DMD VI and 9-DMD VIIa**

Transduced cell lines showed a significantly longer growth period compared to their non-transduced counterparts. The latter exhibited a significantly slowed growth and even a reduction in cell confluency and changes in cellular morphology indicating senescence after the last event of splitting on day 59. All cell lines were subject to freeze/thaw cycles on days 42 and 221 of growth. Proliferation of these cell lines was monitored well beyond day 261 with visibly preserved proliferation capacity and expansion capabilities of 9-DMD VIIa and 9-WT VIIa. No quantification took place after day 261. In conclusion, 9-DMD VIIa exhibited more estimated

Results

population doublings than 9-WT VIIa, although both transduced did grow longer and doubled in population sizemore often than their non-transduced age-matched control cell line.

Automated cell counting did not provide consistent cell numbers in duplicates, often leading to non-evaluable results. These effects are most likely being aggravated by the reduced

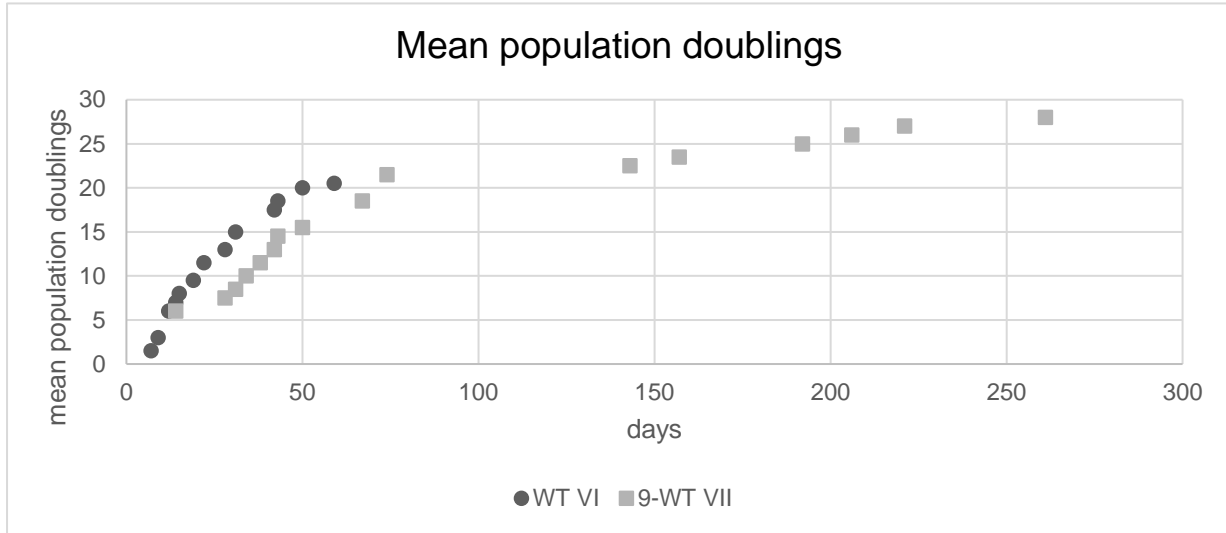


**Figure 59: Estimated mean population doublings WT VI and 9-WT VIIa**

detachment of porcine myoblasts after application of trypsin or Accutase as described above. The data for the figure below was therefore generated by manual counting.

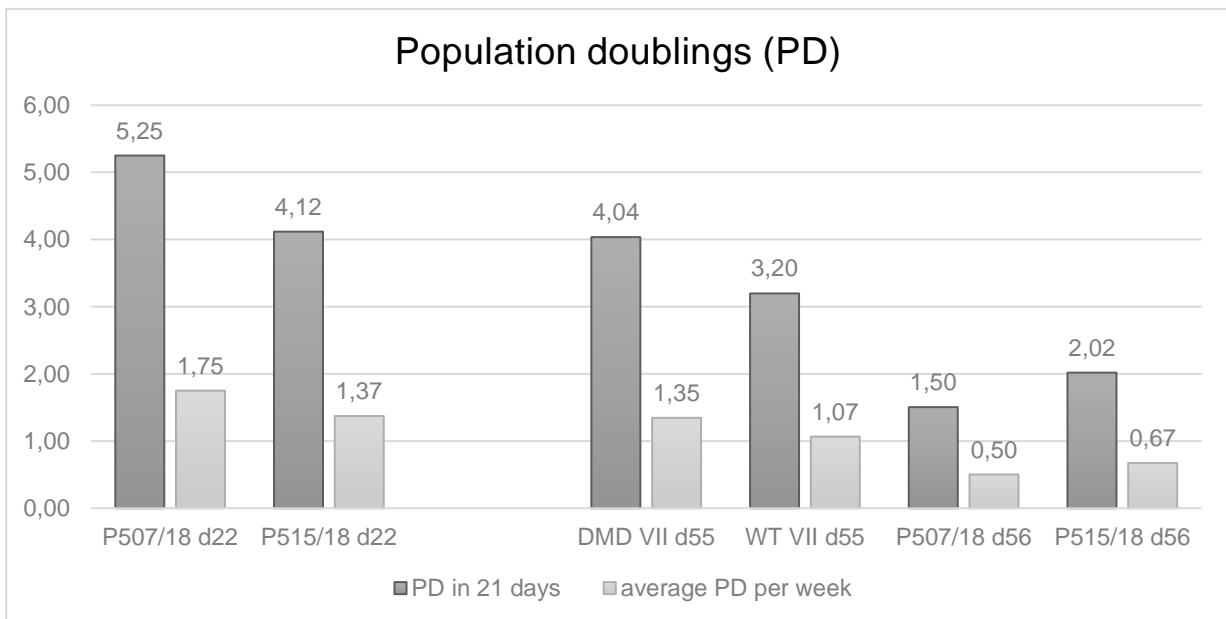


**Figure 60: Calculated population doublings based on consecutive counting for a period of 21 days for transduced and non-transduced porcine myoblasts at different age.**

The younger, non-transduced cell lines P507/18 and P515/18 exhibited significantly more population doublings for the period of time measured than older cultures of the same cell lines. Transduced cell lines, i. e. DMD VII and WT VII from day 55 on, retained their ability for faster population doublings. The figures above represent continuous counts, calculated from the

number of cells at day 1 and 21 of the period of measurement. DMD VII was the only cell line to exhibit negative growth, i. e. loss of confluency, between the points of measurement at days 7 and 14 and accelerated growth after day 14. A week-by-week-assessment would have increased the number of real population doublings to 5.32, i. e. 1.77 per week, a figure comparable to the growth speed of young, non-transduced P507/18 cells.

### VII.5.2. Limited dilution

Approaches of limited dilution were carried out to test colony-forming abilities of transduced cells. DMD VII and WT VII cell lines were diluted according to the indicated protocol. These cells were cultivated using growth medium without selection agent.

Dilution of DMD VII and WT VII cell lines into 96 well cell culture plates, both at day 75 of growth, led to formation of colonies in various wells. Well 30-/31-A12, seeded in normal, non-diluted cell density, served as a positive control with an overgrown cell layer. Two out of 95 wells with WT VII and eight out of 95 wells with DMD VII showed clear colony formation and were transferred to 48 well cell culture plates for further expansion.

Younger cell lines of DMD VII and WT VII, cryo-preserved at day 44 of growth, were diluted as indicated above. This time, colony formation was detected in three out of 95 WT VII-wells and five out of 95 DMD VII-wells.

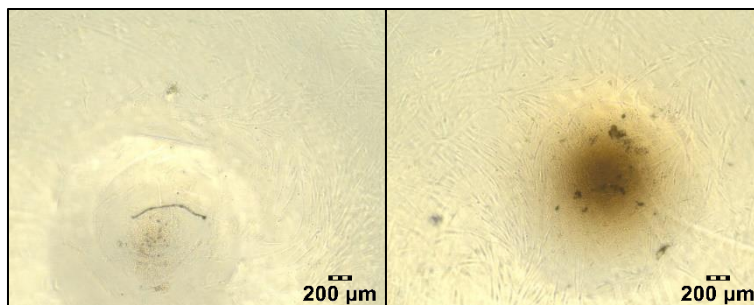


**Figure 61: Growth pattern of cell colonies in 96-well culture plate on day 67; 30-G5 WT VII left, 31-H6 DMD VII right**

Transfer of highly confluent cell colonies in 96 well plates to 48 well plates regularly led to a loss of confluency and increased recovery times. Nevertheless, significant cell colony forming took place in various 48 well culture plates, i. e. for WT VII 30-G5 and DMD VII 31-H1, -H8 and H9.

It was possible to monitor the effect of excessive splitting or, equivalently, the transfer into larger wells regularly leading to a loss in confluency and proliferation capacity, indicating a need of a certain cell density for consistent growth. Less intense splitting led to a significantly better outcome.

### VII.5.4. Fusion of myoblasts

In addition, qualitative fusion experiments in porcine myoblasts in various stages of growth from day 40 to day 259 were conducted to prove comparable characteristics to non-transduced cells and cells with known myogenetic properties. Myotubes featured an increased number of nuclei which were positioned in the cell periphery near the sarcolemma. In cell culture, they differed in terms of length and cell diameter, also featuring birefringent properties of the cell membrane in conventional light microscopy.

Although development of spontaneous multi-nucleated cells did occur in cell culture, fusion experiments lead to an increased number of cells with a higher number of nuclei in cells with increased length. Additionally, these cells showed a typical birefringent sarcolemmal silhouette against the background of the cell culture plate. Fusion characteristics of transduced cells did not visibly differ from non-transduced myoblasts, although fusion efficiency was more clearly visible in DMD cells than in WT ones. In general, the porcine cells were lagging behind the developmental stages of well characterized human myogenic cells as a control.

#### Transduced cells

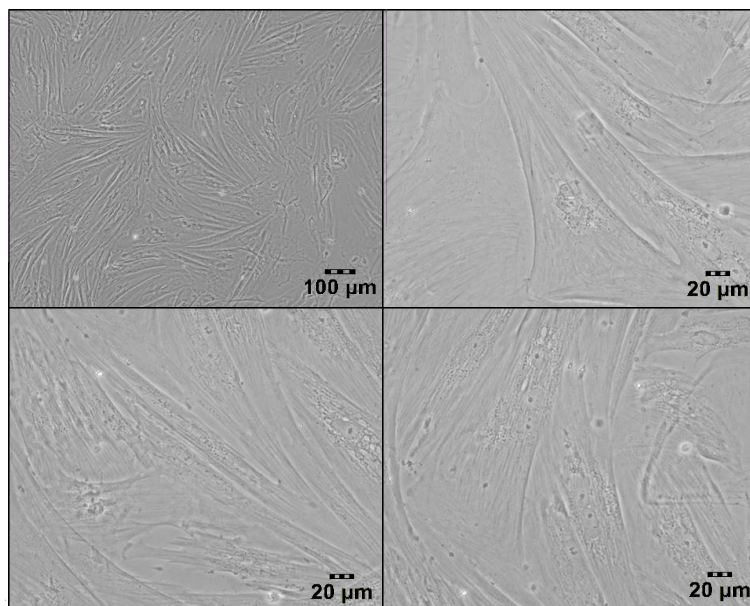


Figure 62: DMD VII d78 after 96 hours of fusion: myotube-like formations with multiple nuclei

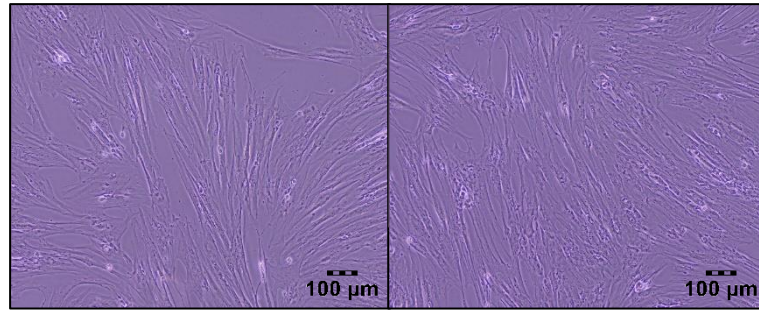


Figure 63: DMD VII d95 after 21 days (left) and 28 days (right) of fusion



Figure 64: 9-DMD VIIa d259 after 96 hours of fusion MG/RC

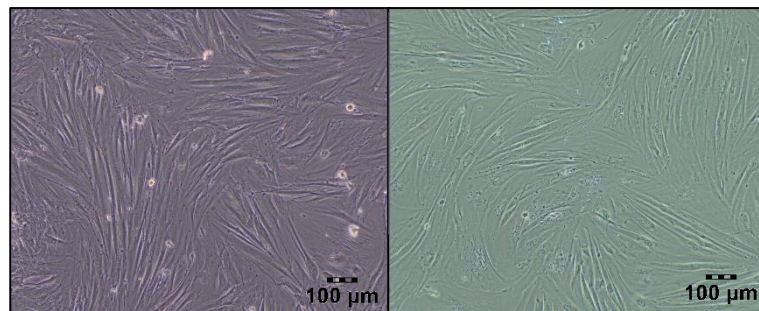


Figure 65: WT VII on day 74 after 24 hours of fusion (left) and on day 78 after 96 hours of fusion (right)

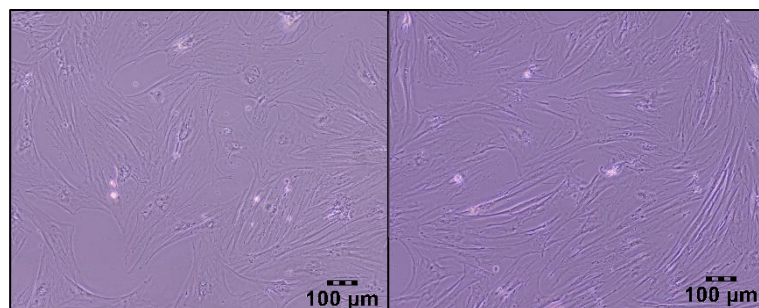
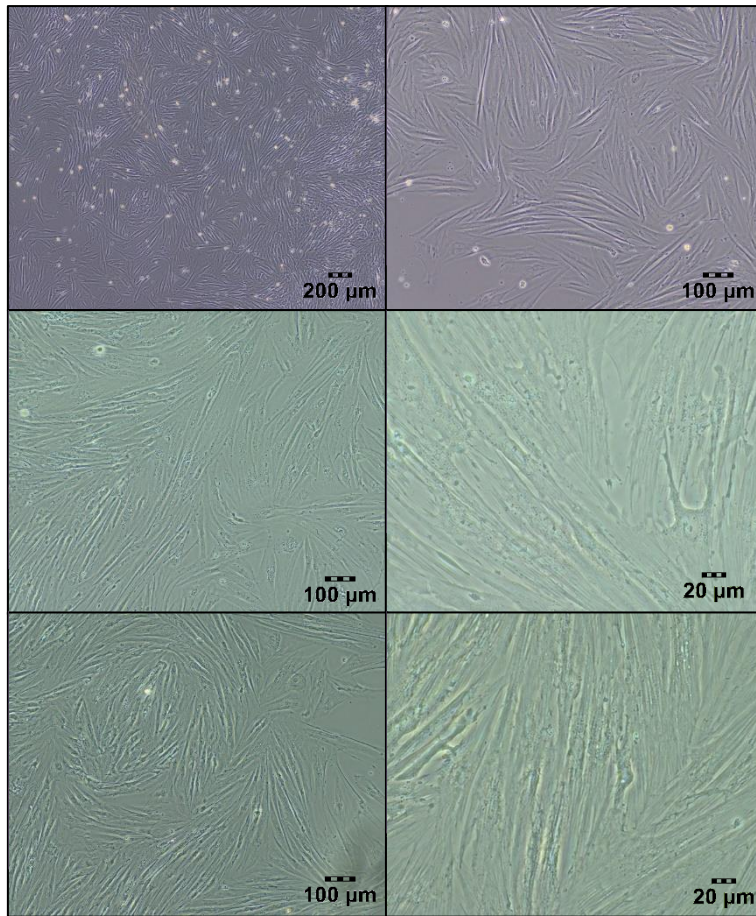
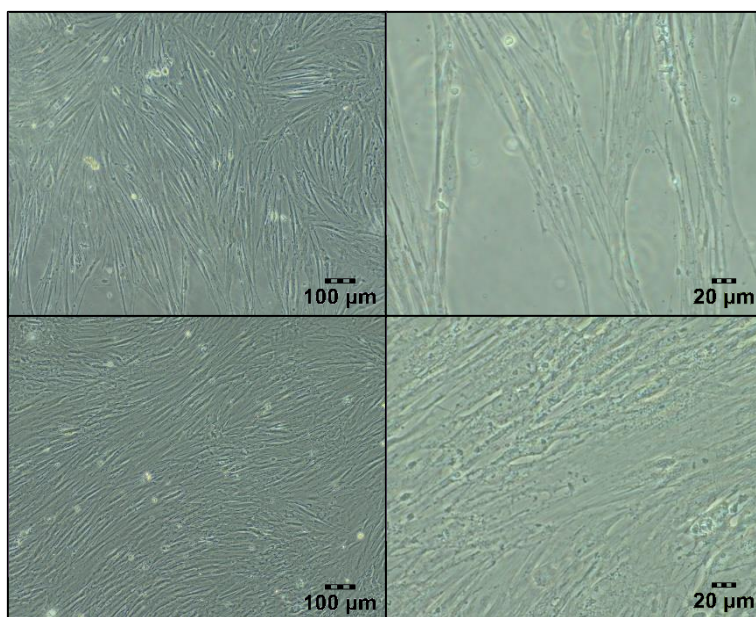


Figure 66: WT VII d95 after 21 days (left) and 28 days (right) of fusion

**Non-transduced cells**



**Figure 67: P507/18 d45, after 24 hours of fusion (upper row); after 96 hours of fusion (middle row), P507/18 d79 after 96 hours of fusion (bottom row)**



**Figure 68: P515/18 on day 45 (top row) and on day 78 (bottom row) after 96 hours of fusion**

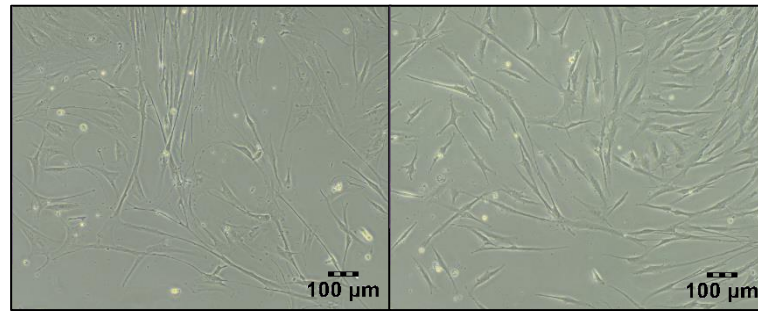


Figure 69: P507/18 (left) and P515/18 (right) on day 38 after 15 days of fusion

### Control cells

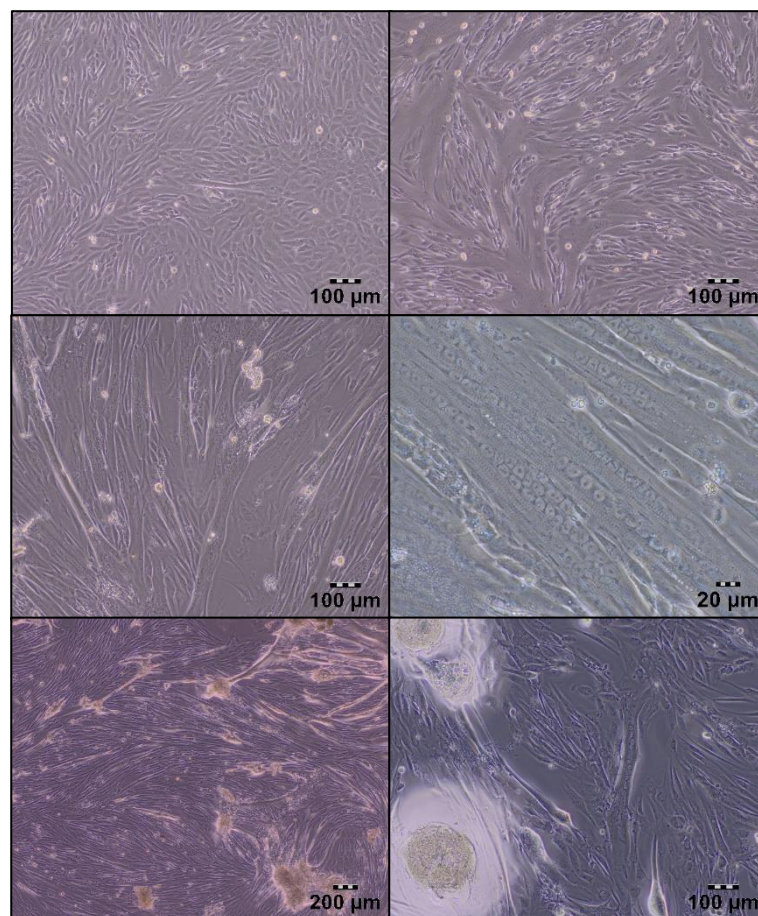


Figure 70: Beginning of myotube fusion on day 3 (upper row), 0208ct7 control cells after 6 days (middle row) and 13 days (bottom left) and 14 days (bottom right) of fusion

To verify the functionality of the used approach, we tested 0208ct7 with known myogenic potential as control culture. 0208ct7 cells began forming myotubes after six days on fusion medium. On day nine, rhythmic contractions of the formed myotubes were visible.

### VII.5.5. Immunofluorescence staining

Immunofluorescence staining for desmin was carried out to monitor expression of myogenic properties in fused DMD VII and WT VII porcine cell cultures before and after transduction. As a result, transduced porcine cell cultures did feature desmin as a stainable marker. Control staining was carried out using non-transduced non-fused and fused P507/18 and P515/18 porcine cell cultures and fused immortalized human myoblasts 0208ct7. Age-matching of non-transduced porcine cell cultures with non-transduced ones in older staining approaches could not be carried out due to the lack of consistent cell proliferation of non-transduced cells.

#### DMD VII

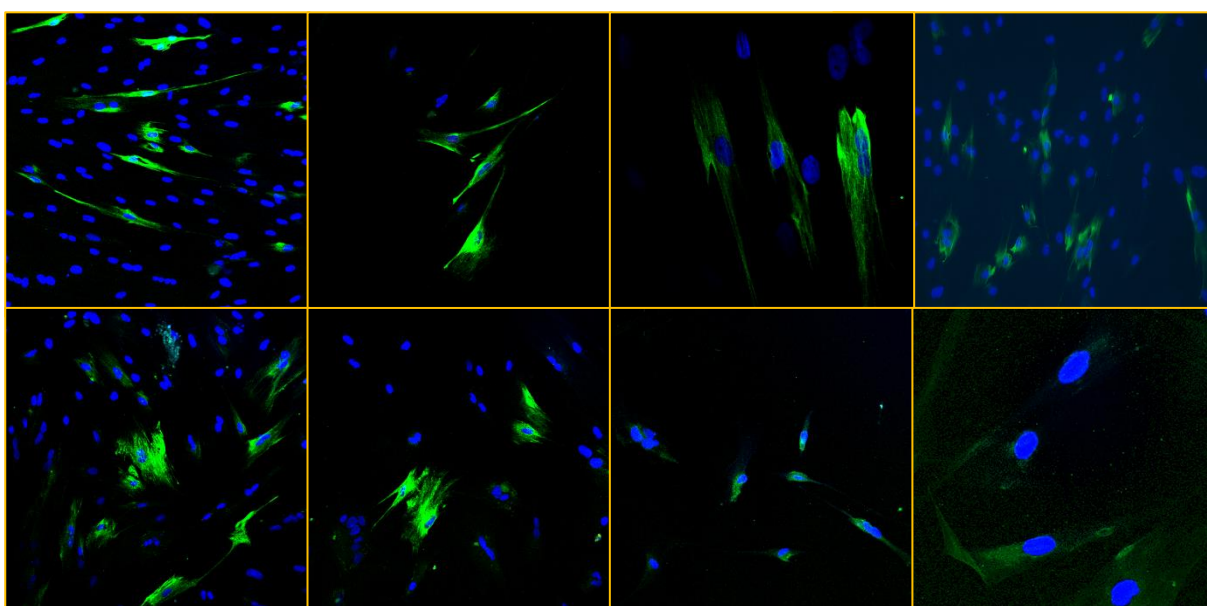


Figure 71: DMD VII cell line, top row from left: on day 60 after 60 hours of fusion (1 to 3), day 54 after 6 days of fusion (4), bottom row from left: day 75 after 24 hours of fusion (1 and 2), day 100 after 4 days of fusion (3) and day 258 after 4 days of fusion (4), stained for desmin and DAPI.

#### WT VII

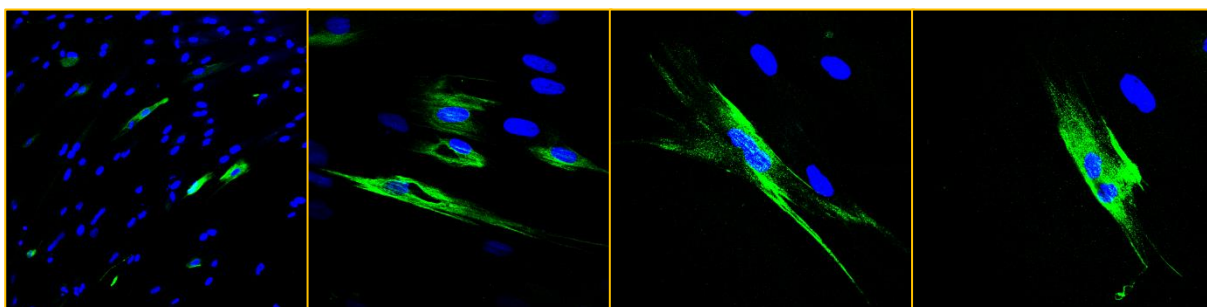
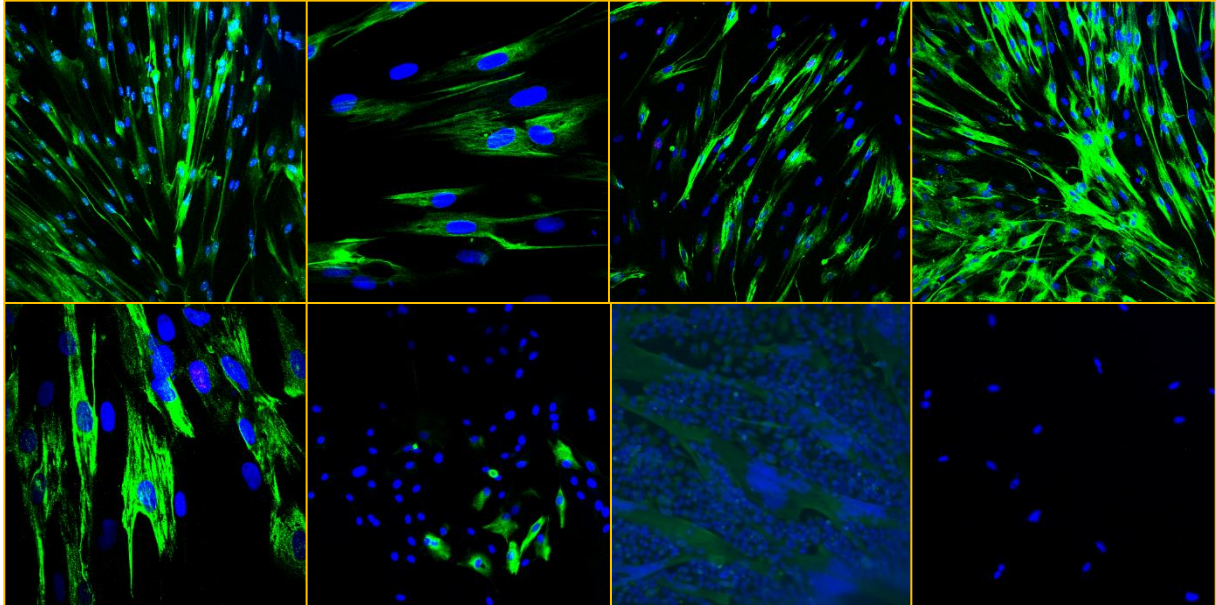


Figure 72: WT VII cell line on day 60 after 60 hours of fusion (1 to 3) and day 75 after 24 hours of fusion (4), stained for desmin and DAPI.

Evidence for desmin expression was found at all tested age stages, up to day 258 for DMD VII and day 75 for WT VII. Although these experiments were designed for qualitative rather than quantitative assessment, the samples suggested a decline in ratio of desmin-positive cells in culture.

#### Non-transduced and control cells



**Figure 73:** First row from left: fused P507/18 cells on day 27 after 60 hours of fusion (1 and 2), day 45 after 24 hours of fusion (3), fused P515/18 cells on day 27 after 60 hours of fusion (4); second row from left: day 41 after 24 hours of fusion (1), non-fused P515/18 cells on day 15 (2), fused 0208ct7 cells (3), all stained for DAPI and desmin, fused DMD VII cells on day 60 after 60 hours of fusion, stained only for secondary antibody (4).

Non-transduced control cells of early passages did express a high ratio of desmin-positive cells after fusion. However, these samples did also suggest a loss of desmin-positive cells over time, supporting a trend visible in the data of the transduced cells. Some non-fused P507/18 and P515/18 cells did also express desmin. Control approaches of desmin staining of fused 0208ct7 led to visualization of myotubes. Application of only secondary antibody as a negative control did not lead to a detectable signal.

### VII.6. Further molecular genetic analyses

Transduced myoblasts and transfected Phoenix amphi producer cells were subject to further molecular genetic analyses.

#### VII.6.1. Sequence analysis in myoblasts

PCR testing of DMD VII and WT VII on day 60 and consequent sequence analyses revealed no detection of env- or gag-pol-gene sequence.

Integration and transcription were verifiable completely in case of the *CDK4* gene and partially for *hTERT* gene in DMD VII cells. Sequencing of cDNA showed proof of adjacent vector sequences at the 3'-end in cases of *hTERT* and *CDK4* and additionally at the 5'-end in case of *CDK4*. Complete genomic integration was detected for *CDK4* in WT VII. Integration of 5'- and 3'-LTR was proven in DMD VII and WT VII by high/low-temperature-annealing. In case of WT VII, 3'-LTR with an adjoining vector sequence of 100 bp seemed to have undergone a recombination event with a chromosomal locus, sharing high homology with the 3'-end of the hemicentin gene, which was also proven by a confirmatory PCR.

### VII.6.2. Sequencing of *CDK4* and *hTERT* genes in producer cell lines

To detect the correct integration of plasmid DNA in the Phoenix amphi cells, either transfected with pBABE-puro-hTERT or pBABE-hygro-CDK4 R24C, gDNA from these cells was extracted and amplified, using the indicated primers pBABE-3' and pBABE-5'. The insert size of *CDK4* is 1'000 bp and 3'500 bp for *hTERT*.

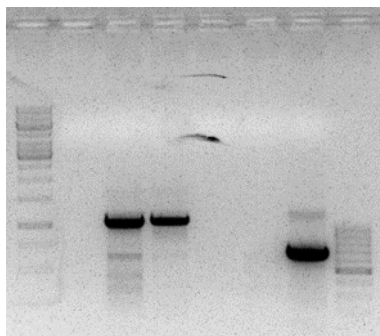


Figure 74: Gel electrophoresis; from left to right: 1'000 bp ladder, no template control pBABE-3'/-5'-primer, pBABE-hygro-CDK 4 R24C Phoenix amphi cell gDNA (III+IV), pBABE-puro-hTERT Phoenix amphi cell gDNA (V+VI), positive control DNA, 100 bp ladder

Agarose gel electrophoresis revealed a PCR product of just over 1'000 bp for the *CDK4* cells. There was no PCR product synthesis in gDNA from *hTERT* cells. A negative control of primers without gDNA template did not show any PCR product synthesis. A positive control of human gDNA amplified with VCP\_2-3R/VCP\_2-3F resulted in the expected band formation of 790 bp.

A BLAST alignment of the sequencing result of the extracted PCR product and the provided sequence of pBABE-hygro-CDK4 R24C confirmed the correct sequence.

### VII.7. Molecular genetic analyses of hereditary degenerative neuromuscular diseases

For further molecular genetic analyses of hereditary degenerative neuromuscular diseases, further investigation of three patients, with assumed mutations in the *VCP* or *GNE* gene, were conducted.

### **VII.7.1. Patient #1**

#### **Clinical course**

Patient #1, aged 62 at genetic examination, developed a steppage gait in his mid-forties. Walking impairment increased until he was not able to walk anymore. Additionally, the patient developed neuropsychiatric symptoms, with episodes of aggression and obsessions, which improved under quetiapine treatment, as well as palilalia and apathy.

The patient's medical history included arterial hypertension and operation for herniated disc at L4 - L5 level. The patient's family history was positive for neurologic disorders. His mother was diagnosed with presenile dementia and eventually died at the age of 63 years. One brother was diagnosed with amyotrophic lateral sclerosis in his forties and died subsequently at 53 years of age. The other brother developed behavioral symptoms at the age of 55 years.

In the clinical neurological examination, a diffuse wasting and severe symmetric muscle weakness in lower and upper extremities was striking, especially in the distal parts of the lower extremities. While pyramidal signs were absent, reflexes of lower and upper extremities were positive. Impaired conceptualization, decreased mental flexibility and disturbed motor programming contributed to an abnormal neuropsychological evaluation. Laboratory results excluded increased levels of creatine kinase or alkaline phosphatase. Electroneurography showed axonal damage and electromyography revealed diffuse myopathic changes and mild spontaneous activity. Skeletal scintigraphy showed no sign of Paget's disease of the bone. Cranial MRI revealed frontal lobe atrophy. Muscle MRI displayed atrophy and fatty degeneration or fibro-adipose tissue replacement in lower and upper limbs with relative sparing of the left M. biceps femoris. Furthermore, muscle biopsy showed severe and non-specific end stage changes with fibro-adipose tissue replacement.

#### **Genetic testing**

Exons 1 to 17 of the *VCP* gene were amplified using PCR according to the standard protocol. Agarose gel electrophoresis showed PCR fragments of appropriate size for all exons.

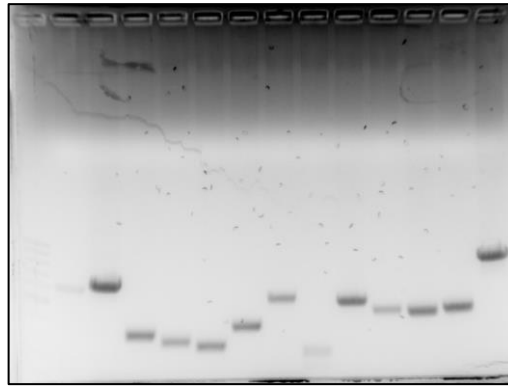


Figure 75: Gel electrophoresis, 100 bp ladder, exon 1, 2-3, 4, 5, 6, 7, 8-9, 10, 11-12, 13, 14, 15, 16-17 of the VCP gene (from left to right)

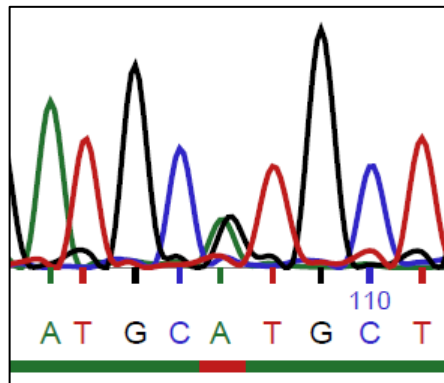


Figure 76: Electropherogram showing c.476G>A mutation in exon 5 of the VCP gene.

Sequencing of exon 1-17 revealed a heterozygous mutation in the *VCP* gene. c.476G>A led to a substitution of guanine by adenine and therefore an amino acid change from arginine to histidine p.R159H. A report of this patient has been published before [280].

## VII.7.2. Patient #2

### Clinical course

Patient #2, aged 80 at genetic examination, at first exhibited a slowly progressive weakness of the left arm at the age of 63, initially while working overhead. Clumsiness of the left hand and a difficulty to raise the left foot properly had been noted. At 66 years of age rising from squatting was no longer possible. Walking distance and speed were gradually decreasing.

The patient's medical history revealed atrial fibrillation treated with beta blocker, digoxin and phenprocoumon as anticoagulant drug and a previous ischemic stroke of the middle cerebral artery in the right capsula interna, most probably due to cardio embolism from atrial fibrillation. The patient's father experienced progressive muscular wasting starting in his forties, before dying from a stroke at age 73. The patient's older brother received a cardiac pacer, but lack of contact between the siblings rendered a more recent detailed family history impossible.

The clinical-neurological examination revealed atrophies, accentuated proximal and left at upper and lower extremities in addition to a hemihypaesthesia on the left side. Muscle strength in all extremities was reduced with emphasis on proximal and left muscles. Functional tests, like walking on heels and tiptoes or single-leg hop, were not possible, while a bilateral positive Trendelenburg sign was detected. Fine movements on the left side were reduced. Reflexes were normal and pyramidal signs not detectable. Laboratory results showed an elevated level of creatine kinase (798 U/l, normal range: < 180 U/l). Evidence of Paget's disease of the bone was not stated, with the exception of slightly elevated serum levels for alkaline phosphatase (161 U/l, normal range: < 135 U/l). Electrocardiogram, electroencephalogram and pulmonary function did not show pathologic results. Neurophysiologic examinations of muscles and nerves revealed no specific signs supporting a myopathy or neuropathy. Cranial MRI imaging detected no abnormalities except a small lacunary defect in the right temporal lobe. Muscular biopsy revealed a degenerative myopathy with autophagic and rimmed vacuoles with lack of inflammatory signs. Earlier suspected diagnosis, like limb-girdle muscular dystrophy 1 B (LGMD1B) or facioscapulohumeral muscular dystrophy (FSHD) were not confirmed in genetic testing.

### Genetic testing

Exon 5 of the *VCP* gene was amplified by PCR according to the protocol. Gel electrophoresis showed a single band for exon 5 size of the predicted size (301 bp).

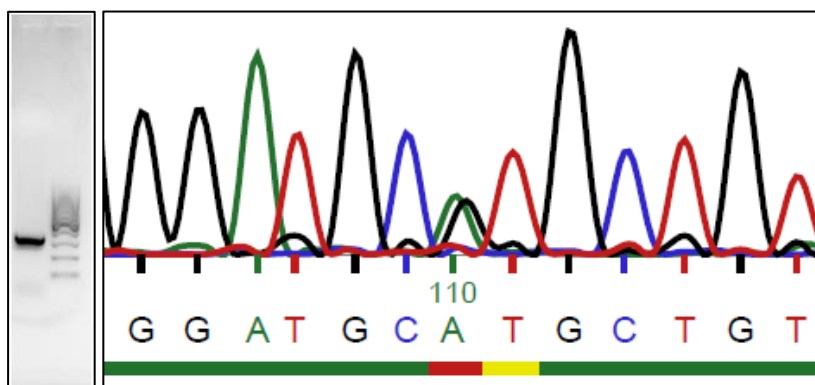


**Figure 77** left: Gel electrophoresis, *VCP* exon 5 (left lane), 100 bp ladder (right lane), right: section of electropherogram of the *VCP* exon 5 sequence showing a heterozygous c.476G>A base exchange.

*VCP* Exon 5 Sanger sequencing was carried out and revealed a heterozygous point mutation, c.476G>A, with a substitution of a guanosine by an adenosine, which leads to an amino acid change from arginine to histidine (p.R159H).

### VII.7.3. Patient #3

#### Clinical course

Patient #3, of Roma ethnicity, presented gait disturbances at age 14. Muscle weakness was progressive as the patient was experiencing difficulties to climb stairs or to rise from squatting at 21. One year later an onset of hand weakness was reported. The patient has had three pregnancies. Unfortunately, further data on family history was not available.

Clinical-neurological examination revealed symmetric atrophy of thigh and calf muscles, especially pronounced for M. tibialis anterior and bilateral wasting of thenar and hypothenar muscles. Muscle strength was overall reduced with main affection of the lower extremities. A steppage-waddling gait and positive Gower's sign was detected. Additionally, Achilles tendon reflexes were absent and stiloradial reflexes reduced. Laboratory results showed a markedly elevated creatine kinase at 16.095 U/l. Ventilatory assessment and echocardiography were normal. Electromyography showed myopathic changes in distal and proximal muscles of lower and upper extremities.

#### Genetic testing

Exons 2 to 12 of the *GNE* gene were amplified with PCR according to the protocol. Gel electrophoresis showed clear bands at the appropriate locations.

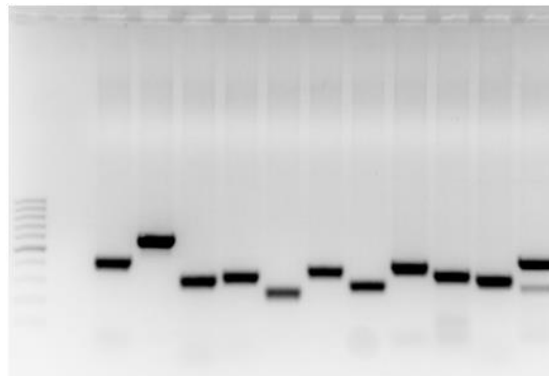


**Figure 78: Gel electrophoresis: 100 bp ladder, *GNE* gene exon 2 to 12 (left to right)**

Sequencing exons 2 to 12 were carried out. It revealed two heterozygous point mutations. c.178A>G in exon 2, changing an adenine to a guanine, leading to an amino acid change from methionine to valine (p.M60V). The second heterozygous point mutation in exon 10, c.1853T>C, led to an amino acid change from isoleucine to threonine (p.I618T).

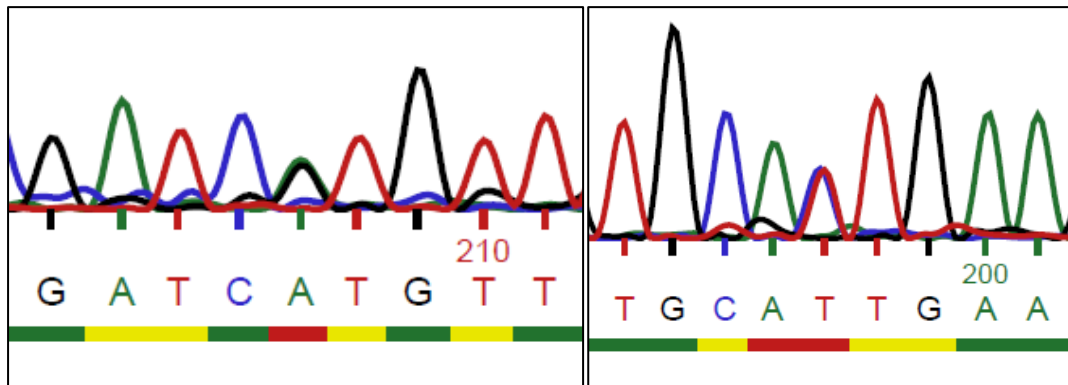


Figure 79: Sections of electropherogram depicting mutations in GNE gene: c.178A>G (left), c.1853T>C (right)

## VIII. Discussion

### VIII.1. The path to immortalized cells

Immortalized cell lines are a common tool for *in vitro* cell culture and will play a more important role to facilitate therapy validation. The new DMD VII and WT VII cell lines have been designed to provide a porcine *in vitro* model for the Duchenne muscular dystrophy and a normal control. The DMDpig as an animal model has the potential to become a great asset for further research, being the closest mimic to humans in terms of size, physiologic functions, and phenotype. DMD VII and WT VII cell lines are a new approach designed to expand the experimental and therapeutic capabilities of an *in vivo* large-scale animal model into an *in vitro* cell culture tool, providing large quantities of cell material for future drug testing. As of November 2021, there is no report of a previously successful immortalization of primary porcine myoblasts.

At the beginning of this project, maintenance and conditions of porcine cell cultures, especially for the required longer cultivation periods, were still under constant evaluation and amendment. The use of established procedures for immortalization of these cells was most promising. The integration of *hTERT* and *CDK4* as cell cycle active genes has been shown to successfully conduct immortalization of human myoblasts, i. e. extension of proliferation capacity while retaining the properties of the primary cells, in particular the *in vitro* differentiation capability [289]. Single application of either *hTERT* or *CDK4* was not sufficient for immortalization of human myoblasts [330, 345].

Likewise, the plasmid backbone pBABE had been used in previous successful immortalization attempts [289, 296, 350]. The application of GFP controls is also widely conducted. The choice of the pBABE backbone limited the available combinations of genes for transduction and antibiotic selection markers. Additionally, careful assessment was conducted to accommodate the limitations posed by the cell lines themselves, i. e. P507/18 and P352/15 featuring an intrinsic neomycin (G418) resistance cassette. Amplification of these plasmids in *E. coli* strains and subsequent preparation of plasmid DNA led to sufficient amounts of satisfactorily pure DNA for transfection of producer cells (Figure 30).

Furthermore, the chosen producer cell line for the retroviral delivery system, Phoenix amphi cell line, is known for stable expression of viral components [351]. Transfection of these HEK293-derived producer cells, facilitated by our procedure combining features of electroporation and chemical-based transfection mechanisms resulted in a sufficient ratio of pmaxGFP®-positive cells (Figure 33). There are reports of higher transfection efficacies using HEK293-producer cells, but the achieved ratio were considered sufficient for the overall goal of

this study [351]. Function of the delivery system and correct integration of the desired genetic information was further validated by a second GFP control (pBABE-neo-IRES-eGFP), with green fluorescent cells starting to appear after 17 days. PCR analyses and genetic sequencing in CDK4-transfected producer cells proved the insertion in their gDNA. In contrast, *hTERT* gDNA was not traceable in PCR amplification and sequencing, most likely due to the larger insert of 3.500 bp, more than three times the size of *CDK4*. Nevertheless, markedly enhanced antibiotic resistance for puromycin in hTERT-transfected compared to non-transfected controls, indicated integration of the plasmid DNA of pBABE-puro-hTERT with its puromycin resistance cassette. All in all, this gave evidence for successful integration of all three plasmid DNAs in their respective transfected producer cell line.

Estimation of the subsequent viral titers produced by these cell lines, using a 3T3 cell assay showed a difference in more than one order of magnitude between mean infectious units of fresh and thawed viral supernatant with viral particles of pBABE-puro-hTERT (Figure 36). This indicated a loss of infectious units in a freeze/thaw cycle and most likely affecting transduction efficacy and providing possible explanations for the different antibiotic resistance for transduced myoblasts in the various approaches [352]. Viral titers containing the DNA sequences of pBABE-hygro-CDK4 R24C and pBABE-neo-IRES-eGFP achieved significantly lower values. Nevertheless, induction of colony formation and appearance of green fluorescent 3T3 and C2C12 cells under antibiotic selection served as proof of production of a virus containing the sequences inducing the respective antibiotic resistance. Interestingly, the dynamic of increase to the final and not the total antibiotic concentration seemed to affect results positively, most likely due to a certain time span needed for successful integration and expression of the particular antibiotic resistance gene. Limiting factors for efficient antibiotic selection of the transfected producer cell lines and therefore of virus production are the overlap of used antibiotic selection agents and intrinsic antibiotic resistances in the producer cells, e. g. hygromycin and neomycin (G418), and the trait of featuring a cluster-like regrowth of cells, possibly also diluting the ratio of successfully transfected producer cells.

All in all, these preliminary systematic experimental approaches resulted in the establishment of a functional delivery system for the intended genes, necessary for immortalization of porcine myoblasts.

## VIII.2. Immortalization of porcine myoblasts

Despite of their advantages, porcine myogenic cells are not a widely used cell type for *in vitro* cell culture, yet. As of November 2021, a search for “porcine myoblast” in the PubMed database showed only 9 results compared to 19’664 for “myoblast” or 12’226 for “murine myoblast”.

Immortalization of porcine myoblasts has not been reported yet. The successful design of the DMDPig, carrying the most common genetic alteration in humans causative for DMD, a deletion of exon 52, enabled the expansion of this animal model's potential for *in vitro* cell culture [237].

The conducted transduction approaches featured a varying setup, utilizing the insights gained from their previous approaches.

The first and second approaches differed from the third one in age of the pigs, when they were euthanized, and myoblasts derived from muscle tissue. Primary cell cultures from younger animals are thought to feature less senescent cells and a higher proliferative capacity, which can be maintained by the transduction with cell cycle active genes. An age difference of 18 and 15 days, respectively, in exon 52-deficient and wild type cells could explain the improvements made in later approaches. Additionally, P507/18 and P515/18 were frozen for only three days or not at all, compared to more than two years in case of P352/15 and P362/15, reducing cellular stress caused by this long-term storage.

Viral titers in this study differed markedly depending on the conduction of freeze/thaw cycles. Consequently, an effect on infectiousness and efficacy of transduction could be expected. Direct comparison of the use of thawed and fresh viral supernatants is particularly striking in the case of single CDK4-transduced myoblasts P352/15 and P362/15, which detached completely after less than 20 days after initiation of hygromycin selection. Single CDK4-transduced P507/18 and P515/18, utilizing fresh viral supernatant, showed clear proliferation for at least 43 days under hygromycin selection in a concentration three times higher than in previous approaches. A similar effect was visible for hTERT-transduction, although not as clearly as the experiments with CDK4-transduced cells. For example, P362 hTERT I featured growth for 113 days after end of transduction, although without antibiotic selection after day 26. The single hTERT-transduced myoblasts in the third approach had not only been cultured for longer than 43 days but exhibited a stronger proliferation rate under markedly higher puromycin concentrations compared to the earlier experiments. In summary, the use of fresh viral supernatant was advantageous, and in case of CDK4-transduction even necessary for successful improvement of proliferation capacities in porcine myoblasts.

Over the course of this study, different sequential transduction procedures were conducted. Previous studies showed the insufficiency of the single use of *CDK4* or *hTERT* for human myogenic cell immortalization [330, 345]. Yet, single transductions were also performed to assess the dynamic of the induced antibiotic resistance and compare growth characteristics. The direct arrangement of *CDK4* and *hTERT* single transduction favored the latter in all approaches, regardless of cells used or antibiotic regimen. Two protocols for double transduction of *hTERT* and *CDK4* were used - a parallel and consecutive one. Parallel and

consecutive transduction using thawed viral supernatant resulted in either fast complete cell detachment or at least a striking decline in confluency, most likely being negatively affected by lower viral titers, especially concerning *CDK4*. In the third approach, using freshly harvested viral supernatant for transduction, double transduction was far better in comparison. In general, all tested sequential procedures of transduction in the last approach resulted in more stable growth and increased resistance towards the antibiotic agents. Observation of first experimental thawing and transduction of porcine myoblasts indicated a high ratio of cell death in these special situations, probably due to cellular stress. Therefore, the initiation of the transduction protocol was deferred in the third approach to day 12 of growth, compared to immediately after thawing in the first two.

Antibiotic agents were used for selection of transduced cells. Porcine myoblasts had a natural threshold for all selection agents used. All concentrations used for selection of transduced cells were well beyond this threshold. When exceeded far too much, large scale cell detachment and growth arrest occurred. Antibiotic agents seemed to induce cellular stress even in resistant cells. This was especially the case for neomycin (G418), which led to distinctive morphologic changes in DMD III (Figure 53). As indicated in the introduction chapter, the lack of dystrophin due to the DMD mutation not only leads to a loss of mechanical mounting of the cytoskeleton and muscle cell membrane damage, but also to deranged intracellular ion homeostasis and signaling cascades, which could lower resilience of these cells for external agents in a dose-dependent manner. Interestingly, these effects were not present under selection with puro- and hygromycin or under neomycin application in non-resistant myoblasts, the latter leading to fast and complete cellular detachment. In conclusion, the exact cellular mechanism of high-dose antibiotic initiation to decline in confluency and contribution to cell death cannot be specified. Gradual increase in antibiotic concentrations, starting beyond the threshold of resistance of non-transduced cells, resulted in visibly more proliferation under higher concentrations in the third approach, reaching dosage levels of more than three times than those from the first two transduction approaches. Furthermore, a trial discontinuation of antibiotic selection was carried out at different times in the protocol. After cessation of antibiotic selection for DMD VIIb and WT VIIb, a higher confluency was visible compared to the other half of the cell line, which was still subject to selection pressure (Figure 47). Likewise, the recovery of P362 hTERT I supported these observations. Potential explanations are a lack of toxicity, which may affect even resistant cells, or overgrowth by cells who lost the corresponding gene due to the absence of selection pressure. Noted higher ratios of senescent cells in non-selected, older cultures could also, at least partially, be explained by cells losing resistance and the inserted *hTERT* or *CDK4*, resulting in exit of the cell cycle. Still, for all cell lines, previously completely detached negative controls corroborated resistance towards the applied selection agent.

In total, the two championed cell lines 9-DMD VIIa and 9-WT VIIa, alongside their WT counterparts were cultured for more than 250 days. Over the course of this long-term observation period, the double transduced cells featured a steady growth, outpacing the non-transduced control cells, who suffered a severe loss in proliferation capabilities after a last splitting of cell culture on day 59 of cultivation and leaving morphologically changed, senescent cells without signs of proliferation as remnants of the non-transduced cell culture. 9-DMD VIIa additionally outpaced their wild type counterpart 9-WT VIIa by estimated population doublings. Week-by-week cell counting proved a preservation of the number of population doublings.

Limited dilution experiments of DMD VII and WT VII proved colony-forming abilities of single cells, being able to grow culture up to 48-well plates. Transfer of these colonies into larger plates usually led to loss of culture. Larger clones overcame this problem with 9-DMD VIIa and 9-WT VIIa being the most durable and longest growing sub-colonies reaching a cultivation period of more than 250 days. Cultivation and expansion were possible well beyond this reference date.

In total, changes in the harvest of viral supernatant, cell lines and transduction or selection protocols resulted in a markedly increased proliferation capacity of the resulting myoblasts. The exact impact of the individually controlled parameters cannot be clearly determined.

Expression of green fluorescent protein in myoblasts proved viral tropism of the retroviral vector based on MMLV for porcine cells and served as a proof of principle check for transduction capability of both DMD and WT porcine cells. The significant difference in the ratio of GFP-positive cells was not surprising, considering the lack of efficient selection in DMD cells due to the intrinsic neomycin (G418) resistance cassette. Nevertheless, the ratio of GFP-positive cells in both cell lines did increase during the observation period, possibly indicating a selection advantage over non-transduced or non-GFP-expressing cells in the same culture.

Genetic sequence analyses of transduced myoblasts on day 60 indicated genomic integration and transcription of the complete *CDK4* and at least the partial *hTERT* gene. Genomic integration of *CDK4* was also detected in WT VII cells.

Additionally, the growth pattern of older transduced cell cultures, even at an age of 258 days, did not differ from the younger non-transduced ones in morphologic appearance in the conventional light microscope. The general morphology of single cells shifted from smaller and bulgier cells of early passages to a longer and slimmer cell body. Spontaneous fusions and senescence also occurred in the transduced cells, but visibly less frequent and mostly in more isolated cells in culture than in non-transduced cultures, which only consisted of cells with morphologic abnormalities without visible proliferation at an older age. Spontaneous myotube formation and frequent senescence in clones derived from transduced cell lines have been

described in other immortalization attempts before [330]. Additionally, transduced cells retained their ability to sustain repeated freeze/thaw cycles, unlike age-matched non-transduced, senescent-imposing cells.

The fusion of primary myoblasts to non-proliferating, terminally differentiated myotubes is considered a hallmark of myogenicity. A qualitative assessment in this study revealed retained fusion capabilities in transduced cells at all tested age stages until day 95 for WT VII and day 258 for DMD VII cells compared to the non-transduced initial cell population.

Desmin is a type III intermediate filament protein, fulfilling a role in cell structure and also intracellular signaling, which serves as an early myogenic marker protein [73]. As indicated in the results section, desmin positive cells were present in all tested age groups up to 258 days of proliferation, indicating preservation of myogenic properties. However, these studies were not designed for quantitative analyses, but suggested a loss in the ratio of desmin positive cells.

All in all, 9-DMD VIIa and 9-WT VIIa featured a significantly improved proliferation capacity compared to non-transduced porcine myoblasts suggesting preservation of the myogenic properties of the non-transduced cells at the start of the study.

### **VIII.3. Limitations**

The lack of broader experience in porcine myoblast cell culture can be viewed as a limitation for use, but during this study and other experimental projects of our working group, a wide range of protocol improvements were established and implemented. The optimal cultivation conditions proved to be highly influential on growth pattern and proliferation capacity. Especially passaging of cells with trypsinization and subsequent splitting caused considerable loss in cell numbers as well as visible cellular density and slowing re-growth. Culture plate size, the interval of culture splitting, and medium changes impacted the pace of expansion, which therefore varied over the course of testing. The initial lack of established culture conditions for porcine myoblasts is a possible explanation for the low number of population doublings in the non-transduced cells and might have impaired the full proliferation potential of the transduced cell lines. With growing knowledge and experience in dealing with porcine myogenic cells, capabilities of these cell lines had the potential for efficient further improvements. Additionally, necessary freezing events might have induced incremental cellular stress and loss of viability.

This study's design was based on reported successful immortalization approaches for murine and human myoblasts [289]. As discussed above, the choice of plasmid resistance genes limited the selection efficacy of the producer cells transfected with *CDK4* and eGFP, correlating with the significantly lower viral titers in their supernatant than in those of hTERT-transfected

producer cells. Low CDK4-titers could be an explanation for the limited proliferation of CDK4-transduced P352/15 and P362/15 cells. Titers of thawed CDK4 supernatant could not be quantified, but if considered analogous to the difference of more than one log level between thawed and frozen hTERT supernatant, fresh CDK4 supernatant with supposedly higher viral titers would explain increased life span of the single CDK4-transduced P507/18 and P515/18 cells [352]. Furthermore, the intrinsic neomycin resistance cassette in the P507/18 cell line limited the quantitative assessment of transduction efficacy measurement.

In genetic sequencing of the transduced cells, detection of the complete sequence of *hTERT* in gDNA and cDNA could not be successfully carried out yet, probably due to the large size of the hTERT insert. Detection of the 5'-LTR and 3'-LTR ends of the vectoral insert and the observed highly elevated resistance towards antibiotic selection with puromycin compared to non-transduced cells, suggested the presence of hTERT. In WT VII cells, an area including the 3'-LTR end with an adjoining vector sequence of 100 bp is suspected to have undergone a recombination event with a chromosomal locus, sharing a high homologue with the 3'-end of the hemicentin 1 gene, which was also proven by a confirmatory PCR. The importance of this alteration remains unknown. *CDK4* integration was proven by gDNA amplification by PCR and subsequent sequencing. Likewise, elevated antibiotic resistance of WT VII towards hygromycin indicated integrity of their coding areas. Clear implications of possible sequence alterations in the hemicentrin 1 gene remain unclear. Animal studies indicate not only a role of the gene in the composition of the ECM but also in mitotic cytokinesis [353]. A possible correlation between this recombination event and slower growth characteristics of WT VII compared to DMD VII cannot be excluded. Further studies are needed for clarification of the functional impact of these alterations. Likewise, in previous studies with human myoblasts, transduction with CDK4 and hTERT did not change the cell characteristics and did not lead to neoplastic transformation [345, 354].

DMD VII and WT VII retained similar fusion capabilities at higher passage numbers than non-transduced cells at lower passages. DMD cells were positive for the myogenic marker desmin until day 258 of growth. However, this study's data indicate a lower ratio of cells positive for desmin in older cultures. Accumulation of non-myogenic cells during extensive amplification is a pre-described side effect in myoblast cultures [289]. Immunofluorescence staining of desmin in young-age non-transduced P507/18 and P515/18 suggested an imperfect myogenic purity for the initial cell population (Figure 73). Cell sorting of the primary cell culture for myogenic markers, i. e. the neural cell adhesion molecule (NCAM) to improve myogenic purity of the initial cell culture, was not carried out. The rationale were unpublished results of preliminary experiments in our working group which indicated a significant loss of proliferation capabilities for porcine myoblasts following this selection procedure. The well-established desmin staining

protocol of human myoblasts had to be adjusted for porcine cells, raising the question of staining sensitivity to assess the true myogenic potential of porcine myoblasts *in vitro*. By contrast, fusion capabilities were retained for DMD VII cells even after 258 days of proliferation. Other detection methods, e. g. western blotting for comparative, quantitative analysis could be used for alternative assessment of protein levels in cell culture. Ultimately, new technologies of cellular transdifferentiation, e. g. by upregulation of MYOD1, could be used to reprogram non-myogenic, transduced cells to restore myogenicity [355, 356].

#### **VIII.4. Molecular genetic analyses of patients**

The male patients #1 and #2 presented with the same heterozygous point mutation c.476G>A in the VCP gene, leading to a change of amino acids from arginine to histidine (p.R159H). This mutation is known to cause VCP proteinopathy with a clinical symptom cluster called IBMPFD. In both patients the clinically leading sign was severely limiting myopathy with tetraparesis and muscle atrophy featuring a diffuse distribution pattern in #1 and accentuation on proximal and left sided muscles in #2 with a variation in age of onset of 20 years. Only #2 showed elevation in CK serum levels. The further distribution of additional clinical symptoms in the two index patients stressed the broad variation in genotype-phenotype-correlation, as indicated in previous studies [277, 281]. Clear evidence for Paget's disease of the bone was not identified in either of the two patients. Neuropsychiatric symptoms, including residual palilalia and apathy under treatment with atypical neuroleptics, were only reported for patient #1 and were associated with frontal lobe atrophy detected in a brain MRI. Muscle biopsies showed degenerative myopathy in both patients with detection of autophagic and rimmed vacuoles in #2.

Additionally, clinical presentation among relatives of both index patients varied widely. Unfortunately, no genetic sequencing of family members could be conducted. Relatives of #1 presented with clinical signs of presenile dementia or behavioral symptoms and ALS, possibly familial, while the father of #2 was suspected of developing a clinically manifest myopathy in his forties. Detailed information on the exact indication for implantation of a cardiac pacemaker in #2's older brother, especially a possible cardiomyopathy, was not available. In conclusion, these two index patients and their relatives add to the presentation of VCP proteinopathy as a wide spectrum disease with great intrafamilial variation. Additionally, the concomitant clinical appearance of ALS and signs of frontotemporal dementia in #1's family adds to previous reports about possible common pathological pathways for these diseases. Familial ALS only cover 5 % of all ALS cases, of which 1-2 % of familial ALS are found to be caused by mutations in the VCP gene [283-285]. Unfortunately, there are no reports about detection of TDP-43 in the muscle

biopsies of the patients, which is a common pathological finding in patients with *VCP* mutations, FTD and ALS [277, 278]. The exact pathomechanism of *VCP* proteinopathy is still unknown.

Genetic sequencing of the *GNE* gene in patient #3 showed two heterozygous mutations, c.178A>G (p.M60V) and c.1853T>C (p.I618T). The female index patient presented with progressive muscle weakness, which initiated with changes in gait at the age of 14 years and progressed to difficulties in climbing of stairs, rising from squatting and hand weakness until the age of 21 with a steppage-waddling gait and positive Gower's sign. Elevated serum CK levels and myopathic changes in electromyography of distal and proximal muscles of lower and upper limbs indicated a myopathy. The clinical examination with typical symmetric atrophy of thigh and calf muscles and focus on the Mm. tibiales anteriores and the Roma ethnicity of the patient eventually raised suspicion of an autosomal-recessive *GNE* myopathy. p.I618T is a known, so-called founder mutation in the population of Bulgarian Roma. Study data show clinical affection for carriers only for homozygous p.I618T mutations, but not for heterozygous ones [269]. The second heterozygous mutation in exon 2, p.M60V, has not been described yet. Two mutations leading to an exchange of the same methionine in the UDP-GlcNAc 2-epimerase domain to arginine (c.179T>C, p.M60R) and threonine (c.179T>G, p.M60T) have been described previously, leading to a medium to severe phenotype of *GNE* myopathy [270]. With no other mutations present, apart from a heterozygous p.I618T, which is insufficient for clinical manifestation, a compound heterozygous state in p.M60T and p.I618T is most likely to cause the patient's clinical phenotype. Further analysis of the p.M60V variant using the Mutationtaster software led to the estimation of being disease causing. In contrast, the PolyPhen2 algorithm considered this variant to be benign but leaving out effects from the presence of a compound heterozygous mutation. To our knowledge, this would be the first description of the p.M60V mutation.

### **VIII.5. Outlook**

The immortalized porcine myoblast cell lines, established in this study, have the potential to serve as a valuable tool for further research of DMD. This is the first report of the generation of immortalized porcine myoblast cell lines until now.

DMD is the most common myopathy, affecting one in 3'500-5'000 boys [14]. New diagnostic criteria requiring genetic sequencing rather than a muscle biopsy result in a scarcity of muscle material of DMD patients, reducing available resources for further research. Multiple animal models of mammalian and non-mammalian species provide *in vitro* and *in vivo* material for experimental studies in order to elucidate the underlying pathophysiological mechanisms of DMD. Small animal models, especially the widely used murine models, feature a dissimilar

phenotype-genotype-correlation compared to humans, limiting the subsequent translation of new insights to humans. The large animal model of the DMD pig reflects the pathological hallmarks and clinical severity of human DMD patients in an accelerated pace and wider extent than the murine models. Additionally, a pig's size is comparable to humans and its genetic alteration is the most frequent mutation occurring in *Homo sapiens* (exon 52 deletion) [237]. Primary porcine myoblasts derived from these animals transfer the advantages of the *in vivo* animal model into *in vitro* cell cultures. The transduction of *hTERT* and *CDK4* induced significantly increased cell proliferation capabilities, therefore enabling longer culture times with greater expansion of the cell lines. The immortalized DMD and WT cell lines and the DMD pig and their WT siblings have the potential to form a unique dual testing system facilitating *in vivo* and *in vitro* experiments, thereby enabling research on pathophysiology and new therapeutic approaches and supporting translational medicine. This disease model could contribute to overcome the scarcity of suitable cell material and promote *in vitro* assessment of new advancements for DMD treatment. Evaluation of new compounds, e. g. AONs, require high through-put screening. These large amounts of cellular material can only be provided by immortalized myogenic cell lines, therefore enabling *in vitro* validation before application *in vivo*. One-of-a-kind advantages of the use of porcine cells is the availability of a large animal, human-like model of the same species and therefore the possibility of *in vivo*, preclinical evaluation of new treatments in the same testing system, leading to a reduction of the number of live pigs and monetary assets needed. Potentially, the porcine model could be further expanded to include *in vitro* muscle tissue models to be able to simulate the structural complexity of the skeletal muscle not only in biopsies. This has been previously and successfully conducted for human skeletal muscle in healthy and disease conditions, including DMD [357, 358].

In total, the immortalized porcine myogenic DMD and WT cell lines established in this study have the potential to become a powerful tool for future preclinical and translational research in Duchenne muscular dystrophy.

## IX. Reference list

1. Rohkamm, R., *Color Atlas of Neurology*. Vol. 2nd. 2014: Thieme.
2. Schmidt, R., Lang, F., Heckmann, M., *Physiologie des Menschen*. Vol. 31. 2010, Heidelberg, Germany: Springer.
3. Cavagna, G., *Fundamentals of Human Physiology*. 2019: Springer.
4. Ottenheijm, C.A.C., L.M.A. Heunks, and R.P.N. Dekhuijzen, *Diaphragm adaptations in patients with COPD*. Respiratory research, 2008. **9**(1): p. 12-12.
5. Buckingham, M., et al., *The formation of skeletal muscle: from somite to limb*. J Anat, 2003. **202**(1): p. 59-68.
6. Morgan, J. and T. Partridge, *Skeletal muscle in health and disease*. Disease models & mechanisms, 2020. **13**(2): p. dmm042192.
7. Musumeci, G., et al., *Somitogenesis: From somite to skeletal muscle*. Acta Histochem, 2015. **117**(4-5): p. 313-28.
8. Horn, A., et al., *Mitochondrial redox signaling enables repair of injured skeletal muscle cells*. Sci Signal, 2017. **10**(495).
9. Barthelemy, F., et al., *Muscle Cells Fix Breaches by Orchestrating a Membrane Repair Ballet*. J Neuromuscul Dis, 2018. **5**(1): p. 21-28.
10. Emery, A.E., *The muscular dystrophies*. The Lancet, 2002. **359**(9307): p. 687-695.
11. Hoffman, E.P., R.H. Brown, Jr., and L.M. Kunkel, *Dystrophin: the protein product of the Duchenne muscular dystrophy locus*. Cell, 1987. **51**(6): p. 919-28.
12. Deschauer, M. *Leitlinien der DGN - Diagnostik von Myopathien*. 2016 [cited 2020 03.03.2020]; Available from: <https://www.dgn.org/leitlinien/3260-030-115-diagnostik-von-myopathien-2016>.
13. Moser, H., *Duchenne muscular dystrophy: pathogenetic aspects and genetic prevention*. Hum Genet, 1984. **66**(1): p. 17-40.
14. Aartsma-Rus, A., et al., *Entries in the Leiden Duchenne muscular dystrophy mutation database: An overview of mutation types and paradoxical cases that confirm the reading-frame rule*. Muscle & Nerve, 2006. **34**(2): p. 135-144.
15. Ryder, S., et al., *The burden, epidemiology, costs and treatment for Duchenne muscular dystrophy: an evidence review*. Orphanet J Rare Dis, 2017. **12**(1): p. 79.
16. Moat, S.J., et al., *Newborn bloodspot screening for Duchenne muscular dystrophy: 21 years experience in Wales (UK)*. Eur J Hum Genet, 2013. **21**(10): p. 1049-53.
17. Mendell, J.R., et al., *Evidence-based path to newborn screening for Duchenne muscular dystrophy*. Ann Neurol, 2012. **71**(3): p. 304-13.
18. Rosalki, S.B., *Serum enzymes in disease of skeletal muscle*. Clin Lab Med, 1989. **9**(4): p. 767-81.
19. Birnkrant, D.J., et al., *Diagnosis and management of Duchenne muscular dystrophy, part 1: diagnosis, and neuromuscular, rehabilitation, endocrine, and gastrointestinal and nutritional management*. Lancet Neurol, 2018. **17**(3): p. 251-267.
20. Gowers, W., *Clinical Lecture ON PSEUDO-HYPERTROPHIC MUSCULAR PARALYSIS*. The Lancet, 1879. **114**(2916): p. 73-75.
21. Darras, B.T., *Duchenne and Becker muscular dystrophy: Clinical features and diagnosis*. 2018: UpToDate.
22. Jacques, M.F., et al., *Frequency of reported pain in adult males with muscular dystrophy*. PLoS One, 2019. **14**(2): p. e0212437.
23. Nigro, G., et al., *The incidence and evolution of cardiomyopathy in Duchenne muscular dystrophy*. Int J Cardiol, 1990. **26**(3): p. 271-7.
24. Spurney, C.F., *Cardiomyopathy of Duchenne muscular dystrophy: current understanding and future directions*. Muscle Nerve, 2011. **44**(1): p. 8-19.
25. Takami, Y., et al., *High incidence of electrocardiogram abnormalities in young patients with duchenne muscular dystrophy*. Pediatr Neurol, 2008. **39**(6): p. 399-403.
26. Melacini, P., et al., *Cardiac and respiratory involvement in advanced stage Duchenne muscular dystrophy*. Neuromuscul Disord, 1996. **6**(5): p. 367-76.
27. Birnkrant, D.J., E. Ararat, and M.J. Mhanna, *Cardiac phenotype determines survival in Duchenne muscular dystrophy*. Pediatr Pulmonol, 2016. **51**(1): p. 70-6.
28. Eiholzer, U., et al., *Short stature: a common feature in Duchenne muscular dystrophy*. Eur J Pediatr, 1988. **147**(6): p. 602-5.
29. Wood, C.L. and V. Straub, *Bones and muscular dystrophies: what do we know?* Curr Opin Neurol, 2018. **31**(5): p. 583-591.
30. McDonald, D.G., et al., *Fracture prevalence in Duchenne muscular dystrophy*. Dev Med Child Neurol, 2002. **44**(10): p. 695-8.
31. King, W.M., et al., *Orthopedic outcomes of long-term daily corticosteroid treatment in Duchenne muscular dystrophy*. Neurology, 2007. **68**(19): p. 1607-13.
32. Doorenweerd, N., et al., *Timing and localization of human dystrophin isoform expression provide insights into the cognitive phenotype of Duchenne muscular dystrophy*. Sci Rep, 2017. **7**(1): p. 12575.
33. Heald, A., et al., *Becker muscular dystrophy with onset after 60 years*. Neurology, 1994. **44**(12): p. 2388-2388.
34. Bradley, W.G., et al., *Becker-type muscular dystrophy*. Muscle Nerve, 1978. **1**(2): p. 111-32.
35. Yazawa, M., et al., *A family of Becker's progressive muscular dystrophy with severe cardiomyopathy*. Eur Neurol, 1987. **27**(1): p. 13-9.
36. Melacini, P., et al., *Myocardial involvement is very frequent among patients affected with subclinical Becker's muscular dystrophy*. Circulation, 1996. **94**(12): p. 3168-75.
37. Takeshima, Y., et al., *Amino-terminal deletion of 53% of dystrophin results in an intermediate Duchenne-Becker muscular dystrophy phenotype*. Neurology, 1994. **44**(9): p. 1648-1648.
38. Muntoni, F., S. Torelli, and A. Ferlini, *Dystrophin and mutations: one gene, several proteins, multiple phenotypes*. Lancet Neurol, 2003. **2**(12): p. 731-40.
39. Nakamura, A., *X-Linked Dilated Cardiomyopathy: A Cardiospecific Phenotype of Dystrophinopathy*. Pharmaceuticals (Basel), 2015. **8**(2): p. 303-20.
40. Berko, B.A. and M. Swift, *X-linked dilated cardiomyopathy*. N Engl J Med, 1987. **316**(19): p. 1186-91.
41. Ortiz-Lopez, R., et al., *Evidence for a dystrophin missense mutation as a cause of X-linked dilated cardiomyopathy*. Circulation, 1997. **95**(10): p. 2434-40.

42. Towbin, J.A., et al., *X-linked dilated cardiomyopathy. Molecular genetic evidence of linkage to the Duchenne muscular dystrophy (dystrophin) gene at the Xp21 locus*. Circulation, 1993. **87**(6): p. 1854-65.
43. Hoogerwaard, E.M., et al., *Signs and symptoms of Duchenne muscular dystrophy and Becker muscular dystrophy among carriers in The Netherlands: a cohort study*. Lancet, 1999. **353**(9170): p. 2116-9.
44. Nozoe, K.T., et al., *Phenotypic contrasts of Duchenne Muscular Dystrophy in women: Two case reports*. Sleep Sci, 2016. **9**(3): p. 129-133.
45. Soltanzadeh, P., et al., *Clinical and genetic characterization of manifesting carriers of DMD mutations*. Neuromuscul Disord, 2010. **20**(8): p. 499-504.
46. Florian, A., et al., *Cardiac involvement in female Duchenne and Becker muscular dystrophy carriers in comparison to their first-degree male relatives: a comparative cardiovascular magnetic resonance study*. Eur Heart J Cardiovasc Imaging, 2016. **17**(3): p. 326-33.
47. Melacini, P., et al., *Cardiac transplantation in a Duchenne muscular dystrophy carrier*. Neuromuscul Disord, 1998. **8**(8): p. 585-90.
48. Landfeldt, E., et al., *Life expectancy at birth in Duchenne muscular dystrophy: a systematic review and meta-analysis*. Eur J Epidemiol, 2020.
49. Schreiber-Katz, O., et al., *Comparative cost of illness analysis and assessment of health care burden of Duchenne and Becker muscular dystrophies in Germany*. Orphanet J Rare Dis, 2014. **9**: p. 210.
50. Duchenne, *The Pathology of Paralysis with Muscular Degeneration (Paralysie Myosclerotique), or Paralysis with Apparent Hypertrophy*. Br Med J, 1867. **2**(363): p. 541-2.
51. Meryon, E., *On Granular and Fatty Degeneration of the Voluntary Muscles*. Med Chir Trans, 1852. **35**: p. 73-84.1.
52. Schumacher, J., *Beitrag zur Kasuistik der Dystrophia muscularis progressiva*, in *Medizinische Fakultät*. 1892, Rheinische Friedrich-Wilhelms-Universität zu Bonn: Bonn.
53. Becker, P.E. and F. Kiener, *[A new x-chromosomal muscular dystrophy]*. Arch Psychiatr Nervenkr Z Gesamte Neurol Psychiatr, 1955. **193**(4): p. 427-48.
54. Monaco, A.P., et al., *Isolation of candidate cDNAs for portions of the Duchenne muscular dystrophy gene*. Nature, 1986. **323**(6089): p. 646-50.
55. Ahn, A.H. and L.M. Kunkel, *The structural and functional diversity of dystrophin*. Nature Genetics, 1993. **3**(4): p. 283-291.
56. Singh, S.M., et al., *Missense mutations in dystrophin that trigger muscular dystrophy decrease protein stability and lead to cross- $\beta$  aggregates*. Proceedings of the National Academy of Sciences, 2010. **107**(34): p. 15069-15074.
57. Ervasti, J.M. and K.P. Campbell, *A role for the dystrophin-glycoprotein complex as a transmembrane linker between laminin and actin*. J Cell Biol, 1993. **122**(4): p. 809-23.
58. Matsumura, K. and K.P. Campbell, *Dystrophin-glycoprotein complex: its role in the molecular pathogenesis of muscular dystrophies*. Muscle Nerve, 1994. **17**(1): p. 2-15.
59. Koenig, M. and L.M. Kunkel, *Detailed analysis of the repeat domain of dystrophin reveals four potential hinge segments that may confer flexibility*. J Biol Chem, 1990. **265**(8): p. 4560-6.
60. Koenig, M., A.P. Monaco, and L.M. Kunkel, *The complete sequence of dystrophin predicts a rod-shaped cytoskeletal protein*. Cell, 1988. **53**(2): p. 219-228.
61. Singh, S.M., S. Bandi, and K.M. Mallela, *The N- and C-Terminal Domains Differentially Contribute to the Structure and Function of Dystrophin and Utrophin Tandem Calponin-Homology Domains*. Biochemistry, 2015. **54**(46): p. 6942-50.
62. Haenggi, T. and J.M. Fritschy, *Role of dystrophin and utrophin for assembly and function of the dystrophin glycoprotein complex in non-muscle tissue*. Cell Mol Life Sci, 2006. **63**(14): p. 1614-31.
63. Ayalon, G., et al., *An ankyrin-based mechanism for functional organization of dystrophin and dystroglycan*. Cell, 2008. **135**(7): p. 1189-200.
64. Bhosle, R.C., et al., *Interactions of intermediate filament protein synemin with dystrophin and utrophin*. Biochem Biophys Res Commun, 2006. **346**(3): p. 768-77.
65. Sadoulet-Puccio, H.M., M. Rajala, and L.M. Kunkel, *Dystrobrevin and dystrophin: an interaction through coiled-coil motifs*. Proc Natl Acad Sci U S A, 1997. **94**(23): p. 12413-8.
66. Rentschler, S., et al., *The WW domain of dystrophin requires EF-hands region to interact with beta-dystroglycan*. Biol Chem, 1999. **380**(4): p. 431-42.
67. Ponting, C.P., et al., *ZZ and TAZ: new putative zinc fingers in dystrophin and other proteins*. Trends Biochem Sci, 1996. **21**(1): p. 11-13.
68. Blake, D.J., et al., *Coiled-coil regions in the carboxy-terminal domains of dystrophin and related proteins: potentials for protein-protein interactions*. Trends Biochem Sci, 1995. **20**(4): p. 133-5.
69. Ilsley, J.L., M. Sudol, and S.J. Winder, *The WW domain: linking cell signalling to the membrane cytoskeleton*. Cell Signal, 2002. **14**(3): p. 183-9.
70. Kobayashi, Y.M., et al., *Sarcolemma-localized nNOS is required to maintain activity after mild exercise*. Nature, 2008. **456**(7221): p. 511-5.
71. Fong, P.Y., et al., *Increased activity of calcium leak channels in myotubes of Duchenne human and mdx mouse origin*. Science, 1990. **250**(4981): p. 673-6.
72. Turner, P.R., et al., *Increased protein degradation results from elevated free calcium levels found in muscle from mdx mice*. Nature, 1988. **335**(6192): p. 735-738.
73. Henderson, C.A., et al., *Overview of the Muscle Cytoskeleton*. Compr Physiol, 2017. **7**(3): p. 891-944.
74. Brancaccio, A., *A molecular overview of the primary dystroglycanopathies*. J Cell Mol Med, 2019. **23**(5): p. 3058-3062.
75. Crosbie, R.H., et al., *Sarcospan, the 25-kDa transmembrane component of the dystrophin-glycoprotein complex*. J Biol Chem, 1997. **272**(50): p. 31221-4.
76. Ozawa, E., et al., *Molecular and cell biology of the sarcoglycan complex*. Muscle Nerve, 2005. **32**(5): p. 563-76.
77. Bredt, D.S., *Knocking signalling out of the dystrophin complex*. Nat Cell Biol, 1999. **1**(4): p. E89-91.
78. Guiraud, S., et al., *The potential of utrophin and dystrophin combination therapies for Duchenne muscular dystrophy*. Hum Mol Genet, 2019. **28**(13): p. 2189-2200.
79. Deconinck, A.E., et al., *Utrophin-dystrophin-deficient mice as a model for Duchenne muscular dystrophy*. Cell, 1997. **90**(4): p. 717-27.
80. Tinsley, J.M., et al., *Primary structure of dystrophin-related protein*. Nature, 1992. **360**(6404): p. 591-3.
81. Love, D.R., et al., *An autosomal transcript in skeletal muscle with homology to dystrophin*. Nature, 1989. **339**(6219): p. 55-8.

## Reference list

---

82. Nudel, U., et al., *Duchenne muscular dystrophy gene product is not identical in muscle and brain*. *Nature*, 1989. **337**(6202): p. 76-8.
83. Holder, E., M. Maeda, and R.D. Bies, *Expression and regulation of the dystrophin Purkinje promoter in human skeletal muscle, heart, and brain*. *Hum Genet*, 1996. **97**(2): p. 232-9.
84. D'Souza, V.N., et al., *A novel dystrophin isoform is required for normal retinal electrophysiology*. *Hum Mol Genet*, 1995. **4**(5): p. 837-42.
85. Whewey, J.M. and R.G. Roberts, *The dystrophin lymphocyte promoter revisited: 4.5-megabase intron, or artifact?* *Neuromuscul Disord*, 2003. **13**(1): p. 17-20.
86. Lidov, H.G., S. Selig, and L.M. Kunkel, *Dp140: a novel 140 kDa CNS transcript from the dystrophin locus*. *Hum Mol Genet*, 1995. **4**(3): p. 329-35.
87. Byers, T.J., H.G. Lidov, and L.M. Kunkel, *An alternative dystrophin transcript specific to peripheral nerve*. *Nat Genet*, 1993. **4**(1): p. 77-81.
88. Austin, R.C., et al., *Cloning and characterization of alternatively spliced isoforms of Dp71*. *Hum Mol Genet*, 1995. **4**(9): p. 1475-83.
89. Lederfein, D., et al., *A 71-kilodalton protein is a major product of the Duchenne muscular dystrophy gene in brain and other nonmuscle tissues*. *Proceedings of the National Academy of Sciences of the United States of America*, 1992. **89**(12): p. 5346-5350.
90. Tinsley, J.M., D.J. Blake, and K.E. Davies, *Apo-dystrophin-3: a 2.2kb transcript from the DMD locus encoding the dystrophin glycoprotein binding site*. *Hum Mol Genet*, 1993. **2**(5): p. 521-4.
91. Koenig, M., et al., *Complete cloning of the Duchenne muscular dystrophy (DMD) cDNA and preliminary genomic organization of the DMD gene in normal and affected individuals*. *Cell*, 1987. **50**(3): p. 509-17.
92. Koenig, M., et al., *The molecular basis for Duchenne versus Becker muscular dystrophy: correlation of severity with type of deletion*. *Am J Hum Genet*, 1989. **45**(4): p. 498-506.
93. Bladen, C.L., et al., *The TREAT-NMD DMD Global Database: analysis of more than 7,000 Duchenne muscular dystrophy mutations*. *Hum Mutat*, 2015. **36**(4): p. 395-402.
94. Takeshima, Y., et al., *Mutation spectrum of the dystrophin gene in 442 Duchenne/Becker muscular dystrophy cases from one Japanese referral center*. *J Hum Genet*, 2010. **55**(6): p. 379-88.
95. Monaco, A.P., et al., *An explanation for the phenotypic differences between patients bearing partial deletions of the DMD locus*. *Genomics*, 1988. **2**(1): p. 90-5.
96. Aartsma-Rus, A., et al., *Therapeutic modulation of DMD splicing by blocking exonic splicing enhancer sites with antisense oligonucleotides*. *Ann N Y Acad Sci*, 2006. **1082**: p. 74-6.
97. Nicolas, A., et al., *Becker muscular dystrophy severity is linked to the structure of dystrophin*. *Hum Mol Genet*, 2015. **24**(5): p. 1267-79.
98. Kesari, A., et al., *Integrated DNA, cDNA, and protein studies in Becker muscular dystrophy show high exception to the reading frame rule*. *Hum Mutat*, 2008. **29**(5): p. 728-37.
99. Aartsma-Rus, A., I.B. Ginjaar, and K. Bushby, *The importance of genetic diagnosis for Duchenne muscular dystrophy*. *Journal of medical genetics*, 2016. **53**(3): p. 145-151.
100. Gloss, D., et al., *Practice guideline update summary: Corticosteroid treatment of Duchenne muscular dystrophy: Report of the Guideline Development Subcommittee of the American Academy of Neurology*. *Neurology*, 2016. **86**(5): p. 465-72.
101. Lebel, D.E., et al., *Glucocorticoid treatment for the prevention of scoliosis in children with Duchenne muscular dystrophy: long-term follow-up*. *J Bone Joint Surg Am*, 2013. **95**(12): p. 1057-61.
102. McDonald, C.M., et al., *Long-term effects of glucocorticoids on function, quality of life, and survival in patients with Duchenne muscular dystrophy: a prospective cohort study*. *Lancet*, 2018. **391**(10119): p. 451-461.
103. Merlini, L., et al., *Early corticosteroid treatment in 4 Duchenne muscular dystrophy patients: 14-year follow-up*. *Muscle Nerve*, 2012. **45**(6): p. 796-802.
104. Lamb, M.M., et al., *Corticosteroid Treatment and Growth Patterns in Ambulatory Males with Duchenne Muscular Dystrophy*. *J Pediatr*, 2016. **173**: p. 207-213.e3.
105. Mendell, J.R., et al., *Randomized, double-blind six-month trial of prednisone in Duchenne's muscular dystrophy*. *N Engl J Med*, 1989. **320**(24): p. 1592-7.
106. Donovan, J.M., et al., *A Novel NF- $\kappa$ B Inhibitor, Edasalonexent (CAT-1004), in Development as a Disease-Modifying Treatment for Patients With Duchenne Muscular Dystrophy: Phase 1 Safety, Pharmacokinetics, and Pharmacodynamics in Adult Subjects*. *Journal of clinical pharmacology*, 2017. **57**(5): p. 627-639.
107. Hoffman, E.P., et al., *Vamorolone trial in Duchenne muscular dystrophy shows dose-related improvement of muscle function*. *Neurology*, 2019. **93**(13): p. e1312-e1323.
108. Walter, M.C., et al., *Creatine monohydrate in muscular dystrophies: A double-blind, placebo-controlled clinical study*. *Neurology*, 2000. **54**(9): p. 1848-50.
109. Tarnopolsky, M.A., et al., *Creatine monohydrate enhances strength and body composition in Duchenne muscular dystrophy*. *Neurology*, 2004. **62**(10): p. 1771-7.
110. Louis, M., et al., *Beneficial effects of creatine supplementation in dystrophic patients*. *Muscle Nerve*, 2003. **27**(5): p. 604-10.
111. Birnkrant, D.J., et al., *Diagnosis and management of Duchenne muscular dystrophy, part 2: respiratory, cardiac, bone health, and orthopaedic management*. *Lancet Neurol*, 2018. **17**(4): p. 347-361.
112. Muenster, T., et al., *Anaesthetic management in patients with Duchenne muscular dystrophy undergoing orthopaedic surgery: a review of 232 cases*. *Eur J Anaesthesiol*, 2012. **29**(10): p. 489-94.
113. Segura, L.G., et al., *Anesthesia and Duchenne or Becker muscular dystrophy: review of 117 anesthetic exposures*. *Paediatr Anaesth*, 2013. **23**(9): p. 855-64.
114. Birnkrant, D.J., et al., *Diagnosis and management of Duchenne muscular dystrophy, part 3: primary care, emergency management, psychosocial care, and transitions of care across the lifespan*. *Lancet Neurol*, 2018. **17**(5): p. 445-455.
115. Nicholson, L.V., et al., *Functional significance of dystrophin positive fibres in Duchenne muscular dystrophy*. *Arch Dis Child*, 1993. **68**(5): p. 632-6.
116. Wells, D.J., et al., *Expression of human full-length and minidystrophin in transgenic mdx mice: implications for gene therapy of Duchenne muscular dystrophy*. *Hum Mol Genet*, 1995. **4**(8): p. 1245-50.
117. Welch, E.M., et al., *PTC124 targets genetic disorders caused by nonsense mutations*. *Nature*, 2007. **447**(7140): p. 87-91.
118. Finkel, R.S., *Read-through strategies for suppression of nonsense mutations in Duchenne/Becker muscular dystrophy: aminoglycosides and ataluren (PTC124)*. *J Child Neurol*, 2010. **25**(9): p. 1158-64.

119. European Medicines Agency. *Translarna*. 2019 [cited 2020 09.03.2020]; Available from: <https://www.ema.europa.eu/en/medicines/human/EPAR/translarna>.
120. Bushby, K., et al., *Ataluren treatment of patients with nonsense mutation dystrophinopathy*. *Muscle Nerve*, 2014. **50**(4): p. 477-87.
121. McDonald, C.M., et al., *Ataluren in patients with nonsense mutation Duchenne muscular dystrophy (ACT DMD): a multicentre, randomised, double-blind, placebo-controlled, phase 3 trial*. *Lancet*, 2017. **390**(10101): p. 1489-1498.
122. Aartsma-Rus, A., et al., *Theoretic applicability of antisense-mediated exon skipping for Duchenne muscular dystrophy mutations*. *Hum Mutat*, 2009. **30**(3): p. 293-9.
123. Aartsma-Rus, A., et al., *Targeted exon skipping as a potential gene correction therapy for Duchenne muscular dystrophy*. *Neuromuscul Disord*, 2002. **12 Suppl 1**: p. S71-7.
124. Pasteuning-Vuhman, S. and A. Aartsma-Rus, *What We Have Learned from 10 Years of DMD Exon-Skipping Trials*, in *Muscle Gene Therapy*, D. Duan and J.R. Mendell, Editors. 2019, Springer International Publishing: Cham. p. 745-758.
125. van Deutekom, J.C., et al., *Local dystrophin restoration with antisense oligonucleotide PRO051*. *N Engl J Med*, 2007. **357**(26): p. 2677-86.
126. Sharp, P.S., H. Bye-a-Jee, and D.J. Wells, *Physiological characterization of muscle strength with variable levels of dystrophin restoration in mdx mice following local antisense therapy*. *Mol Ther*, 2011. **19**(1): p. 165-71.
127. Dunckley, M.G., et al., *Modification of splicing in the dystrophin gene in cultured Mdx muscle cells by antisense oligoribonucleotides*. *Hum Mol Genet*, 1998. **7**(7): p. 1083-90.
128. Verhaart, I.E., et al., *The Dynamics of Compound, Transcript, and Protein Effects After Treatment With 2OMePS Antisense Oligonucleotides in mdx Mice*. *Mol Ther Nucleic Acids*, 2014. **3**: p. e148.
129. Blain, A.M., et al., *Peptide-conjugated phosphodiarnidate oligomer-mediated exon skipping has benefits for cardiac function in mdx and Cmah-/-mdx mouse models of Duchenne muscular dystrophy*. *PLoS One*, 2018. **13**(6): p. e0198897.
130. Echigoya, Y., et al., *Effects of systemic multiexon skipping with peptide-conjugated morpholinos in the heart of a dog model of Duchenne muscular dystrophy*. *Proc Natl Acad Sci U S A*, 2017. **114**(16): p. 4213-4218.
131. Moulton, H.M. and J.D. Moulton, *Morpholinos and their peptide conjugates: therapeutic promise and challenge for Duchenne muscular dystrophy*. *Biochim Biophys Acta*, 2010. **1798**(12): p. 2296-303.
132. Goemans, N., et al., *A randomized placebo-controlled phase 3 trial of an antisense oligonucleotide, drisapersen, in Duchenne muscular dystrophy*. *Neuromuscul Disord*, 2018. **28**(1): p. 4-15.
133. Tandon, V., Yan, S., Rao, A., *FDA Efficacy Review - Drisapersen*. 2015.
134. Food and Drug Administration. *Drug Approval Package: Exondys 51 ijection (eteplirsen)*. 2016 [cited 2020 09.03.2020]; Available from: [https://www.accessdata.fda.gov/drugsatfda\\_docs/nda/2016/206488\\_TOC.cfm](https://www.accessdata.fda.gov/drugsatfda_docs/nda/2016/206488_TOC.cfm).
135. Aartsma-Rus, A. and A.M. Krieg, *FDA Approves Eteplirsen for Duchenne Muscular Dystrophy: The Next Chapter in the Eteplirsen Saga*. *Nucleic Acid Ther*, 2017. **27**(1): p. 1-3.
136. Alfano, L.N., et al., *Long-term treatment with eteplirsen in nonambulatory patients with Duchenne muscular dystrophy*. *Medicine (Baltimore)*, 2019. **98**(26): p. e15858.
137. Mendell, J.R., et al., *Eteplirsen for the treatment of Duchenne muscular dystrophy*. *Ann Neurol*, 2013. **74**(5): p. 637-47.
138. European Medicines Agency, *Versagung der Genehmigung für das Inverkehrbringen von Exondys (Eteplirsen)*. 2018.
139. Shirley, M., *Casimersen: First Approval*. *Drugs*, 2021. **81**(7): p. 875-879.
140. Heo, Y.A., *Golodirsen: First Approval*. *Drugs*, 2020. **80**(3): p. 329-333.
141. Chapdelaine, P., et al., *Meganucleases can restore the reading frame of a mutated dystrophin*. *Gene Ther*, 2010. **17**(7): p. 846-58.
142. Rousseau, J., et al., *Endonucleases: tools to correct the dystrophin gene*. *J Gene Med*, 2011. **13**(10): p. 522-37.
143. Ousterout, D.G., et al., *Reading frame correction by targeted genome editing restores dystrophin expression in cells from Duchenne muscular dystrophy patients*. *Mol Ther*, 2013. **21**(9): p. 1718-26.
144. Mata Lopez, S., et al., *Challenges associated with homologous directed repair using CRISPR-Cas9 and TALEN to edit the DMD genetic mutation in canine Duchenne muscular dystrophy*. *PLoS One*, 2020. **15**(1): p. e0228072.
145. Ousterout, D.G., et al., *Correction of dystrophin expression in cells from Duchenne muscular dystrophy patients through genomic excision of exon 51 by zinc finger nucleases*. *Mol Ther*, 2015. **23**(3): p. 523-32.
146. Moretti, A., et al., *Somatic gene editing ameliorates skeletal and cardiac muscle failure in pig and human models of Duchenne muscular dystrophy*. *Nat Med*, 2020.
147. Bengtsson, N.E., et al., *Muscle-specific CRISPR/Cas9 dystrophin gene editing ameliorates pathophysiology in a mouse model for Duchenne muscular dystrophy*. *Nat Commun*, 2017. **8**: p. 14454.
148. Amoasii, L., et al., *Gene editing restores dystrophin expression in a canine model of Duchenne muscular dystrophy*. *Science*, 2018. **362**(6410): p. 86-91.
149. Nelson, C.E., et al., *In vivo genome editing improves muscle function in a mouse model of Duchenne muscular dystrophy*. *Science*, 2016. **351**(6271): p. 403-407.
150. Long, C., et al., *Postnatal genome editing partially restores dystrophin expression in a mouse model of muscular dystrophy*. *Science*, 2016. **351**(6271): p. 400-3.
151. Tabeordbar, M., et al., *In vivo gene editing in dystrophic mouse muscle and muscle stem cells*. *Science*, 2016. **351**(6271): p. 407-411.
152. McCarter, G.C., et al., *Lipofection of a cDNA plasmid containing the dystrophin gene lowers intracellular free calcium and calcium leak channel activity in mdx myotubes*. *Gene Ther*, 1997. **4**(5): p. 483-7.
153. Pichavant, C., et al., *Electrotransfer of the full-length dog dystrophin into mouse and dystrophic dog muscles*. *Hum Gene Ther*, 2010. **21**(11): p. 1591-601.
154. Acsadi, G., et al., *Human dystrophin expression in mdx mice after intramuscular injection of DNA constructs*. *Nature*, 1991. **352**(6338): p. 815-8.
155. Romero, N.B., et al., *Phase I study of dystrophin plasmid-based gene therapy in Duchenne/Becker muscular dystrophy*. *Hum Gene Ther*, 2004. **15**(11): p. 1065-76.
156. Akkaraju, G.R., et al., *Herpes simplex virus vector-mediated dystrophin gene transfer and expression in MDX mouse skeletal muscle*. *The journal of gene medicine*, 1999. **1**(4): p. 280-289.
157. Haecker, S.E., et al., *In vivo expression of full-length human dystrophin from adenoviral vectors deleted of all viral genes*. *Human gene therapy*, 1996. **7**(15): p. 1907-1914.
158. DelloRusso, C., et al., *Functional correction of adult mdx mouse muscle using gutted adenoviral vectors expressing full-length dystrophin*. *Proceedings of the National Academy of Sciences of the United States of America*, 2002. **99**(20): p. 12979-12984.

## Reference list

---

159. Wang, Z., et al., *Immunity and AAV-Mediated Gene Therapy for Muscular Dystrophies in Large Animal Models and Human Trials*. Front Microbiol, 2011. **2**: p. 201.
160. Miller, D.G., M.A. Adam, and A.D. Miller, *Gene transfer by retrovirus vectors occurs only in cells that are actively replicating at the time of infection*. Molecular and cellular biology, 1990. **10**(8): p. 4239-4242.
161. Koo, T., et al., *Triple trans-splicing adeno-associated virus vectors capable of transferring the coding sequence for full-length dystrophin protein into dystrophic mice*. Hum Gene Ther, 2014. **25**(2): p. 98-108.
162. Lostal, W., et al., *Full-length dystrophin reconstitution with adeno-associated viral vectors*. Human gene therapy, 2014. **25**(6): p. 552-562.
163. Bish, L.T., et al., *Long-term restoration of cardiac dystrophin expression in golden retriever muscular dystrophy following rAAV6-mediated exon skipping*. Mol Ther, 2012. **20**(3): p. 580-9.
164. Goyenville, A., et al., *Rescue of dystrophic muscle through U7 snRNA-mediated exon skipping*. Science, 2004. **306**(5702): p. 1796-9.
165. Brun, C., et al., *U7 snRNAs induce correction of mutated dystrophin pre-mRNA by exon skipping*. Cell Mol Life Sci, 2003. **60**(3): p. 557-66.
166. England, S.B., et al., *Very mild muscular dystrophy associated with the deletion of 46% of dystrophin*. Nature, 1990. **343**(6254): p. 180-2.
167. Vincent, N., et al., *Long-term correction of mouse dystrophic degeneration by adenovirus-mediated transfer of a minidystrophin gene*. Nat Genet, 1993. **5**(2): p. 130-4.
168. Ragot, T., et al., *Efficient adenovirus-mediated transfer of a human minidystrophin gene to skeletal muscle of mdx mice*. Nature, 1993. **361**(6413): p. 647-50.
169. Bowles, D.E., et al., *Phase 1 gene therapy for Duchenne muscular dystrophy using a translational optimized AAV vector*. Mol Ther, 2012. **20**(2): p. 443-55.
170. ClinicalTrials.gov, *AAV9 U7snRNA Gene Therapy to Treat Boys With DMD Exon 2 Duplications*. 2020.
171. ClinicalTrials.gov, *A Study to Evaluate the Safety and Tolerability of PF-06939926 Gene Therapy in Duchenne Muscular Dystrophy*. 2017.
172. ClinicalTrials.gov, *Systemic Gene Delivery Clinical Trial for Duchenne Muscular Dystrophy*. 2017.
173. Fu, H., et al., *Differential Prevalence of Antibodies Against Adeno-Associated Virus in Healthy Children and Patients with Mucopolysaccharidosis III: Perspective for AAV-Mediated Gene Therapy*. Hum Gene Ther Clin Dev, 2017. **28**(4): p. 187-196.
174. Buyse, G.M., et al., *Long-term blinded placebo-controlled study of SNT-MC17/idebenone in the dystrophin deficient mdx mouse: cardiac protection and improved exercise performance*. European heart journal, 2009. **30**(1): p. 116-124.
175. Servais, L., et al., *Long-term data with idebenone on respiratory function outcomes in patients with Duchenne muscular dystrophy*. Neuromuscul Disord, 2020. **30**(1): p. 5-16.
176. Xu, R., et al., *rAAVrh74.MCK.GALGT2 Protects against Loss of Hemodynamic Function in the Aging mdx Mouse Heart*. Mol Ther, 2019. **27**(3): p. 636-649.
177. Wagner, K.R., et al., *Loss of myostatin attenuates severity of muscular dystrophy in mdx mice*. Ann Neurol, 2002. **52**(6): p. 832-6.
178. McPherron, A.C., A.M. Lawler, and S.J. Lee, *Regulation of skeletal muscle mass in mice by a new TGF-beta superfamily member*. Nature, 1997. **387**(6628): p. 83-90.
179. Wagner, K.R., et al., *A phase I/II trial of MYO-029 in adult subjects with muscular dystrophy*. Ann Neurol, 2008. **63**(5): p. 561-71.
180. Pfizer, *Pfizer Terminates Domagrozumab (PF-06252616) Clinical Studies for the Treatment of Duchenne Muscular Dystrophy* 2018.
181. Gussoni, E., H.M. Blau, and L.M. Kunkel, *The fate of individual myoblasts after transplantation into muscles of DMD patients*. Nat Med, 1997. **3**(9): p. 970-7.
182. Gussoni, E., et al., *Dystrophin expression in the mdx mouse restored by stem cell transplantation*. Nature, 1999. **401**(6751): p. 390-4.
183. Skuk, D., et al., *Dystrophin expression in myofibers of Duchenne muscular dystrophy patients following intramuscular injections of normal myogenic cells*. Mol Ther, 2004. **9**(3): p. 475-82.
184. Cerletti, M., et al., *Highly efficient, functional engraftment of skeletal muscle stem cells in dystrophic muscles*. Cell, 2008. **134**(1): p. 37-47.
185. Shieh, P.B., *Emerging Strategies in the Treatment of Duchenne Muscular Dystrophy*. Neurotherapeutics : the journal of the American Society for Experimental NeuroTherapeutics, 2018. **15**(4): p. 840-848.
186. U.S. National Library of Medicine, *ClinicalTrials.gov*. 2021.
187. Wells, D.J., *Tracking progress: an update on animal models for Duchenne muscular dystrophy*. Dis Model Mech, 2018. **11**(6).
188. McGreevy, J.W., et al., *Animal models of Duchenne muscular dystrophy: from basic mechanisms to gene therapy*. Dis Model Mech, 2015. **8**(3): p. 195-213.
189. Bulfield, G., et al., *X chromosome-linked muscular dystrophy (mdx) in the mouse*. Proc Natl Acad Sci U S A, 1984. **81**(4): p. 1189-92.
190. Chamberlain, J.S., et al., *Expression of the murine Duchenne muscular dystrophy gene in muscle and brain*. Science, 1988. **239**(4846): p. 1416-8.
191. Sicinski, P., et al., *The molecular basis of muscular dystrophy in the mdx mouse: a point mutation*. Science, 1989. **244**(4912): p. 1578-80.
192. Vainzof, M., et al., *Animal models for genetic neuromuscular diseases*. J Mol Neurosci, 2008. **34**(3): p. 241-8.
193. Chamberlain, J.S., et al., *Dystrophin-deficient mdx mice display a reduced life span and are susceptible to spontaneous rhabdomyosarcoma*. Faseb j, 2007. **21**(9): p. 2195-204.
194. Stedman, H.H., et al., *The mdx mouse diaphragm reproduces the degenerative changes of Duchenne muscular dystrophy*. Nature, 1991. **352**(6335): p. 536-9.
195. Tanabe, Y., K. Esaki, and T. Nomura, *Skeletal muscle pathology in X chromosome-linked muscular dystrophy (mdx) mouse*. Acta Neuropathol, 1986. **69**(1-2): p. 91-5.
196. Lefaucheur, J.P., C. Pastoret, and A. Sebillé, *Phenotype of dystrophinopathy in old mdx mice*. Anat Rec, 1995. **242**(1): p. 70-6.
197. Fukada, S., et al., *Genetic background affects properties of satellite cells and mdx phenotypes*. Am J Pathol, 2010. **176**(5): p. 2414-24.

198. Chapman, V.M., et al., *Recovery of induced mutations for X chromosome-linked muscular dystrophy in mice*. Proc Natl Acad Sci U S A, 1989. **86**(4): p. 1292-6.
199. Araki, E., et al., *Targeted disruption of exon 52 in the mouse dystrophin gene induced muscle degeneration similar to that observed in Duchenne muscular dystrophy*. Biochem Biophys Res Commun, 1997. **238**(2): p. 492-7.
200. Kudoh, H., et al., *A new model mouse for Duchenne muscular dystrophy produced by 2.4 Mb deletion of dystrophin gene using Cre-loxP recombination system*. Biochem Biophys Res Commun, 2005. **328**(2): p. 507-16.
201. t Hoen, P.A., et al., *Generation and characterization of transgenic mice with the full-length human DMD gene*. J Biol Chem, 2008. **283**(9): p. 5899-907.
202. Rodrigues, M., et al., *Current Translational Research and Murine Models For Duchenne Muscular Dystrophy*. J Neuromuscul Dis, 2016. **3**(1): p. 29-48.
203. Rooney, J.E., et al., *Severe muscular dystrophy in mice that lack dystrophin and alpha7 integrin*. J Cell Sci, 2006. **119**(Pt 11): p. 2185-95.
204. Guo, C., et al., *Absence of alpha 7 integrin in dystrophin-deficient mice causes a myopathy similar to Duchenne muscular dystrophy*. Hum Mol Genet, 2006. **15**(6): p. 989-98.
205. Partridge, T.A., *The mdx mouse model as a surrogate for Duchenne muscular dystrophy*. Febs j, 2013. **280**(17): p. 4177-86.
206. Nakamura, K., et al., *Generation of muscular dystrophy model rats with a CRISPR/Cas system*. Sci Rep, 2014. **4**: p. 5635.
207. Larcher, T., et al., *Characterization of dystrophin deficient rats: a new model for Duchenne muscular dystrophy*. PLoS One, 2014. **9**(10): p. e110371.
208. Sui, T., et al., *A novel rabbit model of Duchenne muscular dystrophy generated by CRISPR/Cas9*. Dis Model Mech, 2018. **11**(6).
209. Groenen, M.A., et al., *Analyses of pig genomes provide insight into porcine demography and evolution*. Nature, 2012. **491**(7424): p. 393-8.
210. Gieseler, K., K. Grisoni, and L. Segalat, *Genetic suppression of phenotypes arising from mutations in dystrophin-related genes in Caenorhabditis elegans*. Curr Biol, 2000. **10**(18): p. 1092-7.
211. Lloyd, T.E. and J.P. Taylor, *Flightless flies: Drosophila models of neuromuscular disease*. Ann N Y Acad Sci, 2010. **1184**: p. e1-20.
212. Berger, J. and P.D. Currie, *Zebrafish models flex their muscles to shed light on muscular dystrophies*. Dis Model Mech, 2012. **5**(6): p. 726-32.
213. Sharp, N.J., et al., *An error in dystrophin mRNA processing in golden retriever muscular dystrophy, an animal homologue of Duchenne muscular dystrophy*. Genomics, 1992. **13**(1): p. 115-21.
214. Cooper, B.J., et al., *The homologue of the Duchenne locus is defective in X-linked muscular dystrophy of dogs*. Nature, 1988. **334**(6178): p. 154-6.
215. Shimatsu, Y., et al., *Canine X-linked muscular dystrophy in Japan (CXMDJ)*. Exp Anim, 2003. **52**(2): p. 93-7.
216. Walmsley, G.L., et al., *A duchenne muscular dystrophy gene hot spot mutation in dystrophin-deficient cavalier king charles spaniels is amenable to exon 51 skipping*. PLoS One, 2010. **5**(1): p. e8647.
217. Smith, B.F., et al., *An intronic LINE-1 element insertion in the dystrophin gene aborts dystrophin expression and results in Duchenne-like muscular dystrophy in the corgi breed*. Lab Invest, 2011. **91**(2): p. 216-31.
218. Banks, G.B. and J.S. Chamberlain, *The value of mammalian models for duchenne muscular dystrophy in developing therapeutic strategies*. Curr Top Dev Biol, 2008. **84**: p. 431-53.
219. Kornegay, J.N., et al., *Golden retriever muscular dystrophy (GRMD): Developing and maintaining a colony and physiological functional measurements*. Methods Mol Biol, 2011. **709**: p. 105-23.
220. Kornegay, J.N., et al., *Canine models of Duchenne muscular dystrophy and their use in therapeutic strategies*. Mamm Genome, 2012. **23**(1-2): p. 85-108.
221. Brinkmeyer-Langford, C., et al., *Genome-wide association study to identify potential genetic modifiers in a canine model for Duchenne muscular dystrophy*. BMC Genomics, 2016. **17**: p. 665.
222. Gaschen, L., et al., *Cardiomyopathy in dystrophin-deficient hypertrophic feline muscular dystrophy*. J Vet Intern Med, 1999. **13**(4): p. 346-56.
223. Carpenter, J.L., et al., *Feline muscular dystrophy with dystrophin deficiency*. Am J Pathol, 1989. **135**(5): p. 909-19.
224. Winand, N.J., et al., *Deletion of the dystrophin muscle promoter in feline muscular dystrophy*. Neuromuscul Disord, 1994. **4**(5-6): p. 433-45.
225. Yu, X., et al., *Dystrophin-deficient large animal models: translational research and exon skipping*. Am J Transl Res, 2015. **7**(8): p. 1314-31.
226. Gambino, A.N., et al., *Emergent presentation of a cat with dystrophin-deficient muscular dystrophy*. J Am Anim Hosp Assoc, 2014. **50**(2): p. 130-5.
227. Chen, Y., et al., *Functional disruption of the dystrophin gene in rhesus monkey using CRISPR/Cas9*. Hum Mol Genet, 2015. **24**(13): p. 3764-74.
228. Nonneman, D.J., et al., *A defect in dystrophin causes a novel porcine stress syndrome*. BMC Genomics, 2012. **13**: p. 233.
229. Horiuchi, N., et al., *Becker muscular dystrophy-like myopathy regarded as so-called "fatty muscular dystrophy" in a pig: a case report and its diagnostic method*. J Vet Med Sci, 2014. **76**(2): p. 243-8.
230. Frantz, L.A.F., et al., *Ancient pigs reveal a near-complete genomic turnover following their introduction to Europe*. Proc Natl Acad Sci U S A, 2019. **116**(35): p. 17231-17238.
231. Perleberg, C., A. Kind, and A. Schnieke, *Genetically engineered pigs as models for human disease*. Dis Model Mech, 2018. **11**(1).
232. Clauss, S., et al., *Animal models of arrhythmia: classic electrophysiology to genetically modified large animals*. Nature Reviews Cardiology, 2019.
233. Klymiuk, N., et al., *Tailored Pig Models for Preclinical Efficacy and Safety Testing of Targeted Therapies*. Toxicol Pathol, 2016. **44**(3): p. 346-57.
234. Aigner, B., et al., *Transgenic pigs as models for translational biomedical research*. J Mol Med (Berl), 2010. **88**(7): p. 653-64.
235. Wolf, E., et al., *Transgenic technology in farm animals--progress and perspectives*. Exp Physiol, 2000. **85**(6): p. 615-25.
236. Bordais, A., et al., *Molecular cloning and protein expression of Duchenne muscular dystrophy gene products in porcine retina*. Neuromuscul Disord, 2005. **15**(7): p. 476-87.

## Reference list

---

237. Klymiuk, N., et al., *Dystrophin-deficient pigs provide new insights into the hierarchy of physiological derangements of dystrophic muscle*. Hum Mol Genet, 2013. **22**(21): p. 4368-82.
238. Estrada, J., et al., *Swine generated by somatic cell nuclear transfer have increased incidence of intrauterine growth restriction (IUGR)*. Cloning Stem Cells, 2007. **9**(2): p. 229-36.
239. Zhao, J., J. Whyte, and R.S. Prather, *Effect of epigenetic regulation during swine embryogenesis and on cloning by nuclear transfer*. Cell Tissue Res, 2010. **341**(1): p. 13-21.
240. Matsunari, H., et al., *Modeling lethal X-linked genetic disorders in pigs with ensured fertility*. Proc Natl Acad Sci U S A, 2018. **115**(4): p. 708-713.
241. Rogers, C.S. and J.R. Swart, *Animal models of Duchenne muscular dystrophy*. 2014: United States of America.
242. Rogers, C.S., et al., *Disruption of the CFTR gene produces a model of cystic fibrosis in newborn pigs*. Science, 2008. **321**(5897): p. 1837-41.
243. White, K.A., et al., *A porcine model of neurofibromatosis type 1 that mimics the human disease*. JCI Insight, 2018. **3**(12).
244. Amuzie, C., et al., *A Translational Model for Diet-related Atherosclerosis: Effect of Statins on Hypercholesterolemia and Atherosclerosis in a Minipig*. Toxicol Pathol, 2016. **44**(3): p. 442-9.
245. Yu, H.H., et al., *Porcine Zygote Injection with Cas9/sgRNA Results in DMD-Modified Pig with Muscle Dystrophy*. Int J Mol Sci, 2016. **17**(10).
246. Krause, S., et al., *A novel homozygous missense mutation in the GNE gene of a patient with quadriceps-sparing hereditary inclusion body myopathy associated with muscle inflammation*. Neuromuscul Disord, 2003. **13**(10): p. 830-4.
247. Krause, S., *Insights into muscle degeneration from heritable inclusion body myopathies*. Front Aging Neurosci, 2015. **7**: p. 13.
248. Mitrani-Rosenbaum, S., et al., *Hereditary inclusion body myopathy maps to chromosome 9p1-q1*. Hum Mol Genet, 1996. **5**(1): p. 159-163.
249. Eisenberg, I., et al., *The UDP-N-acetylglucosamine 2-epimerase/N-acetylmannosamine kinase gene is mutated in recessive hereditary inclusion body myopathy*. Nat Genet, 2001. **29**(1): p. 83-7.
250. Nishino, I., et al., *Distal myopathy with rimmed vacuoles is allelic to hereditary inclusion body myopathy*. Neurology, 2002. **59**(11): p. 1689-93.
251. Hinderlich, S., et al., *A bifunctional enzyme catalyzes the first two steps in N-acetylneuraminic acid biosynthesis of rat liver. Purification and characterization of UDP-N-acetylglucosamine 2-epimerase/N-acetylmannosamine kinase*. J Biol Chem, 1997. **272**(39): p. 24313-8.
252. Keppler, O.T., et al., *UDP-GlcNAc 2-epimerase: a regulator of cell surface sialylation*. Science, 1999. **284**(5418): p. 1372-6.
253. Schwarzkopf, M., et al., *Sialylation is essential for early development in mice*. Proc Natl Acad Sci U S A, 2002. **99**(8): p. 5267-70.
254. Krause, S., et al., *GNE protein expression and subcellular distribution are unaltered in HIBM*. Neurology, 2007. **69**(7): p. 655-9.
255. Savelkoul, P.J., et al., *Normal sialylation of serum N-linked and O-GalNAc-linked glycans in hereditary inclusion-body myopathy*. Mol Genet Metab, 2006. **88**(4): p. 389-90.
256. Gagiannis, D., et al., *Reduced sialylation status in UDP-N-acetylglucosamine-2-epimerase/N-acetylmannosamine kinase (GNE)-deficient mice*. Glycoconj J, 2007. **24**(2-3): p. 125-30.
257. Krause, S., et al., *Localization of UDP-GlcNAc 2-epimerase/ManAc kinase (GNE) in the Golgi complex and the nucleus of mammalian cells*. Exp Cell Res, 2005. **304**(2): p. 365-79.
258. Cho, A., et al., *Sialic acid deficiency is associated with oxidative stress leading to muscle atrophy and weakness in GNE myopathy*. Hum Mol Genet, 2017. **26**(16): p. 3081-3093.
259. Weidemann, W., et al., *Lessons from GNE-deficient embryonic stem cells: sialic acid biosynthesis is involved in proliferation and gene expression*. Glycobiology, 2010. **20**(1): p. 107-17.
260. Harazi, A., et al., *Survival-apoptosis associated signaling in GNE myopathy-cultured myoblasts*. J Recept Signal Transduct Res, 2015. **35**(4): p. 249-57.
261. Nonaka, I., et al., *Distal myopathy with rimmed vacuoles*. Neuromuscul Disord, 1998. **8**(5): p. 333-7.
262. Nonaka, I., et al., *Familial distal myopathy with rimmed vacuole and lamellar (myeloid) body formation*. J Neurol Sci, 1981. **51**(1): p. 141-55.
263. Argov, Z. and R. Yarom, *"Rimmed vacuole myopathy" sparing the quadriceps. A unique disorder in Iranian Jews*. J Neurol Sci, 1984. **64**(1): p. 33-43.
264. Pogoryelova, O., et al., *Phenotypic stratification and genotype-phenotype correlation in a heterogeneous, international cohort of GNE myopathy patients: First report from the GNE myopathy Disease Monitoring Program, registry portion*. Neuromuscul Disord, 2018. **28**(2): p. 158-168.
265. Carrillo, N., M.C. Malicdan, and M. Huizing, *GNE Myopathy: Etiology, Diagnosis, and Therapeutic Challenges*. Neurotherapeutics, 2018. **15**(4): p. 900-914.
266. Chai, Y., T.E. Bortorini, and F.A. McGrew, *Hereditary inclusion-body myopathy associated with cardiomyopathy: report of two siblings*. Muscle Nerve, 2011. **43**(1): p. 133-6.
267. Nishino, I., et al., *Molecular pathomechanism of distal myopathy with rimmed vacuoles*. Acta Myol, 2005. **24**(2): p. 80-3.
268. Mori-Yoshimura, M., et al., *Heterozygous UDP-GlcNAc 2-epimerase and N-acetylmannosamine kinase domain mutations in the GNE gene result in a less severe GNE myopathy phenotype compared to homozygous N-acetylmannosamine kinase domain mutations*. J Neurol Sci, 2012. **318**(1-2): p. 100-5.
269. Chamova, T., et al., *GNE myopathy in Roma patients homozygous for the p.I618T founder mutation*. Neuromuscul Disord, 2015. **25**(9): p. 713-8.
270. Celeste, F.V., et al., *Mutation update for GNE gene variants associated with GNE myopathy*. Hum Mutat, 2014. **35**(8): p. 915-26.
271. Eisenberg, I., et al., *Mutations spectrum of GNE in hereditary inclusion body myopathy sparing the quadriceps*. Hum Mutat, 2003. **21**(1): p. 99.
272. Watts, G.D., et al., *Inclusion body myopathy associated with Paget disease of bone and frontotemporal dementia is caused by mutant valosin-containing protein*. Nat Genet, 2004. **36**(4): p. 377-81.
273. Kovach, M.J., et al., *Clinical delineation and localization to chromosome 9p13.3-p12 of a unique dominant disorder in four families: hereditary inclusion body myopathy, Paget disease of bone, and frontotemporal dementia*. Mol Genet Metab, 2001. **74**(4): p. 458-75.
274. Evangelista, T., et al., *215th ENMC International Workshop VCP-related multi-system proteinopathy (IBMPFD) 13-15 November 2015, Heemskerk, The Netherlands*. Neuromuscul Disord, 2016. **26**(8): p. 535-47.

275. Ju, J.S., et al., *Valosin-containing protein (VCP) is required for autophagy and is disrupted in VCP disease*. J Cell Biol, 2009. **187**(6): p. 875-88.
276. Fernandez-Saiz, V. and A. Buchberger, *Imbalances in p97 co-factor interactions in human proteinopathy*. EMBO Rep, 2010. **11**(6): p. 479-85.
277. Mehta, S.G., et al., *Genotype-phenotype studies of VCP-associated inclusion body myopathy with Paget disease of bone and/or frontotemporal dementia*. Clin Genet, 2013. **83**(5): p. 422-31.
278. Neumann, M., et al., *Ubiquitinated TDP-43 in frontotemporal lobar degeneration and amyotrophic lateral sclerosis*. Science, 2006. **314**(5796): p. 130-3.
279. Weihl, C.C., A. Pestronk, and V.E. Kimonis, *Valosin-containing protein disease: inclusion body myopathy with Paget's disease of the bone and fronto-temporal dementia*. Neuromuscul Disord, 2009. **19**(5): p. 308-15.
280. Papadimas GK, P.G., Zambelis T, Karagiaouris C., B.A. Bourbouli M, Walter MC, Schumacher NU., and K.S.a.K. E, *The multifaceted clinical representation of VCP-proteinopathy in a Greek family*. Acta Myol, 2017.
281. van der Zee, J., et al., *Clinical heterogeneity in 3 unrelated families linked to VCP p.Arg159His*. Neurology, 2009. **73**(8): p. 626-32.
282. Nalbandian, A., et al., *The multiple faces of valosin-containing protein-associated diseases: inclusion body myopathy with Paget's disease of bone, frontotemporal dementia, and amyotrophic lateral sclerosis*. J Mol Neurosci, 2011. **45**(3): p. 522-31.
283. Byrne, S., et al., *Rate of familial amyotrophic lateral sclerosis: a systematic review and meta-analysis*. J Neurol Neurosurg Psychiatry, 2011. **82**(6): p. 623-7.
284. Koppers, M., et al., *VCP mutations in familial and sporadic amyotrophic lateral sclerosis*. Neurobiol Aging, 2012. **33**(4): p. 837.e7-13.
285. Johnson, J.O., et al., *Exome sequencing reveals VCP mutations as a cause of familial ALS*. Neuron, 2010. **68**(5): p. 857-64.
286. Hayflick, L. and P.S. Moorhead, *The serial cultivation of human diploid cell strains*. Exp Cell Res, 1961. **25**: p. 585-621.
287. Bodnar, A.G., et al., *Extension of life-span by introduction of telomerase into normal human cells*. Science, 1998. **279**(5349): p. 349-52.
288. Scherer, W.F., J.T. Syverton, and G.O. Gey, *Studies on the propagation in vitro of poliomyelitis viruses. IV. Viral multiplication in a stable strain of human malignant epithelial cells (strain HeLa) derived from an epidermoid carcinoma of the cervix*. The Journal of experimental medicine, 1953. **97**(5): p. 695-710.
289. Mamchaoui, K., et al., *Immortalized pathological human myoblasts: towards a universal tool for the study of neuromuscular disorders*. Skelet Muscle, 2011. **1**: p. 34.
290. Todaro, G.J. and H. Green, *Quantitative studies of the growth of mouse embryo cells in culture and their development into established lines*. The Journal of cell biology, 1963. **17**(2): p. 299-313.
291. Yaffe, D. and O. Saxel, *Serial passaging and differentiation of myogenic cells isolated from dystrophic mouse muscle*. Nature, 1977. **270**(5639): p. 725-7.
292. Ahuja, D., M.T. Sáenz-Robles, and J.M. Pipas, *SV40 large T antigen targets multiple cellular pathways to elicit cellular transformation*. Oncogene, 2005. **24**(52): p. 7729-7745.
293. Pańcyszyn, A., E. Boniewska-Bernacka, and G. Głąb, *Telomeres and Telomerase During Human Papillomavirus-Induced Carcinogenesis*. Molecular diagnosis & therapy, 2018. **22**(4): p. 421-430.
294. Speiseder, T., et al., *Efficient Transformation of Primary Human Mesenchymal Stromal Cells by Adenovirus Early Region 1 Oncogenes*. J Virol, 2017. **91**(1).
295. Ip, W.H. and T. Dobner, *Cell transformation by the adenovirus oncogenes E1 and E4*. FEBS Lett, 2019.
296. Yoon, S., et al., *Immortalized myogenic cells from congenital muscular dystrophy type1A patients recapitulate aberrant caspase activation in pathogenesis: a new tool for MDC1A research*. Skelet Muscle, 2013. **3**(1): p. 28.
297. Meselson, M. and F.W. Stahl, *THE REPLICATION OF DNA IN ESCHERICHIA COLI*. Proceedings of the National Academy of Sciences of the United States of America, 1958. **44**(7): p. 671-682.
298. Watson, J.D. and F.H. Crick, *Molecular structure of nucleic acids; a structure for deoxyribose nucleic acid*. Nature, 1953. **171**(4356): p. 737-8.
299. Olovnikov, A.M., *A theory of marginotomy. The incomplete copying of template margin in enzymic synthesis of polynucleotides and biological significance of the phenomenon*. J Theor Biol, 1973. **41**(1): p. 181-90.
300. Harley, C.B., A.B. Futcher, and C.W. Greider, *Telomeres shorten during ageing of human fibroblasts*. Nature, 1990. **345**(6274): p. 458-60.
301. Hastie, N.D., et al., *Telomere reduction in human colorectal carcinoma and with ageing*. Nature, 1990. **346**(6287): p. 866-8.
302. von Zglinicki, T., R. Pilger, and N. Sitte, *Accumulation of single-strand breaks is the major cause of telomere shortening in human fibroblasts*. Free Radic Biol Med, 2000. **28**(1): p. 64-74.
303. Makarov, V.L., Y. Hirose, and J.P. Langmore, *Long G tails at both ends of human chromosomes suggest a C strand degradation mechanism for telomere shortening*. Cell, 1997. **88**(5): p. 657-66.
304. Harley, C.B., *Telomere loss: mitotic clock or genetic time bomb?* Mutat Res, 1991. **256**(2-6): p. 271-82.
305. Hemann, M.T., et al., *The shortest telomere, not average telomere length, is critical for cell viability and chromosome stability*. Cell, 2001. **107**(1): p. 67-77.
306. Maciejowski, J. and T. de Lange, *Telomeres in cancer: tumour suppression and genome instability*. Nature reviews. Molecular cell biology, 2017. **18**(3): p. 175-186.
307. Cohen, S.B., et al., *Protein composition of catalytically active human telomerase from immortal cells*. Science, 2007. **315**(5820): p. 1850-3.
308. Schwartz, S., et al., *Transcriptome-wide mapping reveals widespread dynamic-regulated pseudouridylation of ncRNA and mRNA*. Cell, 2014. **159**(1): p. 148-162.
309. de Lange, T., *Shelterin: the protein complex that shapes and safeguards human telomeres*. Genes Dev, 2005. **19**(18): p. 2100-10.
310. Doksan, Y., et al., *Super-resolution fluorescence imaging of telomeres reveals TRF2-dependent T-loop formation*. Cell, 2013. **155**(2): p. 345-356.
311. Griffith, J.D., et al., *Mammalian telomeres end in a large duplex loop*. Cell, 1999. **97**(4): p. 503-14.
312. Fleisig, H.B., et al., *Telomerase reverse transcriptase expression protects transformed human cells against DNA-damaging agents, and increases tolerance to chromosomal instability*. Oncogene, 2016. **35**(2): p. 218-27.

## Reference list

---

313. Smith, L.L., H.A. Collier, and J.M. Roberts, *Telomerase modulates expression of growth-controlling genes and enhances cell proliferation*. *Nat Cell Biol*, 2003. **5**(5): p. 474-9.
314. Park, J.I., et al., *Telomerase modulates Wnt signalling by association with target gene chromatin*. *Nature*, 2009. **460**(7251): p. 66-72.
315. Bryan, T.M., et al., *Evidence for an alternative mechanism for maintaining telomere length in human tumors and tumor-derived cell lines*. *Nat Med*, 1997. **3**(11): p. 1271-4.
316. Bryan, T.M., et al., *Telomere elongation in immortal human cells without detectable telomerase activity*. *Embo j*, 1995. **14**(17): p. 4240-8.
317. Pickett, H.A. and R.R. Reddel, *Molecular mechanisms of activity and derepression of alternative lengthening of telomeres*. *Nature Structural & Molecular Biology*, 2015. **22**(11): p. 875-880.
318. Rivera, T., et al., *A balance between elongation and trimming regulates telomere stability in stem cells*. *Nat Struct Mol Biol*, 2017. **24**(1): p. 30-39.
319. Pickett, H.A. and R.R. Reddel, *The role of telomere trimming in normal telomere length dynamics*. *Cell Cycle*, 2012. **11**(7): p. 1309-1315.
320. Blackburn, E.H. and J.G. Gall, *A tandemly repeated sequence at the termini of the extrachromosomal ribosomal RNA genes in Tetrahymena*. *J Mol Biol*, 1978. **120**(1): p. 33-53.
321. Watson, J.D., *Origin of concatemeric T7 DNA*. *Nat New Biol*, 1972. **239**(94): p. 197-201.
322. Zakian, V.A., *Telomeres: the beginnings and ends of eukaryotic chromosomes*. *Exp Cell Res*, 2012. **318**(12): p. 1456-60.
323. McClintock, B., *The Stability of Broken Ends of Chromosomes in Zea Mays*. *Genetics*, 1941. **26**(2): p. 234-282.
324. Szostak, J.W. and E.H. Blackburn, *Cloning yeast telomeres on linear plasmid vectors*. *Cell*, 1982. **29**(1): p. 245-55.
325. Greider, C.W. and E.H. Blackburn, *A telomeric sequence in the RNA of Tetrahymena telomerase required for telomere repeat synthesis*. *Nature*, 1989. **337**(6205): p. 331-7.
326. Greider, C.W. and E.H. Blackburn, *Identification of a specific telomere terminal transferase activity in Tetrahymena extracts*. *Cell*, 1985. **43**(2 Pt 1): p. 405-13.
327. Blackburn, E.H., et al., *Recognition and elongation of telomeres by telomerase*. *Genome*, 1989. **31**(2): p. 553-60.
328. Greider, C.W. and E.H. Blackburn, *The telomere terminal transferase of Tetrahymena is a ribonucleoprotein enzyme with two kinds of primer specificity*. *Cell*, 1987. **51**(6): p. 887-98.
329. Nobel Foundation *The Nobel Prize in Physiology or Medicine 2009*. 2009.
330. Di Donna, S., et al., *Telomerase can extend the proliferative capacity of human myoblasts, but does not lead to their immortalization*. *Mol Cancer Res*, 2003. **1**(9): p. 643-53.
331. Lundberg, A.S. and R.A. Weinberg, *Functional inactivation of the retinoblastoma protein requires sequential modification by at least two distinct cyclin-cdk complexes*. *Mol Cell Biol*, 1998. **18**(2): p. 753-61.
332. Duronio, R.J., et al., *The transcription factor E2F is required for S phase during Drosophila embryogenesis*. *Genes Dev*, 1995. **9**(12): p. 1445-55.
333. Santamaría, D., et al., *Cdk1 is sufficient to drive the mammalian cell cycle*. *Nature*, 2007. **448**(7155): p. 811-815.
334. Cao, L., et al., *Phylogenetic analysis of CDK and cyclin proteins in premetazoan lineages*. *BMC Evol Biol*, 2014. **14**: p. 10.
335. Lim, S. and P. Kaldis, *Cdks, cyclins and CKIs: roles beyond cell cycle regulation*. *Development*, 2013. **140**(15): p. 3079-93.
336. Serrano, M., G.J. Hannon, and D. Beach, *A new regulatory motif in cell-cycle control causing specific inhibition of cyclin D/CDK4*. *Nature*, 1993. **366**(6456): p. 704-7.
337. Hannon, G.J. and D. Beach, *p15INK4B is a potential effector of TGF-beta-induced cell cycle arrest*. *Nature*, 1994. **371**(6494): p. 257-61.
338. Hirai, H., et al., *Novel INK4 proteins, p19 and p18, are specific inhibitors of the cyclin D-dependent kinases CDK4 and CDK6*. *Molecular and cellular biology*, 1995. **15**(5): p. 2672-2681.
339. Wolfel, T., et al., *A p16INK4a-insensitive CDK4 mutant targeted by cytolytic T lymphocytes in a human melanoma*. *Science*, 1995. **269**(5228): p. 1281-1284.
340. Sotillo, R., et al., *Wide spectrum of tumors in knock-in mice carrying a Cdk4 protein insensitive to INK4 inhibitors*. *The EMBO journal*, 2001. **20**(23): p. 6637-6647.
341. Reynisdottir, I., et al., *Kip/Cip and Ink4 Cdk inhibitors cooperate to induce cell cycle arrest in response to TGF-beta*. *Genes Dev*, 1995. **9**(15): p. 1831-45.
342. Pavletich, N.P., *Mechanisms of cyclin-dependent kinase regulation: structures of Cdks, their cyclin activators, and Cip and INK4 inhibitors*. *J Mol Biol*, 1999. **287**(5): p. 821-8.
343. Goldstein, S., *Replicative senescence: the human fibroblast comes of age*. *Science*, 1990. **249**(4973): p. 1129-33.
344. Ramirez, R.D., et al., *Bypass of telomere-dependent replicative senescence (M1) upon overexpression of Cdk4 in normal human epithelial cells*. *Oncogene*, 2003. **22**(3): p. 433-444.
345. Stadler, G., et al., *Establishment of clonal myogenic cell lines from severely affected dystrophic muscles - CDK4 maintains the myogenic population*. *Skelet Muscle*, 2011. **1**(1): p. 12.
346. ATCC. *Phoenix-AMPHO (ATCC CRL-3213)*. 2016 [cited 2020 26.02.2020]; Available from: [https://www.lgcstandards-atcc.org/products/all/CRL-3213.aspx?geo\\_country=de#generalinformation](https://www.lgcstandards-atcc.org/products/all/CRL-3213.aspx?geo_country=de#generalinformation).
347. Nolan, G. *Phoenix helper-free retrovirus producer lines*. n.d.; Available from: [https://web.stanford.edu/group/nolan/\\_OldWebsite/retroviral\\_systems/phx.html](https://web.stanford.edu/group/nolan/_OldWebsite/retroviral_systems/phx.html).
348. Wheaton, K., et al., *Progerin-Induced Replication Stress Facilitates Premature Senescence in Hutchinson-Gilford Progeria Syndrome*. *Mol Cell Biol*, 2017. **37**(14).
349. Sebastian, S., et al., *Extended 2D myotube culture recapitulates postnatal fibre type plasticity*. *BMC Cell Biol*, 2015. **16**: p. 23.
350. Morgenstern, J.P. and H. Land, *Advanced mammalian gene transfer: high titre retroviral vectors with multiple drug selection markers and a complementary helper-free packaging cell line*. *Nucleic Acids Res*, 1990. **18**(12): p. 3587-96.
351. Swift, S., et al., *Rapid production of retroviruses for efficient gene delivery to mammalian cells using 293T cell-based systems*. *Curr Protoc Immunol*, 2001. **Chapter 10**: p. Unit 10.17C.
352. Jiang, W., et al., *An optimized method for high-titer lentivirus preparations without ultracentrifugation*. *Sci Rep*, 2015. **5**: p. 13875.
353. Xu, X., et al., *Specific structure and unique function define the hemicentin*. *Cell Biosci*, 2013. **3**(1): p. 27.
354. Thorley, M., et al., *Skeletal muscle characteristics are preserved in hTERT/cdk4 human myogenic cell lines*. *Skelet Muscle*, 2016. **6**(1): p. 43.

- 
355. Boularaoui, S.M., et al., *Efficient transdifferentiation of human dermal fibroblasts into skeletal muscle*. J Tissue Eng Regen Med, 2018. **12**(2): p. e918-e936.
  356. Xu, B., A. Siehr, and W. Shen, *Functional skeletal muscle constructs from transdifferentiated human fibroblasts*. Sci Rep, 2020. **10**(1): p. 22047.
  357. Urciuolo, A., et al., *Engineering a 3D in vitro model of human skeletal muscle at the single fiber scale*. PLoS One, 2020. **15**(5): p. e0232081.
  358. Maffioletti, S.M., et al., *Three-Dimensional Human iPSC-Derived Artificial Skeletal Muscles Model Muscular Dystrophies and Enable Multilineage Tissue Engineering*. Cell Rep, 2018. **23**(3): p. 899-908.

## X. Annex

### X.1. List of abbreviations

---

#### 0

0208ct7 · *immortalized human myoblasts*

---

#### 2

2OMePS · *2'-O-methyl-RNA with phosphorothioate backbone*

---

#### 3

3T3 · *immortalized embryonic mouse fibroblasts*

---

#### A

AAV · *adeno-associated virus vector*  
 ABD · *actin binding domain*  
 ACE · *angiotensin converting enzyme*  
 ALS · *amyotrophic lateral sclerosis*  
 ALT · *alternative lengthening of telomeres*  
 AON · *antisense oligonucleotides*  
 ATP · *adenosine triphosphate*

---

#### B

BAC · *bacterial artificial chromosome*  
 BLAST · *Basic Local Alignment Search Tool*  
 BMD · *Becker muscular dystrophy*  
 bp · *base pairs*  
 bvFD · *early-onset frontotemporal dementia with prominent neuropsychiatric symptoms -behavioral variant*

---

#### C

C2C12 · *immortalized mouse myoblast cell line*  
 CDK4 · *cyclin-dependent kinase 4*  
 cDNA · *chromosomal DNA*  
 CK · *creatine kinase*  
 CKCS · *Cavalier King Charles Spaniel animal model*  
 CRISPR/CAS9 · *clustered regularly interspaced short palindromic repeats with CRISPR-associated protein 9*  
 CXMDj · *canine X-linked muscular dystrophy model*

---

#### D

DAPI · *4',6-diamidino-2-phenylindole*  
 DCM · *dilated cardiomyopathy*  
 ddH<sub>2</sub>O · *double-distilled water*  
 DGC · *dystrophin-glycoprotein complex*  
 DGN · *Deutsche Gesellschaft für Neurologie - German Society of Neurology*  
 DH5alpha-E. coli · *Escherichia coli of DH5 Alpha strain*  
 DMD · *Duchenne muscular dystrophy*  
 DMEM · *Dulbecco's Modified Eagle's Medium*  
 DMSO · *dimethyl sulfoxide*

DNA · *deoxyribonucleic acid*

---

#### E

ECM · *extracellular matrix*  
 EF-hand motifs · *helix-loop-helix structural domain*  
 eGFP · *enhanced green fluorescent protein*  
 EMA · *European Medicines Agency*  
 env · *envelope protein*

---

#### F

fALS · *familial amyotrophic lateral sclerosis*  
 FBS · *fetal bovine serum*  
 FDA · *U.S. Food and Drug Administration*

---

#### G

G418 · *Geneticin*  
 gag · *group antigens*  
 GALGT2 · *beta-1,4-N-acetyl-galactosaminyltransferase 2*  
 gDNA · *genomic DNA*  
 GMOs · *genetically modified organisms*  
 GNE · *bifunctional UDP-N-acetylglucosamine 2-epimerase/N-acetylmannosamine kinase*  
 GRMD · *Golden Retriever muscular dystrophy dog model*

---

#### H

HEK · *human embryonic kidney cells*  
 HFMD · *hypertrophic feline muscular dystrophy model*  
 hIBM · *hereditary inclusion body myopathy*  
 HPV · *human papillomavirus*  
 hTERT · *human telomerase reverse transcriptase*  
 hTR · *telomerase RNA*

---

#### I

IBMPFD · *inclusion body myopathy with Paget's disease of the bone and early-onset frontotemporal dementia*  
 IRES · *internal ribosome entry site*

---

#### K

kb · *kilo bases*  
 kbp · *kilo base pairs*  
 kD · *kilo Dalton*  
 KOH · *potassium hydroxide*

---

#### L

LB · *lysogeny broth*  
 LINE-1 · *long interspersed repetitive element-1*

---

**M**

MEDLINE · *Medical Literature Analysis and Retrieval System Online*  
 MLPA · *multiplex ligation-dependent probe amplification*  
 MMLV · *Moloney Murine Leukemia Virus*  
 MRF · *myogenic regulatory factors*  
 MRI · *magnetic resonance imaging*  
 mRNA · *messenger ribonucleic acid*  
 Myf5 · *myogenic factor 5*  
 MyoD · *myoblast determination protein 1*

---

**N**

N-ABD · *N-terminal actin binding domain*  
 Nbs1 · *nibrin gene*  
 ncRNA · *non-coding RNA*  
 NGS · *next generation sequencing*  
 nNOS · *neuronal nitric oxidase synthase*

---

**P**

Pax3 · *paired box gene 3*  
 Pax7 · *paired box gene 7*  
 pBABE · *pBABE plasmid backbone*  
 PBS · *phosphat buffered saline*  
 PCR · *polymerase chain reaction*  
 PFA · *paraformaldehyde*  
 PMO · *phosphorodiamidate morpholino oligomers*  
 pol · *reverse transcriptase gene with integrase and RNase H activity*  
 polyA · *polyadenylation*  
 PPMO · *peptide-conjugated phosphorodiamidate morpholino oligomers*  
 pRB · *retinoblastoma protein*

---

**R**

RNA · *ribonucleic acid*

RT-PCR · *reverse transcription polymerase chain reaction*

---

**S**

SCNT · *somatic cell nuclear transfer*  
 sgRNA · *single guide RNA*  
 siBM · *sporadic inclusion body myositis*  
 snRNA · *small nuclear RNA*

---

**T**

TAE buffer · *Tris-acetate-EDTA buffer*  
 TALEN · *transcription activator-like effector nucleases*  
 TDP-43 · *TAR DNA binding protein-43*  
 TE buffer · *Tris-EDTA buffer*  
 TREAT-NMD · *treat NeuroMuscular Disease - global academic network*  
 TRF2 · *telomeric repeat-binding factor 2*  
 Tween-20 · *polysorbate 20*

---

**V**

VCP · *valosin-containing protein*

---

**W**

WW domain · *rsp5-domain or WWP repeating motif*

---

**X**

XRCC3 · *X-Ray Repair Cross-Complementing Protein 3*

---

**Z**

ZZ · *zinc finger motif*

## X.2. Plasmid sequences

### X.2.1. pBABE-puro-hTERT

Full sequence available from Addgene (<https://www.addgene.org/1771/sequences/>).

> Addgene NGS Result

```
CCCCGAAAAGTGCCACCTGCAGCCTGAATATGGGCCAAACAGGATATCTGTGGTAAGCAGTTCCTGCCCCGGCTCAGGGCC
AAGAACAGATGGAACAGCTGAATATGGGCCAAACAGGATATCTGTGGTAAGCAGTTCCTGCCCCGGCTCAGGGCCAAAGAAC
AGATGGTCCCAGATGCGGTCCAGCCCTCAGCAGTTTCTAGAGAACCATCAGATGTTTCCAGGGTGCCCAAGGACCTGAA
ATGACCCTGTGCCTTATTTGAACTAACCAATCAGTTCGCTTCTCGTCTCTGTTGCGCGCTTCTGCTCCCCGAGCTCAATAAA
AGAGCCACAACCCCTCACTCGGGGCGCAGTCTCCGATTGACTGAGTCGCCCGGGTACCCGTGTATCCAATAAACCCCTC
TTGCAATTGCATCCGACTTGTGGTCTCGCTGTTCCCTGGGAGGGTCTCCTCTGAGTGATTGACTACCCGTACAGCGGGGTCT
TTCATTTGGGGGCTCGTCCGGGATCGGGAGACCCCTGCCAGGGACCACCGACCCACCACCGGGAGGCAAGCTGGCCAGC
AACTTATCTGTCTGTCGGATTGTCTAGTGTCTATGACTGATTTTTATGCGCCTGCGTCTGTTACTAGTTAGCTAACTAGTCTG
TATCTGGCGGACCCGTGGTGGAACTGACGAGTTCTGAACACCCGCGCCGCAACCCTGGGAGACGTCCAGGGACTTTGGGG
GCCGTTTTGTGGCCGACCTGAGGAAGGGAGTGCATGTGGAATCCGACCCGTCAGGATATGTGGTTCTGGTAGGAGACG
AGAACCTAAAACAGTTCGCCGCTCCGTCTGAATTTTTGCTTTCCGTTTTGAAACCGAAGCCGCGCTTGTCTGCTGCAGCG
CTGCAGCATCGTTCTGTGTTGTCTCTGTCTGACTGTGTTTCTGTATTTGCTGAAAATTAGGGCCAGACTGTTACCACTCCCTT
AAGTTTGACCTTAGTCACTGGAAGATGTGAGCGGATCGTCCACAACCAGTCGGTAGATGTCAAGAGAGACGTTGGGTT
ACCTTCTGCTCTGAGAATGGCCAACTTTAACCTGGATGGCCGAGACGCGCACCTTTAACCGACCTCATCCAGTTCGGG
GTTAAGATCAAGGCTTTTTACCTGGCCGCATGGACACCCAGACCAGTCCCTACATCGTGACCTGGGAAGCCTTGGCTT
TTGACCCCTCCCTGGGTCAAGCCCTTTGTACACCCTAAGCCTCCGCTCCTCTTCCCTCCATCCGCCCGTCTCTCCCCCT
TGAACCTCCTCGTTCGACCCCGCTCGATCCTCCCTTTATCCAGCCCTCACTCCTTCTCTAGGCGCCGGCCGATCCAGTG
TGGTGGTACGTAGGAATTCGTCTGCTGCGCAGCTGGGAAGCCCTGGCCCGGGCCACCCCGCGATGCCGCGCGCTCCCC
GCTGCCGAGCCGTGCGCTCCCTGCTGCGCAGCCACTACCGCGAGGTGCTGCCGCTGGCCAGTTCGTGCGGCGCTGGG
GCCCAAGGCTGCGGCTGTTGTCAGCGCGGGGACCCGCGGCTTTCCGCGCGCTGGTGGCCAGTGCTGGTGGTGCCTG
CCCTGGGACGCACGGCCGCCCGCCCGCCCTCCTTCCGCCAGGTGCTCTGCCTGAAGGAGCTGGTGGCCGAGTGC
TGCAGAGGCTGTGCGAGCGCGGCGCAAGAAGCTGCTGGCCTTCGGCTTCGCGCTGCTGGACGGGGCCCGCGGGGCC
CCCCGAGGCTTACCACCAGCGTGCAGCTACCTGCCAACACGGTGACCGACGCACTGCGGGGAGCGGGGCGTGG
GGGCTGCTGCTGCGCCGCTGGGCGACGACGTGCTGGTTCACCTGCTGGCAGCTGCGCGCTCTTTGTGCTGGTGGCTCC
CAGCTGCGCCTACCAGGTGTGCGGGCCCGCTGTACCAGCTCGGCGTCCACTCAGGCCCGGCCCGCCACACGCT
AGTGGACCCCGAAGGCTCTGGGATGCCAACGGCCCTGGAACCATAGCGTACGGGAGGCGGGGTCCCTGGCCCTGC
CAGCCCCGGGTGCGAGGAGGCGCGGGGCGAGTGCCAGCCGAAGTCTGCCGTTGCCAAGAGGCCAGGCGTGGCGCTG
CCCCTGAGCCGGAGCGGACGCCGTTGGGCGAGGGTCTGGGCCACCCGGGCAGGACGCGTGGACCGAGTGACCGTG
GTTTCTGTGTGGTGTACCTGCCAGACCCGCCGAAGAGCCACCTCTTTGGAGGTTGCGCTCTCTGGCACGCGCCACTCC
ACCCATCCGTGGGCGCCAGCACACGCGGGCCCCCATCCACATCGCGGCCACCACGTCCTGGGACACGCTTGTCCC
CCGTTGACCGCCGAGACCAAGCACTTCTCTACTCTCAGGCGACAAGGACAGCTGCGGCCCTCCTTCTACTCAGCTCT
CTGAGGCCAGCTGACTGGCGCTCGGAGGCTGCTGGAGACCATTTTCTGGGTTCCAGGCCCTGGATGCCAGGACTCC
CCGCAAGTTGCCCGCCTGCCAGCGCTACTGGCAATGCGGCCCTGTTTCTGGAGCTGCTTGGGAACCACGCGCAGT
GCCCTACGGGGTGTCTCTCAAGACGCACTGCCCGCTGCGAGCTGCGGTACCCAGCAGCCGGTGTCTGTGCCGGGAG
AAGCCCCAGGGCTCTGTGGCGGCCCGGAGGAGGAGACAGACCCCGTGCCTGGTGCAGCTGCTCCGCCAGCACA
GCAGCCCTCGCAGGTGTACGGTTCGTGCGGGCCTGCTGCGCCGCTGGTGGCCAGGCCCTCTGGGGTCCAGGCA
CAACGAAACGCGCTTCTCAGGAACACCAAGAAGTTCTCCTCTCCGGAAGCATGCCAAGCTCTCGTGCAGGCTGAC
GTGGAAGATGAGCGTGGGGGCTGCGCTTGGCTGCGCAGGAGCCAGGGGTTGGCTGTGTTCCGGCCGACAGCACCGT
CTGCGTGAGGAGATCCTGGCCAAGTTCTGCACTGGCTGATGAGTGTGTACGTCGTCGAGCTGCTCAGGTCTTTTATG
TCACGGAGACCAGTTTCAAAGAAGAGGCTCTTTTTCTACCAGGAGAGTGTCTGGAGCAAGTTGCAAAGCATTGGAATCAG
ACAGCACTTGAAGAGGGTGCAGCTGCGGGAGCTGTGGAAGCAGAGGTACGGCAGCATCGGGAAGCCAGGCCCGCCCTG
CTGAGTCCAGACTCCGTTTATCCCCAAGCCTGACGGGCTGCGGCCGATTGTGAACATGGACTACGTCGTGGGAGCCAGA
ACGTTCCGCAGAGAAAAGAGGGCCGAGCGTCTCACCTCAGGGTGAAGGCACTGTTACGCGTGTCAACTACGAGCGGG
GCGGGCGCCCGCCCTCCTGGGCGCTCTGTGCTGGGCTGGACGATATCCACAGGGCCTGGCGCACCTTCGTGCTGCGT
TGCGGGCCAGGACCCGCGCCTGAGCTGTACTTTGTAAGGTGGATGTGACGGGCGGTACGACACCATCCCCAGGAC
AGGCTCACGGAGGTATCGCCAGCATCATCAAACCCAGAACACGTAAGTGCCTGCGTGGTATGCCGTGGTCCAGAAAGCC
GCCATGGGACAGTCCGCAAGGCCCTCAAGAGCCAGCTCTACTCTGACAGACCTCCAGCCGTAATGCGACAGTTCGTG
GCTCACCTGCAGGAGACCCCGCTGAGGGATCCGCTGTCATCGAGCAGAGCTCCTCCCTGAATGAGGCCAGCAGTGG
CCTCTTCGACGCTTCTACGCTTTCATGTGCCACCACGCGTGCATCAAGGGCAAGTCTACGTCAGTGCAGGGGAT
CCCGCAGGGCTCCATCCTCTCCAGCTGCTCTGCAGCCTGTGCTACGGCGACATGGAGAACAAGCTGTTTGGGGGATTTCG
GCGGGACGGGCTGCTCCTGCGTTTGGTGGATGATTTCTTGTGGTGCACCTCACCTCACCCACGCAAAACCTTCTCAG
GACCCTGGTCCGAGGTGTCCCTGAGTATGGCTGCGTGGTGAACCTTGCAGGAGACAGTGGTGAACCTTCCCTGTAGAAGACGA
GGCCCTGGGTGGCAGGCTTTTGTTCAGATGCGGGCCACGGCCATTTCCCTGGTGCGGCTGCTGCTGGATCCCGGA
CCTGGAGGTGCAGAGCTCAGACTCAGCTATGCCCGGACCTCATCAGAGCCAGTCTACCTTCAACCCGCGCTTCAAGG
CTGGGAGGAACATGCGTGCAAACTCTTTGGGGTCTTGCGGCTGAAGTGCACAGCCTGTTTCTGGATTTGAGGTGAACAG
CCTCCAGACGGTGTGCACCAACATCTACAAGATCCTCCTGCTGCAGGCGTACAGGTTTACGCATGTGTGCTGCAGCTCCCA
TTTCATCAGCAAGTTTGAAGAACCCACATTTTCTGCGCGTCTCTGACACGGCCTCCCTCTGCTACTCCATCCTGAA
AGCCAAGAACGCAGGGATGTGCGTGGGGGCCAAGGGCGCCCGCCCTCTGCCCTCCGAGGCCGTGCAGTGGCTGTGC
CACCAAGATTCCTGCTCAAGCTGACTCGACACCGTGTACCTACGTCGACCTCCTGGGTCACTCAGGACAGCCAGCG
CAGCTGAGTCCGAAGCTCCGGGACGACGCTGACTGCCCTGAGGCGGAGCCAGCCAGCCAAACCCGGCACTGCCACAGTTCAA
GACCATCCTGGACTGAGTCGACCCGTGGAATGTGTGTCAGTTAGGGTGTGGAAAGTCCCAGGCTCCCAGCAGGCAGAA
```

GTATGCAAAGCATGCATCTCAATTAGTCAGCAACCAGGTGTGGAAAGTCCCAGGCTCCCCAGCAGGCAGAAGTATGCAAAG  
CATCGATCTCAATTAGTCAGCAACCATAGTCCCAGCCCTAACTCCGCCATCCCGCCCTAACTCCGCCAGTTCCGCCCAT  
TCTCCGCCCCATGGCTGACTAATTTTTTTATTTATGTCAGAGGCCGAGCCGCTCGGCCCTGAGCTTCCAGAAGTAGT  
GAGGAGGCTTTTTTGGAGGCTTAGGCTTTTGCAAAAAGCTTACCATGACCGAGTACAAAGCCACAGGTATCGCCTCGCCACCC  
GCGACGACGTCCCCAGGGCCGTACGCACCCCTCGCCGCCGCTTCCGCGACTACCCCGCCACGCGCCACACCGTCGATCC  
GGACCGCCACATCGAGCGGGTACCGAGCTGCAAGAAGTCTTCTCACGCGCTCGGGCTCGACATCGGCAAGGTGTGGG  
TCGCGGACGACGGCGCCGCGGTGGCGGTCTGGACCACGCCGAGAGCGTGAAGCGGGGGCGGTGTTCCGCCGAGATCG  
GCCCAGCATGGCCGAGTTGAGCGGTTCCCGGCTGGCCGCGCAGCAACAGATGGAAGGCCCTCTGGCGCCGACCCGGCC  
CAAGGAGCCCGGTGTTCCCTGGCCACCGTCCGCGTCTCGCCGACCACAGGGCAAGGCTCTGGGCAGCGCCGTCGTG  
CTCCCCGGAGTGGAGGCGCCGAGCGCGCCGGGTGCCCGCTTCTGGAGACCTCCGCGCCCGCAACCTCCCTTCT  
ACGAGCGGCTCGGCTTACCCTCACCGCCGACGTGAGGTGCCGAAGGACCGCGCACCTGGTGCATGACCCGCAAGCCC  
GGTGCCTGACGCCCCGCCACGACCCGACGCGCCGACCGAAAGGAGCGCACGACCCCATGCATCGATAAAAATAAAGAT  
TTTTTTAGTCTCCAGAAAAAGGGGGGAATGAAAGACCCACCTGTAGGTTTGGCAAGCTAGCTTAAAGTAACGCCATTTTGA  
AGGCATGGAAAAATACATAACTGAGAATAGAGAAGTTCAGATCAAGGTGAGAACAGATGGAACAGCTGAATATGGGCCAAA  
CAGGATATCTGGTAAGCAGTTTCTGCCCGGCTCAGGGCCAAGAACAGATGGAACAGCTGAATATGGGCCAAAACAGGAT  
ATCTGTGGTAAGCAGTTTCTGCCCGGCTCAGGGCCAAGAACAGATGGTCCCAGATGCGGTCCAGCCCTCAGCAGTTTCT  
AGAGAACCATCAGATGTTCCAGGGTGCCCAAGGACCTGAAATGACCCTGTGCCTATTTGAACTAACCAATCAGTTCGCTT  
CTCGCTTCTGTTCCGCGCTTCTGCTCCCCGAGCTCAATAAAGAGCCCAACCCCTCACTCGGGGCGCCAGTCTCCGA  
TTGACTGAGTCGCCGGGTACCCGTGTATCCAATAAACCCCTTTCAGTTCATCCGACTTGTGGTCTCGCTGTTCTTGGG  
AGGTCTCTCTGAGTGATTGACTACCCGTACGCGGGGCTTTTACATGCAGCATGTACAAAATAATTTGGTTTTTTTTTCT  
TAAGTATTTACATTAATGGCCATAGTTGCATTAATGAATCGGCCAACGCGGGGAGAGGCGGTTTGCATTTGGCGCTC  
TTCCGCTTCTCGCTACTGACTCGCTGCGCTCGGTGTTGGGCTGCGGCGAGCGGTATCAGCTCACTCAAAGGCGGTAAT  
ACGGTTATCCACAGAATCAGGGGATAACGCAGGAAAGAACATGTGAGCAAAGGCCAGCAAAGGCCAGGAACCGTAAAAA  
GGCCGCGTTGCTGGCGTTTTTCCATAGGCTCCGCCCCCTGACGAGCATCAAAAAATCGACGCTCAAGTCAGAGGTGGCG  
AAACCCGACAGGACTATAAGATACCAGGCGTTTTCCCTGGAAGCTCCCTCGTGCCTCTCTGTTCCGACCCCTGCCGCTT  
ACCGGATACCTGCCGCTTCTCCCTTCGGGAAGCGTGGCGCTTCTCATAGCTCACGCTGTAGGTATCTCAGTTCGGGTG  
AGGTCTTCCGTCGAAGCTGGGCTGTGTGCACGAACCCCGTTTCAGCCCGACCGCTGCGCCTTATCCGGTAACTATCGTC  
TTGAGTCCAACCCGGTAAGACACGACTTATCGCCACTGGCAGCAGCCACTGGTAACAGGATTAGCAGAGCGAGGTATGTAG  
GCGGTGCTACAGAGTCTTGAAGTGGTGGCCTAACTACGGCTACACTAGAAGAACAGTATTTGGTATCTGCGCTCTGCTGAA  
GCCAGTTACCTTCGAAAAAGAGTTGGTAGCTCTTGATCCGGCAACAAACCACCGCTGGTAGCGGTGGTTTTTTTTGTTTGC  
AAGCAGCAGATTACGCGCAGAAAAAAGGATCTCAAGAAGATCTTTGATCTTTTACGGGGTCTGACGCTCAGTGGAAACG  
AAAATCACGTTAAGGGATTTGGTTCATGAGATTATCAAAAAGGATCTTACACTAGATCCTTTTTGCGGCCGCAAACTAATCTAA  
AGTATATATGAGTAACTTGGTCTGACAGTTACCAATGCTTAATCAGTGAGGCACCTATCTCAGCGATCTGTCTATTTCTGTTCA  
TCCATAGTTGCTGACTCCCCGTCGTGTAGATAACTACGATACGGGAGGGCTTACCATCTGGCCCCAGTGTGCAATGATAC  
CGCGAGACCCACGCTCACCGGCTCCAGATTTATCAGCAATAAACAGCCAGCCGGAAGGGCCGAGCGCAGAAGTGGTCT  
GCAACTTTATCCGCTCCATCCAGTCTATTAATTGTTGCCGGGAAGCTAGAGTAAGTAGTTCGCCAGTTAATAGTTTGGCAA  
CGTTGTTGCCATTGCTACAGGCATCGTGGTGTACGCTCGTCTTTGGTATGGCTTCACTCAGCTCCGGTCCCAACGATCA  
AGCGAGTTACATGATCCCCATGTTGTGCAAAAAGCGGTTAGCTCCTTCGGTCCCGATCGTTGTGCAAGTAAGTTGG  
CCGAGTGTATCACTCATGGTTATGGCAGCACTGCATAATTCTTACTGTATGCCATCCGTAAGATGCTTTTCTGTGACT  
GGTGAAGTCAACCAAGTCACTTCTGAGAATAGTGTATGCGGCGACCGAGTTGCTCTTGCCCGCGTCAATACGGGATAATA  
CCGCGCCACATAGCAGAACTTTAAAAGTCTCATATTGAAAACGTTCTTCGGGGCGAAAACCTCTCAAGGATCTTACCGCT  
GTTGAGATCCAGTTCGATGTAACCCACTCGTGCACCCAACTGATCTTACGATCTTTTACTTTACCAGCGTTTCTGGGTGAG  
CAAAAACAGGAAGGCAAAATGCCGCAAAAAGGGAATAAGGGCGACACGGAAATGTTGAATACTCATACTCTTCTTTTTCAA  
TATTATTGAAGCATTTATCAGGGTATTGTCTCATGACGGATACATATTTGAATGTATTTAGAAAAATAAACAAATAGGGGTT  
CGCGCACATTT

## X.2.2. pBABE-hygro-CDK4-R24C

Full sequence available from Addgene (<https://www.addgene.org/11254/sequences/>).

Addgene NGS Result:

gcagcctgaatatggccaaacaggatatctgtgtaagcagttctgccccGGCTCAGGGCCAAGAACAGATGGAACAGCTGAATATGGGCCAAAC  
AGGATATCTGTGGTAAGCAGTTCCTGCCCGGCTCAGGGCCAAGAACAGATGGTCCCCAGATGCGGTCCAGCCCTCAGCAG  
TTTCTAGAGAACCATCAGATGTTTCCAGGGTGCCCCAAGGACCTGAAATGACCCTGTGCCTATTTGAACTAACCAATCAGTT  
CGCTTCTCGTCTGTTCCGCGCTTCTGCTCCCCGAGCTCAATAAAAAGAGCCCAACCCCTCACTCGGGGCGCCAGTCC  
TCCGATTGACTGAGTCGCCCCGGTACCCGTGTATCCAATAAACCCCTTTCAGATTGCATCCGACTTGTGGTCTCGCTGTTCC  
TTGGGAGGGTCTCCTCTGAGTGATTGACTACCCGTACGCGGGGGTCTTTCAATTTGGGGGCTCGTCCGGGATCGGGAGACCC  
CTGCCAGGGACCACCGACCCACCACCGGAGGCAAGCTGGCCAGCACTTATCTGTGTCTGTCCGATTGTCTAGTGTCTA  
TGACTGATTTATGCGCTGCGTCTGACTAGTTAGCTAACTAGCTCTGTATCTGGCGGACCCGTGGTGGAACTGACGAGTT  
CTGAACACCCGCGCAACCCCTGGGAGACGTCCCAGGACTTTGGGGCCGTTTTTGTGGCCGACCTGAGGAAGGGAGT  
CGATGTGAATCCGACCCCGTCAGGATATGGTCTGTTAGGAGACGAGAACCTAAAACAGTTCGCCCTCCGCTCGCTGAATT  
TTTTGTTTTCGTTTTGAAACCGAAGCCGCGCTCTTGTCTGCTGCAGCGCTGCAGCATCGTCTGTGTTGTCTGTCTGACT  
GTGTTTCTGATTTGTCTGAAAATTAGGGCCAGACTGTTACCCTCCCTAAGTTTACCTTAGGTCACTGGAAAGATGTCCA  
GCGGATCGCTCACAACAGTCCGGTAGATGTCAAGAAGAGACGTTGGGTTACCTTCTGCTCTGCAGAAATGGCCAACCTTTAAC  
GTCGGATGGCCGCGAGACGGCACCTTAACCGAGACCTCATACCCAGGTTAAGATCAAGGTCTTTTACCTGGCCCGCAT  
GGACACCCAGACAGTCCCCTACATCGTACCTGGGAAGCCCTTGGCTTTTACCCCTCCCTGGGTCAAGCCCTTTGTA

CACCCTAAGCCTCCGCTCCTCTTCTCCATCCGCCCGTCTCTCCCCCTTGAACCTCCTCGTTCCGACCCCGCCTCGATCCT  
CCCTTTATCCAGCCCTCACTCCTTCTTAGGCGCCGGCCGATCCCAGTGTGGTGGTACGTAGGAATTCCTCGAGCCCGGG  
CTGGCGTGAAGGCTTGTGATCCTCCACAGTGGCCACTTTCGATATGAGCCAGTGGTGAATTTGGTGTGGTGCCTATGG  
GACAGTGTACAAAGCTTGTGATCCTCCACAGTGGCCACTTTCGATCCTCCAGTGTGAGAGTCCCAATGGAGGAGGAGG  
TGGAGGAGGCTTCCCATCAGCACAGTTCGTGAGGTGGCTTACTGAGGCGACTGGAGGCTTTTGGATCCCAATGTTGTC  
CGGCTGATGGACGTCTGTGCCACATCCCGAAGTACCAGGAGTCAAGGTAACCCTGGTGTGAGCATGTAGACCAGGAC  
CTAAGGACATATCTGGACAAGGCACCCACCAGGCTTCCAGCCGAAACGATCAAGGATCTGATGCGCCAGTTTCTAAGA  
GGCCTAGATTTCTTCATGCCAATTGCATCGTTCACCGAGATCTGAAGCCAGAGAACATTCTGGTGACAAGTGGTGGAAACG  
TCAAGTGGTGCATTTGGCTGGCCAGAATCTACAGCTACCAGATGGCACTTACACCCGTGGTTGTACACTCTGGTACC  
AGCTCCCGAAGTCTTCTGCAGTCCACATATGCAACACCTGTGGACATGTGGAGTGTGGCTGTATCTTTCAGAGATGTTTC  
GTGCAAGCCTCTTCTGTGAAACTCTGAAGCCGACAGTTGGGCAAAATCTTTCGACTGATTGGGCTGCCTCCAGAGGA  
TGACTGGCTCGAGATGTATCCCTGCCCGTGGAGCCTTCCCGCCAGAGGGCCCGCCAGTGCAGTCCGGTGGTACCTG  
AGATGGAGGAGTCGGGAGCACAGCTGCTGCTGAAATGCTGACTTTTAAACCCACACAAGCGAATCTCTGCCTTTCGAGCTCT  
GCAGCACTTTATCTACATAAGGATGAAGGTAATCCGGAGTATGATGTGCCAGATTATGCTTGAGGATCCACTAGTTCTAGTC  
GACCTGTGGAATGTGTGTCAGTTAGGGTGTGAAAGTCCCGAGCTCCCGAGCAGGCAAGTATGCAAAAGCATGCATCTCAATTAGTCA  
CAATTAGTCAAGCAACAGGTGTGAAAGTCCCGAGCTCCCGAGCAGGCAAGTATGCAAAAGCATGCATCTCAATTAGTCA  
GCAACCATAGTCCCGCCCTAACTCCGCCATCCCGCCCTAACTCCGCCAGTTCGCGCCATTCTCCGCCCATGGCTGA  
CTAATTTTTTTTTATTTATGCAAGGCGGAGGCGCCTCGGCTCTGAGCTATTCAGAAAGTAGTGAGGAGGCTTTTTGGAGG  
CCTAGGCTTTTGCAAAAGCTTGGCAGCTGGGGCGCCCTCTGGTAAGGTTGGGAAGCCCTGCAGATCTGATCCCGGGGGG  
AATGAGATATGAAAAGCCTGAATCACCAGCAGCTGTGCGAGAAGTTTCTGATCGAAAAGTTCGACACGCTCTCCGACCT  
GATGCAGCTCTCGGAGGGCGAAGAATCTCGTGTCTTCAGCTTCGATGTAGGAGGGCGTGGATGTCTCGCGGTAATAG  
CTGCGCCGATGTTTTCTACAAAGATCGTTATGTTTTATCGGCACCTTTCATCGGCCGCGCTCCCGATTCCGGAAGTCTTGAC  
ATTGGGAATTTAGCGAGAGCCTGACCTATTGCATCTCCCGCCGTGCACAGGTTGTCACGTTGCAAGACCTGCCTGAAACC  
GAACTGCCCGCTGTTCTGCAGCCGGTTCGCGGAGGCCATGGATGCGATCGCTGCGGCCGATCTTAGCCAGACGAGCGGTT  
CGGCCATTCCGACCGCAAGGAATCGGTCAATACACTACATGGCGTGATTCATATGCGCGATTGCTGATCCCATGTGTAT  
CACTGGCAAAGTGTGATGGACGACACCGTCAAGTCCGTCGCGCAGGCTCTCGATGAGCTGATGCTTTGGGCCGAGGAC  
TGCCCGAAGTCCGGCACCTCGTGCACGCGGATTTCCGCTCCAAACATGTCCTGACGGACAATGGCCGCAACAGCGGTC  
ATTGACTGGAGCGAGGCGATGTTCCGGGATTCCCAATACGAGGTCGCCAACATCTTCTTGGAGGCCGTGGTTGGCTTGT  
ATGGAGCAGCAGACGCGCTACTTCGAGCGGAGGCATCCGGAGCTTGCAGGATCGCCGCGGCTCCGGGCGTATATGCTCCG  
CATTGGTCTTGACCAACTCTATCAGAGCTTGGTTGACGGCAATTTTCGATGATGCAAGTTCGCGCAGGGTTCGATGCGACGCA  
ATCGTCCGATCCGGAGCCGGGACTGTCCGGCGTACACAAATCGCCCGAGAAGCGCGGCTCTGGACCGATGGCTGTGT  
AGAAGTCTCGCCGATAGTGGAAACCGACGCCAGCACTCGTCCGAGGGCAAAGGAATAGAGTAGATGCCGACCGGGAT  
CTATCGATGCGCGGGTGTGGTGGTTACGCGTAATCTGCTGCTTGCAAACAAAAAACCACCGCTACCAGCGGTGGTTTTGTT  
TGCCGGATCAAGAGCTACCAACTCTTTTTCCGAAGGTAAGTGGCTTCAGCAGAGCGCAGATACCAATACTGTTCTTCTAGTG  
TAGCCGTAGTTAGGCCACCACTTCAAGAACTCTGTAGCACCGCCTACATACCTCGCTCTGCTAATCCTGTTACCAGTGGCTG  
CTGCCAGTGGCGATAAGTCTGTCTTACCAGGTTGGACTCAAGACGATAGTTACCAGGATAAGGCGCAGCGGTCCGGGCTGAA  
CGGGGGTTCGTGCACACAGCCAGCTTGGAGCGAACGCACTACACCGAAGTGAATACCTACAGCGTGAAGTATGAGAAA  
CGCCACGCTTCCCGAAGGGAGAAAAGCGGACAGGTATCCGGTAAGCCGCGAGGGTTCGGAACAGGAGACGCGACGAGGGA  
GCTTCCAGGGGGAAACGCTGGTATCTTTATAGTCTGTCCGGTTTTCGCCACCTCTGACTTGAAGCGTGCATTTTTGTGATGC  
TCGTACAGGGGGCGGAGCCTATGGAAAACGCCAGCAACGCATCGATAAAATAAAGATTTTTATTTAGTCTCCAGAAAAGG  
GGGAATGAAAGACCCACCTGTAGGTTTGGCAAGCTAGCTTAAGTAACGCCATTTTGAAGGCATGGAAAATACATAACT  
GAGAATAGAGAAGTTCAGATCAAGGTCAGGAACAGATGGAACAGCTGAATATGGGCCAAACAGGATATCTGTGGTAAGCAGT  
TCCTGCCCGGCTCAGGGCCAAGAACAGATGGAACAGCTGAATATGGGCCAAACAGGATATCTGTGGTAAGCAGTTCTCTGC  
CCCGGCTCAGGGCCAAGAACAGATGGAACAGCTGAATATGGGCCAAACAGGATATCTGTGGTAAGCAGTTCTCTGCCCGG  
TCAGGGCCAAGAACAGATGGTCCCGAGATGCGGTCCAGCCCTCAGCAGTTTCTAGAGAACCATCAGATGTTTCCAGGGTGC  
CCCAAGGACCTGAAATGACCCTGTGCCTTATTTGAACTAACCAATCAGTTCGCTTCTCGCTTCTGTTCCGCGCTTCTGCTCC  
CCGAGCTCAATAAAAGAGCCCAACCCCTCACTCGGGGCGCCAGTCTCCGATTGACTGAGTGCAGCGGGTACCCGTGTA  
TCCAATAAACCTCTTGCAGTTGCATCCGACTTGTGGTCTCGCTGTTCTTGGGAGGGTCTCCTCTGAGTGATTGACTACCC  
GTCAGCGGGGTCTTTCACATGCAGCATGATCAAAATTAATTTGGTTTTTTCTTAAGTATTTACATTAATGGCCATAGTG  
CGCCGCAAAATCAATCAAAGTATATAGTAAACTTGGTCTGACAGTTACCAATGTTAATCAGTGAAGCAGCTATCTCAG  
CGATCTGTCTATTTGTTTCATCCATAGTTGCCTGACTCCCCGTCGTGTAGATAACTACGATACGGGAGGGCTTACCATCTGGC  
CCCAGTGTGCAATGATACCGCGAGACCCACGCTCACCAGGCTCCAGATTTATCAGCAATAAACAGCCAGCCGGAAGGGCC  
GAGCGCAGAAGTGGTCTGCAACTTTATCCGCCTCCATCCAGTCTATTAATTGTTGCCGGGAAGCTAGAGTAAGTAGTTCCG  
CAGTTAATAGTTTGGCAGCAAGTGTGGCATTGCTACAGGCATCGTGGTGCACGCTCGTGGTGGTATGGCTTCAATCAGC  
TCCGTTCCCAACGATCAAGCGAGTTACATGATCCCCATGTTGTGCAAAAAGCGGTTAGCTCCTCCGCTCCGATCG  
TTGTGCAAGTAAGTTGGCCGAGTGTATCACTCATGGTTATGGCAGCACTGCATAAATCTCTTACTGTGCATGCCATCCGTA  
AGATGCTTTTCTGTGACTGGTGAAGTACTCAACCAAGTCAATCTGAGAATAGTGTATGCGGCGACCGAGTTGCTCTTGGCCG  
CGTCAATACGGGATAAATCCGCGCCACATAGCAGAATTTAAAGTGTCTCATTTGGAAAACGTTCTTCCGGGGCGAAAAC  
CTCAAGGATCTTACCCTGTTGAGATCCAGTTTCGATGTAACCCCACTCGTGCACCCAACTGATCTTCCAGCATCTTTACTTTCA  
CCAGCTTTTCTGGGTGAGCAAAAACAGGAAGGCAAAATCCCGCAAAAAGGGAATAAGGGCGACACGGAAATGTTGAATAC  
CTACTCTTCTTTTCAATATTGAAAGCATTATCAGGGTATTGTTCTCATGAGCGGATACATATTTGAATGTATTTAGAA  
AAATAACAAATAGGGGTTCCGCGCACATTTCCCGAAAAGTGCCACCT

### X.2.3. pBABE-neo-IRES-eGFP

Full sequence available from Addgene (<https://www.addgene.org/14431/sequences/>) .

> Author sequence

CTGCAGCCTGAATATGGGCCAAACAGGATATCTGTGGTAAGCAGTTCTGCCCGGCTCAGGGCCAAGAACAGATGGAACA  
GCTGAATATGGGCCAAACAGGATATCTGTGGTAAGCAGTTCTGCCCGGCTCAGGGCCAAGAACAGATGGTCCCCAGATG  
CGGTCCAGCCCTCAGCAGTTCTAGAGAACCACAGATGTTCCAGGGTCCCCAAGGACCTGAAATGACCTTGTGCTTAT  
TTGAACTAACCAATCAGTTTCGCTTCTCGCTTCTGTTTCGCGCGCTTCTGCTCCCCGAGCTCAATAAAAAGAGCCCAACCCCTC  
ACTCGGGGCGCCAGTCTCCGATTGACTGAGTCGCCCCGGTACCCGTGTATCCAATAAACCCCTCTTGCACTTGCATCCGACT  
TGTGGTCTCGCTGTTCTTGGGAGGGTCTCCTCTGAGTGATTGACTACCCGTGAGCGGGGGTCTTTCATTTGGGGGCTCGTC  
CGGGATCGGGAGACCCCTGCCAGGGACCACCGACCACCCGGGAGGTAAGCTGGCCAGCAACTTATCTGTGTCTGTC  
CGATTGTCTAGTGTCTATGACTGATTTTATGCGCCTGCGTCCGTTACTAGTAACTAGCTCTGTATCTGGCGGACCCGTG  
GTGGAAGTACGAGTTCTGAACACCCCGCCGCAACCCTGGGAGACGTCCAGGGACTTTGGGGCGTTTTTGTGGCCCG  
ACCTGAGGAAGGGAGTGCATGTGGAATCCGACCCCGTACAGGATATGTGGTTCTGGTAGGAGACGAGAACCTAAAACAGTTC  
CCGCTCCGTCTGAATTTTTGCTTTGCTTTGGAACCGAAGCCGCGCTTGTCTGCTGCAGCATCGTTCTGTGTTGCTCT  
GTCTGACTGTGTTTCTGTATTGTCTGAAAATTAGGGCCAGACTGTTACCACTCCCTTAAAGTTTACCTTAGATCACTGGAAG  
ATGTCGAGCGGCTCGCTACAACAGTCCGTAGATGTCAAGAAGAGACGTTGGTTACCTTCTGCTCTGCAGAATGGCCAAC  
CTTTAACGTCCGATGGCCGCGAGACGGCACCTTAACCGAGACCTCATACCCAGGTTAAGATCAAGGCTTTTTACCTGGC  
CCGATCGACACCCAGACCGTCCCTACATCGTGTAGCGACCCCTTTGCAAGCTTTGACCCCTCCCTGGGTCAAGCCC  
TTTGTACACCCTAAGCCTCCGCCTCCTCTTCCATCCGCGCCGTCTCTCCCTTGAACCTCCTCTTTCGACCCCGCCTCA  
ATCCTCCCTTATCCAGCCCTCACTCCTTCTAGGCGCCGCGGATCCAGTGTGGTGGTACGTAGGAATTCGCCAGCAC  
AGTGGTGCAGCGTACCGCGGGCCCGGATCCGCCCTCTCCCTCCCCCCCCCTAACGTTACTGGCCGAAGCCGCTTGA  
ATAAGGCCGGTGTGCGTTTGTCTATATGTTATTTTCCACCATATTGCCGTCTTTGGCAATGTGAGGGCCCGAAACCTGGCC  
CTGTCTTCTGACGAGCATTCTAGGGTCTTTCCCTCTCGCAAAGGAATGCAAGGTCTGTTGAATGTGCGTAAGGAAGC  
AGTTCTCTGGAAGCTTCTTGAAGACAAACAACGTCTGTAGCGACCCCTTTGCAAGCAGCGGAACCCCTCCCTGGCGACAG  
GTGCTCTGCGGCCAAAAGCCAGTGTATAAGATACACCTGCAAAGCGGCAACAACCCAGTGCCACGTTGTGAGTTGGAT  
AGTTGTGGAAGAGTCAAATGGCTCTCCTCAAGCGTATTCAACAAGGGGCTGAAGGATGCCAGAAGGTACCCATTGTATG  
GGATCTGATCTGGGGCCTCGGTGCACATGCTTTACATGTGTTTGTGAGGTTAAAAAACGCTTAGGCCCCCGAACCAG  
GGGACGTGGTTTTCTTTGAAAACACGATGATAATATGGCCACAACCATGGTGAAGGCGAGGAGCTGTTACCCGGG  
GTGGTGCCATCCTGGTCGAGCTGGACGGCGACGTAACGGCCACAAGTTACGCGTGTCCGGAGGGCGAGGCGGATG  
CCACTACGGCAAGCTGACCCCTGAAGTTCACTGACACCCGGCAAGCTGCCCTGCCCTGACCCACCTCGTGACACCC  
TGACCTACGGCGTGCAGTGTTCAGCCGCTACCCGACCACATGAAGCAGCAGGACTTCTTCAAGTCCGCCATGCCGAAG  
GCTACGTCCAGGAGCGCACCATCTTCTTCAAGGACGACGGCAACTACAAGACCCGCGCGAGGTGAAGTTCGAGGGCGAC  
ACCCTGGTGAACCGCATCGAGCTGAAGGGCATCGACTTCAAGGAGGACGGCAACATCTGGGGCACAAGCTGGAGTACAAC  
TACAACAGCCACAACGCTATATCATGGCCGACAAGCAGAAGAACGGCATCAAGGTAACCTCAAGTCCGCCACAACATCG  
AGGACGGCAGCTGCAGCTCGCCGACCCTACCAGCAGACACCCCATCGGCGACGGCCCTGCTGCTGCCCGACAAAC  
CACTACCTGAGCACCCAGTCCGCCCTGAGCAAAGACCCCAACGAGCAGCGATCACATGGTCTGCTGGAGTTCGTGACC  
GCCGCCGGGATCACTCTCGGCATGGACGAGCTGTACAAGTAAGTGCACCTGTGGAATGTGTGTCAGTTAGGGTGTGGAAG  
TCCCAGGCTCCCCAGCAGGCAAGTATGCAAAGCATGCATCTCAATTAGTCAGCAACCATAGTCCCGCCCTAACTCCGCCATCCCC  
TCCCAGCAGGCAAGTATGCAAAGCATGCATCTCAATTAGTCAGCAACCATAGTCCCGCCCTAACTCCGCCATCCCC  
CCCTAACTCCGCCAGTTCGCGCCATTCTCCGCCCATGGTGACTAATTTTTTTTATTTATGCAGAGGCGGAGGCGCCCTC  
GGCCTCTGAGCTATCCAGAAGTAGTGAGGAGGCTTTTTGGAGGCTAGGCTTTTGCAAAAGCTTACAGCTGCCCGCAAGC  
ACTCAGGGCGCAAGGGCTGCTAAAGGAAGCGGAACACGTAGAAAGCCAGTCCGAGAAACGGTGTGACCCCGGATGAAT  
GTCAGCTACTGGGCTATCTGGACAAGGGAAAACGCAAGCGCAAAGAGAAAGCAGGTAGCTTGCAGTGGGCTTACATGGCGA  
TAGCTAGACTGGGCGTTTTATGGACAGCAAGCGAACCAGGAATTGCCAGCTGGGGCGCCCTCTGGTAAGGTTGGGAAGCC  
TGCAAAGTAACTGGATGGCTTTCTTCCGCCAAGGATCTGATGGCGCAGGGGATCAAGATCTGATCAAGAGACAGGATGA  
GGATCGTTTCGCATGATTGAACAAGATGGATTGCACGAGGTTCTCCGGCCGCTTGGGTGGAGAGGCTATTCGGCTATGACT  
GGCACAACAGACAATCGGCTGCTGTGATGCCCGGTGTTCCGGCTGTGACGCGCAGGGGCGCCCGTTCTTTTTGTCAAGA  
CCGACCTGTCCGGTGCCTGAATGAAGTGCAGGACGAGGACGCGCGGCTATCGTGGCTGGCCACGACGGGCGTTCTTGC  
GCAGCTGTGCTCGACGTTGTCACTGAAGCGGAAGGGACTGGTGTCTATTGGGCGAAGTCCCGGGCAGGATCTCCTGTC  
ATCTCACCTTGTCTGCTGCCGAGAAAGTATCCATCATGGCTGATGCAATGCGGCGGCTGCATACGCTTGTATCCGGTACCTGC  
CCATTCGACCACCAAGCGAAACATCGCATCGAGCGAGCAGTCTGGATGGAAGCCGGTCTTGTGATCAGGATGATCTG  
GACGAAGAGCATCAGGGGCTCGGCCAGCCGAACTGTTCCGACTGCTCAAGGCGCATGCCGACGGGAGGATCTCGT  
CGTACCCATGGCGAGTCTGCTTGGCGAATATGTTGGAAAATGGCCGCTTTTTCTGGATTCACTGACTGTGGCCGGCT  
GGTGTGGCGGACCGCTATCAGGACATAGCGTTGGCTACCCGTGATATTGCTGAAGAGCTTGGCGGCAATGGGCTGACCG  
CTTCTCTGCTTTACGGTATCGCCGCTCCCGATTGCGAGCGCATCGCTTCTATCGCCTTCTTACGAGTCTTCTGAGCG  
GGACTCTGGGGTatcgatCGTAATCTGCTGCTTGAACAAAAAACCCAGCTACCAAGCGGTGGTTTGTGTCGGATCAAG  
AGCTACCAACTCTTTTTCCGAAGGTAAGTGGCTTACGACAGGCGCAGATACCAATACTGCTCTTAGTGTAGCCGTAGTTA  
GGCCACCACCTCAAGAACTCTGTAGCACCCGCTACATACCTGCTGCTAATCCTGTTACGAGTGGCTGCTGCCAGTGCG  
ATAAGTCTGTCTTACCAGGTTGGACTCAAGACGATAGTTACCGGATAAGGCGCAGCGGTCCGGGCTGAACGGGGGTTCTG  
GCACACAGCCCAGCTTGGAGCGAACGACCTACCCGAACTGAGATACCTACAGCGTGAGCTATGAGAAAGCGCCACGCTTC  
CCGAAGGGGAGAAAGGCGGACAGGTATCCGTAAGCGGCAGGGTCCGAACAGGAGAGCGCACGAGGGAGCTTCCAGGGG  
AAACGCCTGGTATCTTTATAGTCTGTCGGGTTTCGCCACCTGACTTGAAGCGTTCGATTTTTGTGATGCTCGTCAGGGGG  
CGGAGCCTATGAAAAACGCCAGCAACGatcgatAAAAATAAAGATTTTATTTAGTCTCCAGAAAAAGGGGGGAATGAAAGACC  
CCACTGTAGGTTTGGCAAGCTAGCTTAAGTAACGCCATTTTGAAGGCATGGAATAATACATAACTGAGAATAGAAAGTTT  
AGATCAAGGTCAGGAACAGATGGAACAGCTGAATATGGGCCAAACAGGATATCTGTGGTAAGCAGTTCTGCCCGGCTCA  
GGGCCAAGAACAGATGGAACAGCTGAATATGGGCCAAACAGGATATCTGTGGTAAGCAGTTCTGCCCGGCTCAGGGCCA  
AGAACAGATGGTCCCCAGATGCGGTCCAGCCCTCAGCAGTTTCTAGAGAACCATCAGATGTTTCCAGGGTCCCCAAGGAC  
CTGAAATGACCTGTGCTTATTTGAACTAACCAATCAGTTCCGTTCTCGCTTCTGTTTCGCGCGCTTCTGCTCCCCGAGCTCA  
ATAAAGAGCCCAACCCCTCACTCGGGCCAGTCTCCGATTGACTGAGTGCAGGCTGACTGAGTGCAGGCTACCCGTATCAATAA  
CCCTCTTGCAGTTGCATCCGACTTGTGCTCGCTGTTCTTGGAGGGTCTCCTCTGAGTGATTGACTACCCGTACGCGGGGCTTC  
GGTCTTTTCACTTCCGACTTGTGGTCTCGCTGCTTGGAGGGTCTCCTCTGAGTGATTGACTACCCGTACGCGGGGCTTTC  
ACATGCAGCATGTATCAAAATTAATTTGGTTTTTTTTCTTAAGTATTTACATTAATGGCCATAGTGGCGCCGCAATCAATCTA





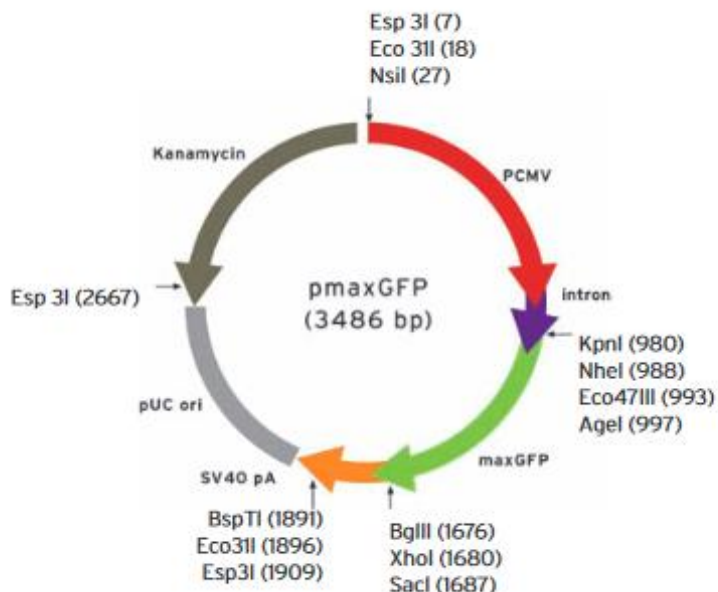


Figure 83: Full sequence of pmaxGFP

([https://bioscience.lonza.com/lonza\\_bs/CH/en/document/download/21442](https://bioscience.lonza.com/lonza_bs/CH/en/document/download/21442); 03.02.2020)

Both plasmids, pBABE-puro-hTERT and pBABE-hygro CDK4 R24C were a gift from Bob Weinberg. pBabe neo IRES-EGFP was a gift from L. Miguel Martins.

### X.3. Primer sequences

#### IX.3.1. pBABE

Name	Sequence	Tm (°C)
pBABE-3'	5'-ACCCTAACTGACACACAT TCC-3'	56.5
pBABE-5'	5'-CTTTATCCAGCCCTCAC-3'	51.1

Figure 84: Primer sequences used for pBABE-backbone

#### X.3.2. GNE

Name of exon and sense (s)/antisense (a)	Sequence	Tm (°C)	PCR product (bp)
2s	5'-GTGGTTAAGGACTTGAAACT-3'	54.0	449
2a	3'-GTGACTACTCTAAGGCCAC-5'	56.7	
3s	5'-CTTCAGAGTTGGTGTTAGATTG-3'	56.5	618
3a	3'-CCAAAAGGATTGAAATAGACGG-5'	56.5	
4s	5'-GCACAGACTTAGAGTCTTGC-3'	57.3	335
4a	3'-GAGCAAGATAGGAAGGCAG-5'	56.7	
5s	5'-GTGGGCTATACTTGCCAATG-3'	58.0	357
5a	3'-GCATACCTTATAACAACCTCACG-5'	58.0	
6s	5'-GGTCTAATTATGAGCATAGTAC-3'	54.7	269
6a	3'-GGATGATTAACAGTGATTGTAG-5'	58.0	
7s	5'-CTGAAGTCTCAGTTTCCATTAC-3'	53.3	369
7a	3'-GTTTCTAGTCTTACCTTCCAAC-5'	51.7	
8s	5'-CCTATAGCAGTGTCTAATTTGTC-3'	64.0	308
8a	3'-GCTCAGGCATGCATCACAAG-5'	62.0	
9s	5'-CGTTTGTCTTAGGAGATCTGG-3'	56.6	424

9a	3'-GCAGAGTTGTAACCACCTGAC-5'	64.0	
10s	5'-GGCTTCAGTGTTCCAGCTGTC-3'	60.0	372
10a	3'-GGCTTCAGTGTTCCAGCTGTC-5'	62.0	
11s	5'-GTGAAAAGAAAACACCGTCTTCC-3'	61.2	344
11a	3'-GACACTGCAAAGCACCTGTC-5'	28.3	
12s	5'-CTTTAACATTTCTGCTGCTGGCTC-3'	64.0	461
12a	3'-ATTTCTCTGCCAAAGTCACCTGC-5'	63.0	

Figure 85: Primer sequences for exons of *GNE* gene

### X.3.3. VCP

Name of exon and sense (F/s)/ antisense (R/a)	Sequence	Tm (°C)	PCR product (bp)
VCP_1F	5'-GAGAATTCCAATCCGTCGAG-3'	52	632
VCP_1R	5'-TCCTGGTCTCCACCTCTCTG-3'	56	
VCP_2-3F	5'-GCTTTCTGGTCTAGGGACAGC-3'	56	790
VCP_2-3R	5'-CAAGAACTTGGTCCTGCCTG-3'	54	
VCP_4s	5'-AAGCCATCCTGCCTTTTCTT-3'	50	385
VCP_4as	5'-AATAAATACAGGGGAAAAGCATAA-3'	49	
VCP_5s	5'-GAGCTTGGCATTGTTGACCC-3'	51	301
VCP_5as	5'-CCCAGTCCTGACAGTTACCAC-3'	56	
VCP_6s	5'-TTTGCACACTAGGTAGTGGAAATG-3'	53	301
VCP_6as	5'-CCCAGGATTAGACATTGGGAC-3'	54	
VCP_7s	5'-CCCTCTCTGGAGCGCTAGTC-3'	58	269
VCP_7as	5'-AAAAGGATGTGTTCCATAAGTGCTC-3'	52	
VCP_8-9F	5'-TTACCACCTTCTCACCCAGG-3'	54	569
VCP_8-9R	5'-TGGACCCAATCACTGTGAAG-3'	52	
VCP_10F	5'-GGTCACCCTAGGCCTGTCTC-3'	58	255
VCP_10R	5'-GTCTCTAGCCAGTCCACAGC-3'	56	
VCP_11-12F	5'-AGCAGTCAGGGGAAGGATTC-3'	54	542
VCP_11-12R	5'-TTGACACCCTGAGATCACCC-3'	54	
VCP_13F	5'-TAATGGAGGGGATGCTTCTG-3'	52	402
VCP_13R	5'-CAGTTGAGCAGCCAGCAC-3'	53	
VCP_14F	5'-GTGTGAGCCACCACGTTTG-3'	53	471
VCP_14R	5'-CCCAGTGAATCTTGTCCAG-3'	54	
VCP_15F	5'-GGGCAAAGTGTAGTTGGGAG-3'	54	325
VCP_15R	5'-ACTCCAGGGCATGGTGG-3'	52	
VCP_16-17F	5'-AAACTGCAGTAATGGGAGGC-3'	52	820
VCP_16-17R	5'-ACTCCATCCCTTTTGGTG-3'	51	

Figure 86: Primer sequences for exons of VCP gene

## X.4. GenBank accession numbers

Gene	gDNA sequence
GNE	NC_000009.12
VCP	NC_000009.12

Figure 87: GenBank accession numbers

## X.5. List of figures and tables

Figure 1: top: Overview of two adjacent sarcomeres; bottom: electron microscopic image of ultrastructural organization of sarcomeres in parallel [4]. (Published under Creative Commons Attribution License - CC BY 2.0.).....	8
Figure 2: Typical sequence of Gowers's sign [20]. (Reprint permission granted from copyright holder.).....	10
Figure 3: Overview of the structure of the dystrophin-glycoprotein complex [56]. (Reprint permission granted from copyright holder.).....	13
Figure 4: Overview of human dystrophin isoforms [32]. (Published under Creative Commons Attribution 4.0 International License – CC BY 4.0.).....	13
Figure 5: Overview of exons coding for Dp427m. The reading frame is restored, when exons flanking the deletion have congruent ends, e. g. skipping of exon 51 and a deletion of exon 52 leads to a restored reading frame between exons 50 and 53 [122]. (Reprint permission granted from copyright holder).....	16
Figure 6: Overview of important DMD mouse models, modified after [188].....	22
Figure 7: Reports of dystrophin-deficient dogs, modified after [188].....	24
Figure 8: Schematic picture of replacement of exon 52 by a neomycin cassette [237]. (Reprint permission granted from copyright holder.).....	25
Figure 9: Pigs used for porcine cell lines.....	36
Figure 10: Antibiotic concentrations used on P507/18 and P515/18.....	41
Figure 11: Antibiotic concentrations used on P352/15 and P362/15.....	41
Figure 12: Antibiotic concentrations used on Phoenix amphi producer cell line.....	41
Figure 13: Antibiotic concentrations used on 3T3.....	41
Figure 14: Plasmid volumes and amounts of DNA used.....	42
Figure 15: Induced resistance by transfected plasmids and maximum selection agent concentration.....	43
Figure 16: Titration of virus scheme.....	44
Figure 17: Overview of antibiotic selection.....	44
Figure 18: Protocol for transduction of myoblasts.....	45
Figure 19: Transduction scheme first approach P352/15 and P562/15.....	45
Figure 20: Range of antibiotic concentrations used in first approach.....	46
Figure 21: Overview of transduction and antibiotic selection of P362/15 cell approaches in second approach.....	46
Figure 22: Transduction scheme third approach P507/18 and P515/18.....	47
Figure 23: Overview of antibiotic selection of different cell approaches in third approach.....	47
Figure 24: List of antibodies.....	50
Figure 25: PCR mixture for <i>hTERT</i> and <i>CDK4</i> cDNA sequence.....	50
Figure 26: PCR protocol for <i>hTERT</i> and <i>CDK4</i> cDNA sequence.....	51
Figure 27: PCR mixture for <i>VCP</i> and <i>GNE</i> gene.....	51
Figure 28: PCR protocols for the <i>VCP</i> and the <i>GNE</i> gene.....	52
Figure 29: Visualization of DNA measurement of pBABE-puro-hTERT (top left), pBABE-hygro-CDK4 R24C (right), pBABE-neo-IRES-eGFP (bottom).....	53
Figure 30: Amount of plasmid DNA.....	53
Figure 31: Comparison of P507/18 cells on day 20 of antibiotic selection: 200 µg/ml G418 (left), 400 µg/ml (middle), 600 µg/ml (right).....	54
Figure 32: Example of myoblast growth (P507/18) under double selection day 20: 0.05 µg/ml puromycin + 5 µg/ml hygromycin (left), 0.1 µg/ml puromycin + 10 µg/ml hygromycin (right).....	54
Figure 33: left: Phoenix amphi cells, stained for DAPI, right: pmaxGFP® as positive control, day 1 after transfection....	56
Figure 34: Typical growth pattern of Phoenix amphi producer cell line in varying confluencies under antibiotic selection (top left & right), examples of expression of pBABE-neo-IRES-eGFP (bottom left & right).....	56
Figure 35: Selection of transfected producer cells.....	57
Figure 36: Mean viral titer (hTERT).....	57
Figure 37: GFP-positive C2C12 cells (top left) and growth pattern top right) 17 days and GFP-positive 3T3 cells (bottom left) and growth pattern (bottom left) 14 days after transduction with pBABE-neo-IRES-eGFP containing viral supernatant and subsequent antibiotic selection up to 500 µg/ml G418.....	58
Figure 38: Cell culture at day 12 before transduction, P507/18 (left) and P515/18 (right).....	61
Figure 39: P507/18 hTERT (DMD I) day 19, 5 days after antibiotic selection initiation (left), day 21, 7 days under antibiotic selection (right).....	61
Figure 40: DMD IV (left) and WT IV (right) on day 28 regained confluency under antibiotic selection with 1.5 µg/ml puromycin.....	62
Figure 41: Visualization of sharp decline in cell confluency on day 19, four days after addition of hygromycin, single cells with signs of colony-like growth (DMD II left; WT II right).....	62
Figure 42: DMD V (left) and WT V (right) on day 28 regained confluency under antibiotic selection.....	63
Figure 43: Insular-shaped regrowth pattern of DMD VII (left) and WT VII (right) on day 19.....	63
Figure 44: Growth pattern of DMD VII (left) and WT VII (right) on day 20.....	64
Figure 45: DMD VII (left) and WT VII (right) on day 28.....	64
Figure 46: DMD VII (left) and WT VII (right) on day 38 under maximum antibiotic selection concentration (0.3 µg/ml puromycin and 30 µg/ml hygromycin).....	64
Figure 47: Comparison of DMD VIIa (top left), DMD VIIb (top right), WT VIIa (bottom left) and WT VIIb (bottom right) on day 57, being under antibiotic selection with 0.2 µg/ml puromycin and 20 µg/ml hygromycin; DMD and WT VIIb were non-selected.....	65
Figure 48: 9-DMD VII (left) and 9-WT VII (right) on day 206.....	65

Figure 49: DMD I (top left) and WT I (top right) and DMD II (bottom left) and WT II (bottom right), all on day 38 under selection with 0.3 µg/ml puromycin and 30 µg/ml hygromycin.....	66
Figure 50: DMD VI (top left) and WT VI (top right) on day 38, DMD VI (bottom left) and WT VI (bottom right) on day 53 ....	67
Figure 51: Irregularly shaped cells on day 129; DMD VI (top left) and WT VI (top right); DMD VI (bottom left) and WT VI (bottom right) on day 221.....	68
Figure 52: (next page): green fluorescent cells: 1. row: WT III on day 23; 2. row: WT III on day 53; 3. row: WT III on day 55; 4. row: WT III on day 82; 5. row: DMD III on day 48; 6. row: DMD III on day 53.....	68
Figure 53: Morphologic features of DMD III on day 14 (left) without selection and on day 28 (right) under selection with 275 µg/ml G418.....	70
Figure 54: Transduction efficacy measured by ratio of GFP-positive transduced porcine myoblasts under antibiotic selection. The timeline shows days after last transduction. ....	70
Figure 55: Comparison of cell morphology of P507/18 on day 9 (left) and 9-DMD VIIa on day 178 (right). ....	71
Figure 56: Typical apoptotic cells with a flat, irregularly shaped morphology on day 213 (upper left) and WT VIIb on day 95 (bottom left); spontaneous myotube-like formation and irregularly shaped P515/18 cells on day 67 (upper right); cluster formations of DMD VII on day 62 (bottom right). ....	71
Figure 57: DMD VII cells under trypsinization exhibiting trabecular-shaped formation of trypsinized cells (left), DMD VI cells after trypsin application with cell remnants (right). ....	72
Figure 58: Estimated mean population doublings DMD VI and 9-DMD VIIa.....	73
Figure 59: Estimated mean population doublings WT VI and 9-WT VIIa.....	74
Figure 60: Calculated population doublings based on consecutive counting for a period of 21 days for transduced and non-transduced porcine myoblasts at different age. ....	74
Figure 61: Growth pattern of cell colonies in 96-well culture plate on day 67; 30-G5 WT VII left, 31-H6 DMD VII right .....	75
Figure 62: DMD VII d78 after 96 hours of fusion: myotube-like formations with multiple nuclei .....	76
Figure 63: DMD VII d95 after 21 days (left) and 28 days (right) of fusion.....	77
Figure 64: 9-DMD VIIa d259 after 96 hours of fusion MG/RC .....	77
Figure 65: WT VII on day 74 after 24 hours of fusion (left) and on day 78 after 96 hours of fusion (right) .....	77
Figure 66: WT VII d95 after 21 days (left) and 28 days (right) of fusion .....	77
Figure 67: P507/18 d45, after 24 hours of fusion (upper row); after 96 hours of fusion (middle row), P507/18 d79 after 96 hours of fusion (bottom row).....	78
Figure 68: P515/18 on day 45 (top row) and on day 78 (bottom row) after 96 hours of fusion .....	78
Figure 69: P507/18 (left) and P515/18 (right) on day 38 after 15 days of fusion.....	79
Figure 70: Beginning of myotube fusion on day 3 (upper row), 0208ct7 control cells after 6 days (middle row) and 13 days (bottom left) and 14 days (bottom right) of fusion .....	79
Figure 71: DMD VII cell line, top row from left: on day 60 after 60 hours of fusion (1 to 3), day 54 after 6 days of fusion (4), bottom row from left: day 75 after 24 hours of fusion (1 and 2), day 100 after 4 days of fusion (3) and day 258 after 4 days of fusion (4), stained for desmin and DAPI. ....	80
Figure 72: WT VII cell line on day 60 after 60 hours of fusion (1 to 3) and day 75 after 24 hours of fusion (4), stained for desmin and DAPI.....	80
Figure 73: First row from left: fused P507/18 cells on day 27 after 60 hours of fusion (1 and 2), day 45 after 24 hours of fusion (3), fused P515/18 cells on day 27 after 60 hours of fusion (4); second row from left: day 41 after 24 hours of fusion (1), non-fused P515/18 cells on day 15 (2), fused 0208ct7 cells (3), all stained for DAPI and desmin, fused DMD VII cells on day 60 after 60 hours of fusion, stained only for secondary antibody (4). ....	81
Figure 74: Gel electrophoresis; from left to right: 1'000 bp ladder, no template control pBABE-3'/-5'-primer, pBABE-hygro-CDK 4 R24C Phoenix ampho cell gDNA (III+IV), pBABE-puro-hTERT Phoenix ampho cell gDNA (V+VI), positive control DNA, 100 bp ladder.....	82
Figure 75: Gel electrophoresis, 100 bp ladder, exon 1, 2-3, 4, 5, 6, 7, 8-9, 10, 11-12, 13, 14, 15, 16-17 of the VCP gene (from left to right).....	84
Figure 76: Electropherogram showing c.476G>A mutation in exon 5 of the VCP gene.....	84
Figure 77 left: Gel electrophoresis, VCP exon 5 (left lane), 100 bp ladder (right lane), right: section of electropherogram of the VCP exon 5 sequence showing a heterozygous c.476G>A base exchange.....	85
Figure 78: Gel electrophoresis: 100 bp ladder, GNE gene exon 2 to 12 (left to right).....	86
Figure 79: Sections of electropherogram depicting mutations in GNE gene: c.178A>G (left), c.1853T>C (right).....	87
Figure 80: Full sequence map for pBABE-puro-hTERT ( <a href="https://www.addgene.org/1771/">https://www.addgene.org/1771/</a> ; 03.02.2020).....	114
Figure 81: Full sequence map pBABE-hygro-CDK4 R24C ( <a href="https://www.addgene.org/11254/">https://www.addgene.org/11254/</a> ; 03.02.2020) .....	115
Figure 82: Addgene full sequence of pBABE-neo-IRES-eGFP ( <a href="https://www.addgene.org/14431/">https://www.addgene.org/14431/</a> ; 03.02.2020) .....	115
Figure 83: Full sequence of pmaxGFP ( <a href="https://bioscience.lonza.com/lonza_bs/CH/en/document/download/21442;03.02.2020">https://bioscience.lonza.com/lonza_bs/CH/en/document/download/21442;03.02.2020</a> ).....	116
Figure 84: Primer sequences used for pBABE-backbone .....	116
Figure 85: Primer sequences for exons of GNE gene.....	117
Figure 86: Primer sequences for exons of VCP gene .....	117
Figure 87: GenBank accession numbers.....	117

## **X.6. Danksagung**

An dieser Stelle möchte ich mich bei allen Personen bedanken, die zum Gelingen dieser Arbeit beigetragen haben.

Ganz besonders würdigen möchte ich Frau Priv.-Doz. Dr. med. Dr. phil. Sabine Krause für die Bereitstellung des Themas und die außerordentliche und enge Betreuung während der Erstellung der Arbeit. Ihre konstruktiven Vorschläge für anfallende Probleme und Fragen halfen mir bei der Erstellung dieser Arbeit sehr.

Weiterhin möchte ich mich bei Frau Univ.-Prof. Dr. med. Marianne Dieterich, Frau Prof. Dr. med. Maggie C. Walter und Herrn Prof. Dr. med. Benedikt Schoser für die Bereitstellung der notwendigen Laborkapazitäten und Materialien bedanken.

Zudem möchte ich meinen Kollegen im Labor für Molekulare Myologie danken, insbesondere Dr. rer. med. Peter Meinke und Dr. rer. nat. Stefan Hintze. Sie standen mir für Fragen und Unterstützung allzeit zur Seite. Zudem gilt mein besonderer Dank Dr. rer. nat. Rolf Stucka, insbesondere für die Unterstützung bei der Durchführung der PCR-Testungen der Myoblasten. Zudem möchte ich mich bei Maria Schmuck, Ira Brandstetter und meinen Mitdotorandinnen Simone Reichert und Tina Donandt bedanken. Weiterhin danken möchte ich unseren Kooperationspartnern um Univ.-Prof. Dr. med. vet. Eckhard Wolf, Prof. Elisabeth Kapaki sowie Dr. rer. nat. Claudia Kalbe.

Zuletzt möchte ich mich herzlich bei meiner Familie, insbesondere meinen Eltern, meiner Schwester Clara, meinem Großvater sowie meiner Freundin Elisabeth für den Rückhalt und die Unterstützung in dieser Zeit bedanken.

## **X.7. Eidesstattliche Versicherung**

Ich erkläre hiermit an Eides statt, dass ich die vorliegende Dissertation mit dem Thema

**“Immortalization of primary myoblasts from the DMD pig -  
hTERT/CDK4 prevent cellular senescence in primary porcine myoblasts“**

selbstständig verfasst, mich außer der angegebenen keiner weiteren Hilfsmittel bedient und alle Erkenntnisse, die aus dem Schrifttum ganz oder annähernd übernommen sind, als solche kenntlich gemacht und nach ihrer Herkunft unter Bezeichnung der Fundstelle einzeln nachgewiesen habe.

Ich erkläre des Weiteren, dass die hier vorgelegte Dissertation nicht in gleicher oder in ähnlicher Form bei einer anderen Stelle zur Erlangung eines akademischen Grades eingereicht wurde.

München, den 18.01.2022

Nicolas Ulrich Schumacher

## **X.8. Curriculum vitae**